Experimental Investigation and Statistical Analysis of Entrainment Rates of Particles in Suspended Load

Yao Qifeng

Doctoral Thesis

Department of Geology and Mineralogy
Division of Earth and Planetary Sciences
Graduate School of Science
Kyoto University

June, 2019

Abstract

Suspended load has been considered as one of the most significant mode of sediment transport in many types of fluid flows, and thus quantitative prediction of suspended load is a critical subject for various research fields including deep-sea sedimentology. Spatio-temporal development of a suspended load is generally predicted by estimating downward and upward fluxes at the near-bed reference level in the water column, which are called as settling and entrainment rates of suspended sediment. Downward flux of suspended load can be easily estimated by products of settling velocity of particles and concentration, while the theoretical prediction of entrainment rates of the suspended load still remains difficult. Therefore, empirical formulation of the entrainment rates has been extensively investigated to establish morphodynamic models considering the suspended load.

The proposed formulations of entrainment rate, however, have several unsolved matters. Only the limited numbers of possible governing parameters were considered in previous analyses, and the performances of existing functions had been compared by the sum of squared residuals even though numbers of employed parameters in those functions were different. Also, the empirical entrainment function established from measurements in open channel flows were applied to density flows. Finally, in previous researches, the artificial saturation values that was set in entrainment functions to avoid unrealistic results. This saturation value should be applied for total concentration of a suspended load, while previous entrainment functions for mixed grain-size sediment misused this saturation value to each grain-size class.

To this end, this research aimed to produce a new empirical function for predicting entrainment rate of the suspended load in open channel flows and turbidity currents. For this purpose, new experiments were conducted to provide additional data pertaining to entrainment of sediment of uniform and mixed grain-size classes. The multiple regression analysis was employed in this study. and the best model was chosen by the model selection using the Akaike Information Criterion (AIC) and the cross-validation.

As a result of the statistical analysis, this research produced new functions for uniform grain-size and non-uniform grain-size sediment. The new functions is obtained by a purely empirical approach, and therefore it can be used for verifying theoretical researches. The three issues in previous research were clarified by the result of the statistical analysis. (1)

First, AIC indicated that the new function provides better predictions than those of existing functions. (2) Secondly, it was implied that the best model for open channel and density flows were clearly different, suggesting that two types of flow show different behavior in transporting suspended load. (3) Thirdly, the new entrainment function for non-uniform sediment was also established, in which the artificial saturation value was not set.

The result of this study contributes to understand the morphodynamics of various environments such as river deltas, coastal managements, and sedimentology of submarine fans, although further theoretical modeling of entrainment processes of basal sediment particles and additional flume experiments as well as field measurements will be required to improve precision of the functions.

Table of Contents

1 Introduction

Sediment loads of bed materials in fluid flows are classified as a bed load and a suspended load. A suspended load is defined as the undissolved solid particles that are lifted upward by turbulent eddies in flows. Comparing to a bed load in which sediment particles frequently contact with bed materials, a suspended load is characterized by finer grain-size distribution and longer travel distance (Figure 1). Suspended load has been considered as one of the most significant mode of sediment transport in various types of fluid flows, such as rivers, ocean currents, turbidity currents, and atmospheric flows. Syvitski, Vorosmarty, Kettner, and Green (2005) estimated that the prehuman global fluxes of supspended sediment is 14 billion metric tons, which is *ca*. 90 wt% of total sediment load delivered from land to ocean. In density flows in deep-sea environments such as turbidity currents, the suspended sediment leads to the density difference between the flow and surrounding water (Parker, Fukushima, & Pantin, 1986), the excess weight of flow makes turbidity current sustainable. Aeolian sediment particles (< 0.1 cm in diameter) are also transported as suspended load (Sarre, 1987).

Quantitative prediction of suspended load is therefore a critical subject for various research fields such as river management, planetary sciences and deep-sea sedimentology. Both in the river flows and turbidity currents, the material exchange at the bed is one of the most important part of this process. The entrainment and deposition of the suspended sediment make the flow being a nonconservative and dynamic substance (Middleton, 1993), which shows complicated behavior rather than a simple conservative flow. Especially, it is a significant process in fine-grained meandering rivers (e.g. Ma et al., 2017), in which development of flood plain is largely governed by rates of suspended sediment transport (Lauer & Parker, 2008). Flood plain management is of the greatest importance in human land-use planning, so that precise relation between discharges of river flows and suspended loads is urgently required. In addition, turbidites which deposited on submarine fans often comprise large-scale reservoir rocks of energy resources, and quantitative understandings of turbidity currents contribute estimation of their geomorphology. As described above, amounts of a suspended load control excess density of turbidity currents, and therefore quantitative prediction of suspended load is a key issue of numerical models of turbidity currents (Kostic & Parker, 2006). In summary, the modeling of suspended sediment is necessary not only

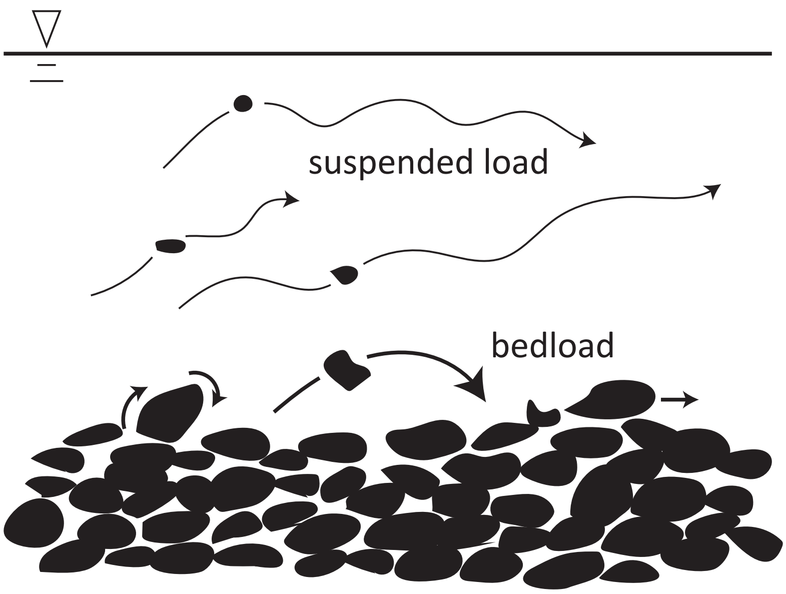

Fig. 1: Sketch of suspended load and bedload. $\triangledown$ denotes the water surface.

for scientific purpose but also for economic requirements.

To model a suspended load, it is necessary to quantify entrainment rates of bed materials to suspension that is defined as upward flux of sediment. The modeling of spatio-temporal development of a suspended load is generally performed by the advection-diffusion equation with consideration of the balance between settling rates (downward flux) and entrainment rates (upward flux) of sediment at the near-bed reference level in the fluid column. The settling rate from the suspended load can be estimated by product of the concentration and the settling velocity of the sediment particles. However, the theoretical modeling of the entrainment of bed materials remains difficult in the near-bed region where collisions, friction and diffusion of particles by turbulence interact each other. Therefore previous research focused on the empirical formulations in which the entrainment rate is related with properties of the flow intensity and sediment properties. For instance, Garcia and Parker (1991) suggested that the dimensionless entrainemnt rate of suspended sediment is proportional to the products of the power of the dimensionless flow shear velocity and the particle Reynolds number. On the other hand, van Rijn (1984) implied that the entrainment rate is a function of "transport stage" that considers the flow shear velocity and the critical shear velocity for initiation of the particle movement. Both of the functions indicate that the entrainment rate can be described by some metrics of the flow intensity and the sediment particle size, and they have been extensively used in numerical models of the morphodynamics (e.g. Kostic & Parker, 2006).

The proposed formulations of the entrainment rate, however, have several unsolved problems. (1) Firstly, statistical consideration was insufficient in previous research. The linear regression analysis was often employed in previous works, whereas only the limited numbers of the possible governing parameters were considered in their analysis. For example, in the function of Garcia and Parker (1991), the exponent of the flow shear velocity is fixed to be 5, and only the coefficient for the product of the flow shear velocity and the particle Reynolds number was fit to the datasets. In addition, the performances of existing functions were compared by the sum of squared residuals even though numbers of employed parameters in those functions were different. (2) Secondly, both datasets pertaining to open channel flows and density flows were mixed when they were analyzed in previous studies (e.g. Elhakeem & Sattar, 2015), or the empirical entrainment function established from measurements in open channel flows were applied to density flows (Garcia & Parker, 1993). The vertical velocity profiles of flows are different between open channel and density flows, so that the diffusion of suspended sediment can vary greatly in these two types of flows. (3) Thirdly, consideration of mixed-grain size sediment in entrainment function was problematic. In previous research, the artificial saturation values were set in entrainment functions to avoid unrealistic results (Garcia & Parker, 1991; van Rijn, 2007). This saturation value should be applied for total concentration of a suspended load, while previous entrainment functions for mixed grain-size sediment misused this saturation value to each grain-size class (Garcia & Parker, 1993). Also, measurements of entrainment of the mixed grain-size sediment were quite limited in number, and therefore reliability of the functions was low.

To this end, this research aimed to produce a new empirical function for predicting entrainment rate of the suspended load in open channel flows and turbidity currents. For this purpose, experiments were conducted to provide additional data pertaining to entrainment of sediment of uniform and mixed grain-size classes. The multiple regression analysis was then conducted in this study. The dimensionless parameters that are potentially significant in predicting entrainment rate of the suspended load were examined in multiple models as many as possible, and the best model and parameter sets were chosen by the model selection using the Akaike Information Criterion and the average values of cross-validation. These procedures solve the problem that the parameters and their exponents were chosen arbitrarily in previous research, and provide more reliable empirical function showing high generalization performance.

2 Theory of suspended sediment transport and previous studies

2.1 Concentration profile of suspended load in turbulent flows

Suspended sediment particles are held up above the bed by the turbulence of the fluid, and the downward volume flux of particles by settling is $-w_s c$ where w_s denotes the settling velocity of sediment particles and c is volumetric concentration of a suspended load. Let x and y be horizontal coordinates and z is vertical coordinate. Mass conservation of the suspended load takes the form:

$$\frac{\partial c}{\partial t} + u\frac{\partial c}{\partial x} + v\frac{\partial c}{\partial y} + (w - w_s)\frac{\partial c}{\partial z} = \frac{\partial}{\partial x}\left(\epsilon_{xs}\frac{\partial c}{\partial x}\right) + \frac{\partial}{\partial y}\left(\epsilon_{ys}\frac{\partial c}{\partial y}\right) + \frac{\partial}{\partial z}\left(\epsilon_{zs}\frac{\partial c}{\partial z}\right) \quad , \tag{1}$$

where u and v are horizontal velocities and w denotes a vertical component of flow velocity. Parameters ϵ_{xs}, ϵ_{ys}, and ϵ_{zs} denote the diffusion coefficients along the x, y, and z axes. Assuming the equilibrium condition where $\partial/\partial t, \partial/\partial x, \partial/\partial y, \partial/\partial z = 0$ and $w = 0$, the Equation 1 can be cast in the respective form:

$$\frac{\partial}{\partial z}\left(\epsilon_{zs}\frac{\partial c}{\partial z}\right) + w_s\frac{\partial c}{\partial z} = 0 \quad . \tag{2}$$

Assuming the equillibrium condition where total vertical flux of suspended sediment is zero at any horizon, the Equation 2 yields the relation:

$$\epsilon_{zs}\frac{\partial c}{\partial z} + w_s C = 0 \quad . \tag{3}$$

At this equilibrium condition, the downward flux of suspended sediment $w_s c_a$ is balanced with the upward sediment flux (i.e. entrainment rate), where c_a is the concentration at the near-bed reference level $z = a$ and w_s is the settling velocity. Thus, the following relation is assumed at the equilibrium condition:

$$w_s c_a = -\epsilon_{zs}\left.\frac{\partial c}{\partial z}\right|_{z=a} = w_s E_s \quad , \tag{4}$$

where E_s is the dimensionless entrainment rate of suspended sediment (i.e., upward flux of sediment devided by the settling velocity w_s) at the reference level $z = a$. The height of the reference level a can be chosen arbitrarily, and most of researchers evaluated $w_s c_a = E$ at the distance at 5% of the flow height (i.e. $a = 0.05h$).

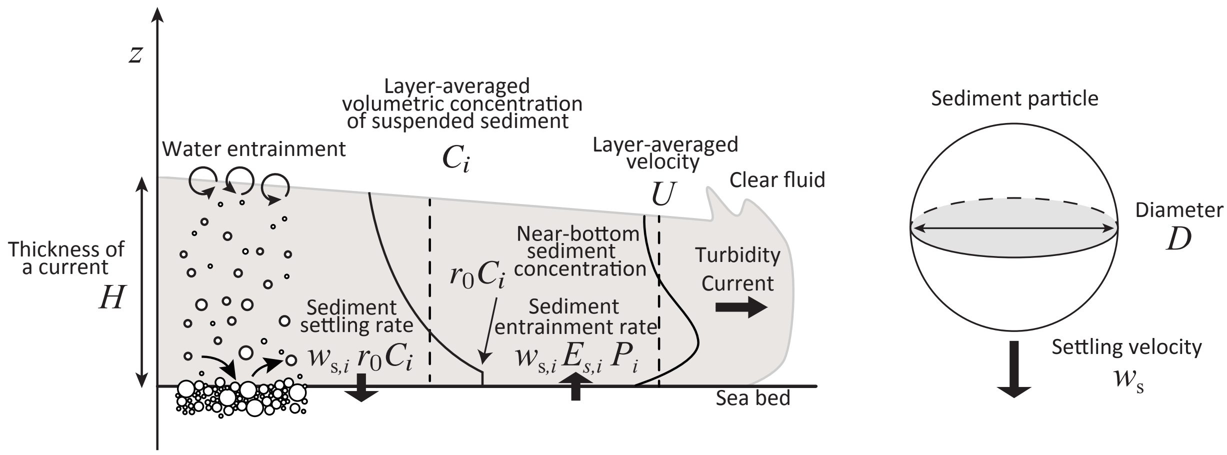

Fig. 2: The schematic figure of parameters related to the transport process of suspended load. C_i denotes the layer-averaged volumetric concentration of particles in the ith size range, and the coefficient r_0 denotes the ratio of near-bottom concentration to the layer-averaged sediment concentration. D and w_s denotes diameter and settling velocity of a sediment particle, respectively. U is the layer-averaged flow velocity, and P_i is the volumetric fraction of the ith grain-size class sediment in the active layer on the bed. H is the flow height.

With these two boundary conditions, the Equation 2 can be integrated in the z-direction to yield the following relation:

$$\frac{c}{c_a} = \exp\left\{\int_a^z -\frac{w_s}{\epsilon_{zs}} dz\right\} \quad . \tag{5}$$

With regard to diffusion coefficient ϵ_{zs}, Rouse (1937) assumed that it is proportional to the eddy viscosity of the fluid ϵ. This relation is thus given by:

$$\epsilon_{zx} = \beta\epsilon = \beta\kappa u_* z(1 - z/h) \quad , \tag{6}$$

where u_* and κ denotes shear velocity and von Karman constant, and H denotes flow thickness. The parameter β denotes an empirical coefficient that takes a value ranging 1.0–1.2. From the Equation 5 and 6, the following relation is obtained:

$$\frac{c}{c_a} = \left(\frac{h - z}{z}\frac{a}{h - a}\right)^Z, \quad Z = \frac{w_s}{\beta\kappa u_*} \quad , \tag{7}$$

where Z is a dimensionless variable called as the Rouse number.

Although this classic theory described above provides the relative distribution of suspended sediment concentration at the equilibrium condition, the near-bed entrainment rate $E_s = c_a$ is required to calculate the absolute values of concentration profile. Thus, the extensive amounts of studies, which are described later, have been conducted to obtain the function for predicting the entrainment rate E_s.

2.2 Governing variables for entrainment rate of suspended load

Models to predict entrainment rates of suspension generally adopt input variables such as flow shear velocity, depth, and sediment properties including density, diameter and/or settling velocity of particles. Lawler, Parker, Anderson, and Fitzsimmons (1977) suggested that the functional relationship of the entrainment rate of the uniform sediment as follows:

$$E_s = f(u_*, w_s, H, D_s, g, \nu, R) \quad , \tag{8}$$

where H denotes the thickness of the current, D_s denotes the geometric diameter of representative sediment grains. The parameter g denotes the gravity acceleration, and ν denotes the kinematic viscosity. $R = (\rho_s - \rho_f)/\rho_f$ denotes the submerged specific density of particles (ρ_s and ρ_f are density of sediment and fluid, respectively) (Figure 2).

Among these variables describing hydraulic and sediment properties of transporting flows, shear velocity has been regarded as one of the most influential variable for entrainment rates of suspended load because it is directly related to the fluid forces supporting suspended load in the flow. The rate of work for supporting suspended load is $g\rho_f RCHw_\mathrm{s}$ (Bagnold, 1966) where C denotes the layer-averaged flow concentration defined as:

$$C = \frac{1}{H}\int_0^H c dz \quad . \tag{9}$$

On the other hand, suspended load is supported by turbulence in the flow, and thus it is expected that the flow power to maintain suspension is correlated to the production rate of turbulent kinetic energy (TKE). The depth-averaged production rate of TKE is proportional to the shear velocity cubed, and thus the following relation can be assumed at the equilibrium condition (Bagnold, 1966; Dorrell, Amy, Peakall, & McCaffrey, 2018):

$$(\rho_s - \rho_f)CHw_\mathrm{s} = \alpha\rho_f u_*^3 \quad , \tag{10}$$

where α is the coefficient indicating the efficiency of the flow to support suspension. This coefficient α is often considered the constant for simplicity.

Instead of the shear velocity, however, Dorrell et al. (2018) proposed to use the competence shear velocity $u_{*\mathrm{i}}$, which is equivalent to the transport stage parameter proposed by van Rijn (1984), for considering the available flow power above that required for incipient particle motion. Here the term competence indicates the maximum particle size that can be transported by a flow, and therefore the entrainment rate must be zero when the shear velocity u_* is below the critical shear velocity $u_{*\mathrm{ci}}$ for incipient motion of the particle. Thus, the competence shear velocity is defined as:

$$u_{*\mathrm{i}} = \max\left(\sqrt{u_*^2 - u_{*\mathrm{ci}}^2}, 0\right) \quad . \tag{11}$$

The critical shear velocity of individual particle incipient motion $u_{*\mathrm{ci}}$ can be calculated under the following relationships suggested by Soulsby (1997):

$$u_{*\mathrm{ci}} = \sqrt{\tau_\mathrm{c} R\, g\, D_s} \quad , \tag{12}$$

$$\tau_\mathrm{c} = \frac{0.3}{1 + 1.2D_*} + 0.055\left\{1 - \exp(-0.02D_*)\right\} \quad , \tag{13}$$

$$D_* = D_s \left(\frac{g}{\nu^2} R\right)^{1/3} = R_{\mathrm{p}}^{2/3} \quad , \tag{14}$$

where τ_{c} is critical Shields number of the particle, D_* is dimensionless grain diameter of the particle, and ν is the kinematic viscosity of water. $R_{\mathrm{p}} = (Rg)^{0.5} D_s^{1.5}/\nu$ is the particle Reynolds number that is equivalent to the dimensionless grain diameter.

2.3 Entrainment functions proposed in previous studies

Considering the mechanical relation and the competence of the flow described above, several research proposed the entrainment functions using the competence shear velocity cubed (van Rijn, 1984; Dorrell et al., 2018).

van Rijn (1984, 2007) proposed the entrainment function based on the transport of all sediment as a bed-load transport and suspended load transport. This study applied the critical shear velocity $u_{*\mathrm{ci}}$ instead of critical boundary shear stress τ_{c} and provided an empirical relationship between $u_{*\mathrm{ci}}$ and w_{s}. The latest study of van Rijn (2007) suggested that the entrainment rate of sediment is saturated with the max value of 5%.

The best fitness between measured and computed data of dimensionless sediment entrainment rate was resulted in:

$$E_s = 0.015 \frac{D_{50}}{a} \frac{T^{1.5}}{D_*^{0.3}} \tag{15}$$

with the reference level at $a = 0.5\Delta$ (bed-form height) or $a = k_s$ (equivalent roughness height), and $a_{\min} = 0.01H$.

The variables in the function are defined as:

$$T = \frac{u_*^2 - u_{*\mathrm{c}}^2}{u_{*\mathrm{c}}^2} \quad , \tag{16}$$

$$D_* = D_{50} \left(\frac{Rg}{\nu^2}\right)^{1/3} \quad . \tag{17}$$

The function was revised in van Rijn (2007) as the following relationship:

$$E_s = 0.015 \left(1 - p_{\mathrm{clay}}\right) f_{\mathrm{silt}} \frac{D_{50}}{a} \frac{T^{1.5}}{D_*^{0.3}} \tag{18}$$

and $E_s < 0.05$ where the silt factor $f_{\mathrm{silt}} = d_{\mathrm{sand}}/d_{50}$, and if $d_{50} > d_{\mathrm{sand}} = 62\,\mu\mathrm{m}$, then $f_{\mathrm{silt}} = 1$. In the sheet flow condition, the reference level $a = 20\,d_{50}$.

On the other hand, Dorrell et al. (2018) proposed a new entrainment function based on the flow power and flux balance, assuming that the suspended load does not strongly stratified. The proposed relation takes the form:

$$E_s = \alpha \frac{u_{*\mathrm{i}}^3}{gHR\, w_\mathrm{s}} \quad , \tag{19}$$

where α is a coefficient = 4.9 and 13.2 for the particle grain-size distribution in uniform and non-uniform type, respectively.

Also, the research of Eggenhuisen, Cartigny, and de Leeuw (2017) introduced a dimensionless suspension capacity formulation by comparing the gravity forces and the vertical turbulent forces of near-bed suspended particles using the peak value of turbulent intensity. The most characteristic statement in this research was that particle size has no first order effect on suspension capacity with relative smaller grains $< 250\,\mu$m. However, the model of Eggenhuisen et al. (2017) can only be applied to the interval from $z^+ = [5, 90]$, where $z^+ = zu_*/\nu$ and thus their model is difficult to compare with other models.

In contrast to the models described above, other models employed the shear velocity with the arbitrary exponents as the input variable (e.g. Garcia & Parker, 1991), despite the theoretical consideration on force balances and flow competence. This could be justified because the efficiency coefficient α in the force balance model (Equation 10) can be not the constant but the function of other variables. Also, the entrainment rate at the specific level in water column can be largely different from the layer-averaged concentration due to the stratification of suspended load.

For example, Garcia and Parker (1991) employed purely empirical approach to estimate the entrainment rate at the level of 5% of the flow height. They compiled previous experimental and observational data in equilibrium or quasi-equilibrium conditions to obtain a new empirical function. Their research suggested that the u_*/w_s and R_p are primary parameters for estimating entrainment rate for uniform sediment.

First, they fitted a curve between c_a and $(u_*/w_\mathrm{s})^1(R_\mathrm{p})^{n_1}$, where n_1 is a coefficient at $0 < n_1 < 1$ to fit the observation of c_a, with a result at $n_1 = 0.6$. Then the coefficient of $((u_*/w_\mathrm{s})(R_\mathrm{p})^{0.6})^{n_2}$ was computed to fit the observation with a result of $n_2 = 5$. After that, the artificial saturation value of entrainement rate was set to the value of 30%, otherwise it may be too high concentration to consider as a suspension (Engelund & Fredsøe, 1976).

The dimensionless sediment entrainment rate E_s proposed by Garcia and Parker (1991) was in the following relationship:

$$E_s = \frac{A\,Z_u^5}{1 + \frac{A}{0.3} Z_u^5} \tag{20}$$

with the reference level $a = 0.05H$, where

$$Z_u = \frac{u_*}{w_\mathrm{s}} R_\mathrm{p}^{0.6} \tag{21}$$

and A is a constant coefficient with value of 1.3×10^{-7}.

Equation 20 was extended for non-uniform sediment as the following relationship (Garcia & Parker, 1991):

$$E_{s,i} = \frac{A\,(\lambda Z_i)^5}{1 + \frac{A}{0.3} (\lambda Z_i)^5} \quad , \tag{22}$$

$$Z_i = \frac{u_*}{w_{\mathrm{s}i}} R_{\mathrm{p}i}^{0.6} \left(\frac{D_i}{D_{50}}\right)^m \quad , \tag{23}$$

where λ denotes a coefficient related to the grain-size deviation of sediment particles, $m = 0.2$ denotes an exponent parameterized to describe the "hiding effect", which represents the mobility under reciprocal action of different size grains.

In lagre scale and low slope rivers, it was suggested by Wright and Parker (2004a, 2004b) that the entrainment rate decreases because the flow turbulence can be suppressed by the density stratification effect. In this situation, Wright and Parker (2004a) proposed the following modification to the model of Garcia and Parker (1991):

$$E_{s,i} = \frac{B\,(\lambda Z_i)^5}{1 + \frac{B}{0.3} (\lambda Z_i)^5} \quad , \tag{24}$$

$$Z_i = \frac{u_*}{w_{\mathrm{s}i}} R_{\mathrm{p}i}^{0.6}\, S^{\,0.08} \left(\frac{D_i}{D_{50}}\right)^m \quad , \tag{25}$$

where B is a constant coefficient with value of 7.8×10^{-7}, S denotes the bed-slope.

Elhakeem and Sattar (2015) also represented a purely empirical model to estimate the entrainment rates of non-uniform sediment by using gene expression programming. This model uses four parameters, namely, Shields stress, critical Shields stress, a coefficient to describe the grain size distribution and dimensionless relative grain size. The dimensionless entrainment rate in mix-size grains condition based on the dimensionless sediment mixture term $\sqrt{R\,g\,D_i}$ was proposed as following relationship:

$$E_{s,i} = (0.024 + 0.021 e^{-132(0.245-c_u)^2})\, d_{*i}^{-0.5}\, (\tau_{*\mathrm{g}} - \tau_{*\mathrm{cg}})^2 \quad , \tag{26}$$

where $d_{*i} = D_i / D_{50}$, $\tau_{*\mathrm{g}}$ is the Shields stress of D_{50}, $\tau_{*\mathrm{cg}}$ is the critical Shields stress of D_{50}, c_u is the Kramer coefficient of uniformity defined as:

$$c_u = \frac{\sum_0^{50} P_i\, d_i}{\sum_0^{100} P_i\, d_i} \quad . \tag{27}$$

The proposed model provided satisfactorily prediction with a deviation less than 25% between the measured and predicted values. However, in this research, the sediment transport rate was calculated by the moving velocity of dunes. As a result, the calculated sediment flux should contain not only suspended load, but also bedload. Therefore, it seems difficult to employ their model as the estimator of suspended load.

2.4 Problems in existing functions

Even though numerous research have been conducted for obtaining the entrainment function, the proposed formulation of entrainment rate have several unsolved matters. For example, the selections of exponent on the dimensionless shear velocity u_* / w_s or $u_{*\mathrm{i}} / w_\mathrm{s}$ vary largely depending on research. The exponent was set at 10 (Akiyama & Fukushima, 1985), 7 (Parker, Garcia, Fukushima, & Yu, 1987), 5 (Garcia & Parker, 1991), 4 (Izumi, Tanaka, Tsuboi, & Date, 2003) and 3 (Dorrell et al., 2018). Theoretical analyses seem to support values close to the cube law, whereas empirical verification is needed to prove it.

Another unsolved matter is the necessity of the artificial saturation value for the entrainment rate. Turbulence is required for sustaining suspended load, so that the extremely large concentration at equilibrium condition (i.e. entrainment rate) is unlikely even for very high-velocity flows because very high concentration of suspended load eliminates turbulent eddies by density stratification and friction/collisions of grains (e.g. Cantero et al., 2012). Therefore, the artificial threshold value of 0.3 to regulate entrainment rates was used in the formulation proposed by Garcia and Parker (1991), and van Rijn (2007) employed 0.05 for the maximum entrainment rate. However, these values lack measured evidences both in experimental or observational datasets.

This artificial threshold value in entrainment rate affects on the expansion of the entrainment function for the mixed-size (non-uniform) sediment. The threshold value should be applied to the total concentration of suspended load, while the entrainment function for multiple grain-size class (e.g. Garcia & Parker, 1991) can reach the maximum value even though the total concentration is still low. This is a logically incorrect application of the entrainment function for uniform sediment, so that the appropriate formulation is required in a new formulation of the entrainment rate of suspended load.

Finally, it should be noted that difference in entrainment rate of suspension between open channel flows and density flows has been rarely discussed in previous studies. Most of the empirical entrainment functions were proposed based on data sets pertaining to open channel flows, and those functions have been applied to density flows without any corrections (Garcia & Parker, 1993). However, the vertical velocity profiles of flows is largely different between two types of flows. In case of open channel flows, flow velocity increases upward following the log law, while the flow velocity becomes maximum at the middle of flows in case of density currents. Therefore, the definition of the flow height may be different between open channle and density flows. This implies that the reference level (at $0.05H$) of density flows may not correspond to that of open channel flows. In addition, it is known that the entrainment of ambient water influences to the pattern of concentration profile of suspended sediment in case of density currents.

3 Methodology for flume experiment

3.1 Experimental settings

The experiments reported in this study were conducted in an acrylic flume of 4 m long, 0.12 m wide and 0.5 m deep that was submerged in the tank (5.5 m long, 2.5 m wide and 1.8 m deep; Figure 3). The bed slope of the submerged flume was adjustable. The tank and flume was initially filled with fresh water before experiments. The diffuser from which the flow was injected was set at the upstream end of the flume, and the head tank with two mixing tanks was connected to the diffuser (Figure 3). Sediment was mixed in the two mixing tanks, and the mixture of sediment and water was pumped to the head tank. The opening of the valve from the head tank to the flume controlled the flow discharge. Water level in the head tank was maintained at the constant level to keep the flow discharge constant during experiments. In addition, the damping tank was located at the downstream end of the flume to prevent reflection of the flow (Figure 3). A supply of fresh water from the top of the damping tank in conjunction with an overflow device guaranteed the maintenance of a constant level of fresh water in the tank.

Two types of sediments were used for experiments: lightweight plastic particles with a specific gravity of 1.45, and siliciclastic sand grains dyed in blue color with a specific gravity of 2.65. Lightweight plastic particles were used in order to reproduce suspension in a relatively small scale. The plastic particles were 3ϕ in geometric mean diameter, and were 0.60 in standard deviation σ on ϕ-scale. The corresponding values for siliciclastic sand were 2ϕ and 0.40 respectively (Figure 4).

Two different types of experiments of density currents were conducted, which were (1) uniform sediment mixture used only plastic particles, (2) non-uniform sediment mixture used both plastic particles and natural sand grains. Also, a straight bed with the slope fixed in a range of 5% to 12% was used in the experiments (Figure 3).

The values of sediment concentration in the mixing tanks range from 0.3% to 6.6% (Table 1). The concentration in the mixing tanks of most experiments ranges from 0.5% to 4%, for which the experimental density flows were capable for transporting sediment.

The proportion of plastic particles and natural siliciclastic sand was varied from 1:9 to 9:1, which provide data set for multiple conditions of bed material, and may reflect “hiding effect” under different environment.

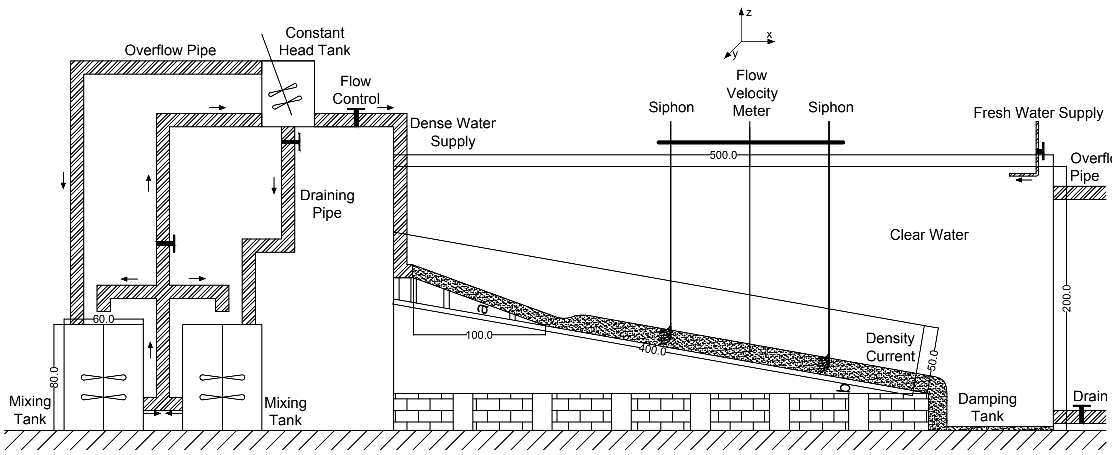

Fig. 3: Schematic diagram showing the experimental flume and sediment mixing tanks. Bed-slope **b** which vary from 5% –12% was used in series of experiments, the small slope **a** at the upstream which fixed at 10% can be put in or brought out from the flume.

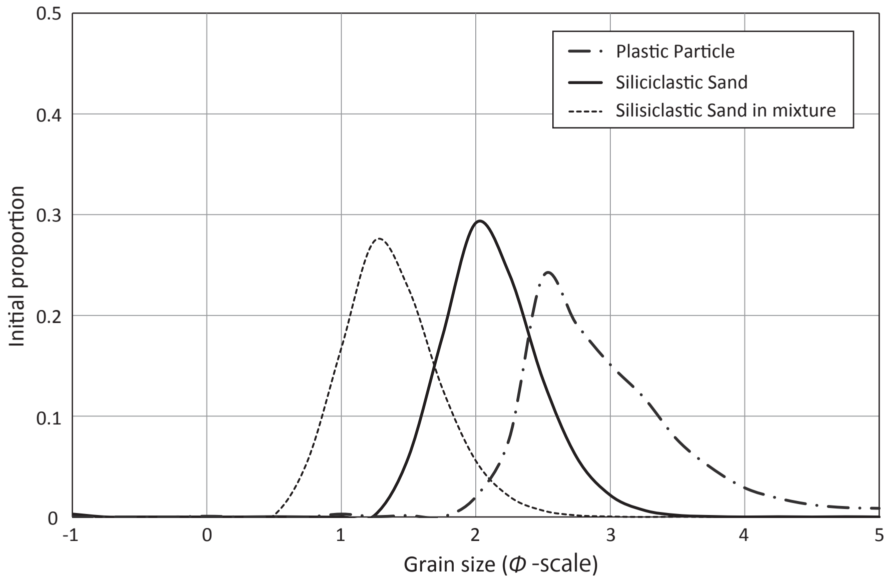

Fig. 4: Grain-size distribution of two types of sediment particles used in experiments. The right curve (chane line) shows the grain-size distribution of plastic particles which measured follow the Gibbs' settling velocity under density of 1.45 g/cm^3. The central curve (solid line) shows the grain-size distribution of siliciclastic sand measured under same method with density of 2.65 g/cm^3. The left curve (dashed line) shows the grain-size distribution of siliciclastic sand in sediment mixture which measured under density of 1.45 g/cm^3, because the software STube can only be set up at only one density value.

Table 1: The conditions conducted and measured in the experiments. The notation Sand (%) and Plastic (%) shows the initial proportion of sediment mixture preparation in mixing tanks. Tank C_p (%) and Tank C_m (%) are the initial total concentration of sediment mixture from preparation of sediment weight and measurement of actual tank mixture.

Run	Particle	Slope (%)	Sand (%)	Plastic (%)	Tank C_p(%)	Tank C_m(%)	Flow C(%)	T (℃)	U (m/s)	H (m)
1	Nonuniform	5	50%	50%	5.0	4.3	1.20	21	0.23	0.22
2	Nonuniform	5	50%	50%	5.0	4.0	0.70	9.3	0.20	0.20
3	Nonuniform	10	10%	90%	3.5	3.2	0.63	21	0.15	0.25
4	Nonuniform	10	90%	10%	8.0	6.6	0.18	22	0.19	0.25
5	Uniform	10	–	100%	2.0	1.7	0.45	16	0.28	0.35
6	Uniform	10	–	100%	0.5	0.3	0.04	12	0.16	0.13
7	Uniform	10	–	100%	0.5	0.3	0.03	12	0.16	0.13
8	Uniform	10	–	100%	1.0	0.8	0.08	12	0.19	0.18
9	Uniform	10	–	100%	1.0	0.8	0.05	12	0.19	0.18
10	Uniform	10	–	100%	1.0	1.0	0.12	16	0.19	0.20
11	Uniform	10	–	100%	1.0	1.0	0.06	16	0.19	0.20
12	Nonuniform	10	50%	50%	3.0	2.9	0.39	14	0.17	0.14
13	Nonuniform	10	50%	50%	3.0	2.9	0.38	14	0.17	0.14
14	Nonuniform	10	50%	50%	3.0	2.7	0.36	20	0.12	0.18
15	Nonuniform	10	50%	50%	3.0	2.7	0.36	20	0.12	0.18
16	Nonuniform	12	33%	66%	3.0	2.0	0.29	13	0.11	0.11
17	Nonuniform	12	66%	33%	6.0	5.2	0.38	9.5	0.19	0.15

3.2 Measurements of flow properties during experiments

In order to measure the flow velocity and suspension concentration, the acoustic Doppler velocity profiler (ADVP; Nortek Vectrino Profiler) and two vertical arrays of siphon tubes were set at arms of actuators which can be moved both horizontally and vertically. The ADVP can measure the vertical profile of three dimensional components of flow velocity in a range of 4–7 cm from the probe. For keeping the elevation of ADVP to be able to measure the near-bed velocity profile, the actuator was operated during the experiments in progress.

Two series of siphon tubes were used to obtain samples of suspension loads at different depth in the flow. The first array of siphon tubes took samples from 0 to 9 cm above the bed with 1 cm interval, and the second array of siphons took samples at unequally spaced interval that was positioned at 0, 1.25, 2.5, 3.75, 5, 7.5, 10, 12.5, 15, 17.5, 20 and 25 cm above bed (Figure 5). The siphon mouths were made of aluminum tubes with 8 mm external diameter and 5 mm internal diameter. The collected samples by siphons were weighed and dried to measure the concentration of suspended sediment. These samples were used to determine vertical profiles of concentration of suspended sediment. The sampling was conducted only when the flow reached the quasi-equilibrium state. The simple way to confirm the quasi-equilibrium condition during the experiment is the observed development of bed thickness and flow properties (velocity, flow thickness and concentration by observation). The accurate method to determine the quasi-equilibrium condition need to confirm that the measured data (velocity and concentration) in different distance from flume inlet is stable.

All the experiments were recorded by single-lens reflex cameras, in order to observe the flow thickness. The temperature of the fresh water in both the flume and the mixing tank were measured before each experiment. The water in the flume was carefully removed to avoid the deformation of bedform after each experiment, and the bed sediment was sampled to analyze its grain-size distribution. Sampling of bed sediment was started at the peak elevation of bed at the upstream region, then the bed sediment along flow direction was sampled by every 20 cm interval.

3.3 Grain-size analysis and calculation of concentration profiles

The grain size distributions of suspension sediment and bed sediment were measured by the 1.8 m long settling-tube grain-size analyzer using the software STube (Naruse, 2005).

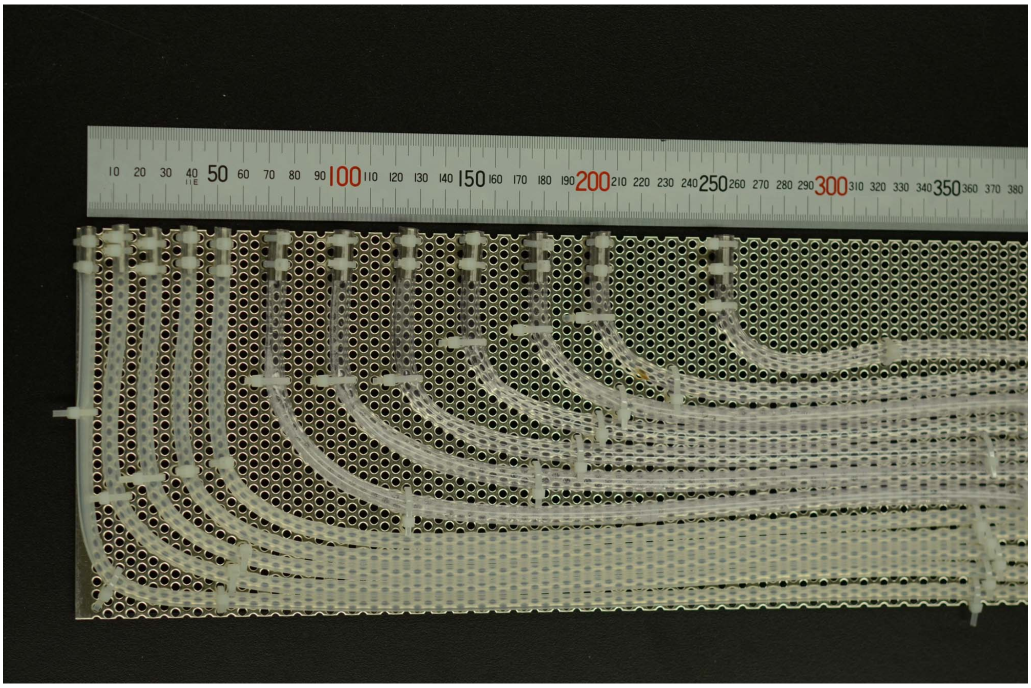

Fig. 5: Photograph showing a series of siphons used in experiments for measuring sediment concentration.

The particle settling velocity was calculated by Gibbs' settling velocity method (Gibbs, 1974). In this study, the grain-size distribution was discretized into 5 classes from 0 to 5 ϕ for every 1 ϕ. The proportion of grain-size class of bed material was used to obtain the parameter P_i. Figure 6 shows difference of the grain-size distribution between bed sediment and suspension at lower region of flow.

The weight concentration of suspension was initially measured from the weight of sampled mixture and dried sediment, and then volume concentration of suspension was calculated. Products of total sediment concentration and fraction of each grain-size class yielded the concentration profile of suspension of each grain-size class (Figure 7). Also, the standard deviation of grain-size distribution of the bed samples was calculated.

Then, the concentration of each grain-size class at the reference level ($z = 0.05H$) was calculated. It has been known that the vertical distribution of the sediment concentration in a suspended load above a reference level can be approximated by the logarithmic curve (Sequeiros et al., 2010). Therefore, the logarithmic curve was fit to the vertical concentration profile measured in the lower regime (from bed to $0.2H$) of the flow, and the concentration at the reference level was calculated from the fit curve.

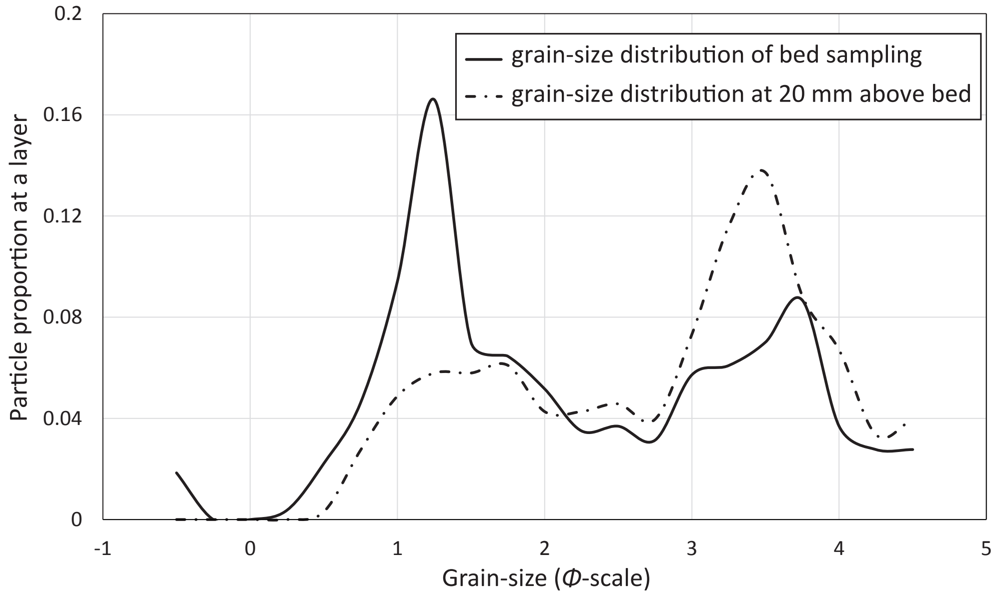

Fig. 6: Example of grain-size distributions measured at bed and at the level h = 20 mm.

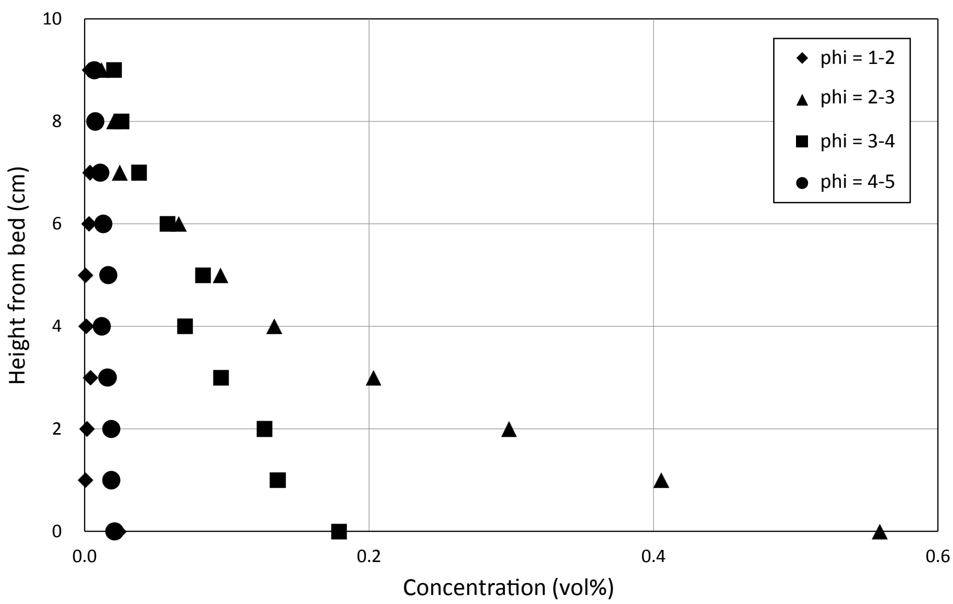

Fig. 7: Example of vertical concentration profiles of each grain-size class measured in experiments using non-uniform sediment. Each point shows the individual concentration of one class range of grain-size at a certain layer.

3.4 Calculation of layer averaged flow properties and shear velocity

In the steady condition of flows, the layer-average flow velocity U and layer-average volume sediment concentration C and flow thickness H are defined in the following relationship (Garcia & Parker, 1993):

$$UH = \int_a^\infty u_z \, dz \quad , \tag{28}$$

$$UCH = \int_a^\infty u_z c_z \, dz \quad . \tag{29}$$

Also, the simplest relationship of C was proposed as (Parker et al., 1987):

$$C = \frac{c_a}{2} \quad . \tag{30}$$

The flow shear velocity was calculated from the velocity profile measured by ADVP. First, the direction of flow velocity was rotated from horizontal coordinate to streamwise coordinate. Then, the shear velocity was computed from:

$$\frac{u}{u_*} = \frac{1}{\kappa} \ln \left(\frac{z}{k_s} \right) + B_s \left(\frac{u_* k_s}{\nu} \right) \quad , \tag{31}$$

where k_s is the effective bed roughness height. In the assumption that the flow is hydraulically rough, the relationship between velocity and distance from bed is represented as:

$$\frac{u}{u_*} = \frac{1}{\kappa} \ln \left(\frac{z}{z_0} \right) \quad , \tag{32}$$

where empirically $z_0 = k_s/30$ is well known, the equation changes to:

$$\frac{u}{u_*} = \frac{1}{\kappa} \ln \left(30 \frac{z}{k_s} \right) \quad , \tag{33}$$

and B_s was computed as:

$$\text{for } (u_* k_s/\nu) > 70, \; B_s = 8.5 \quad , \tag{34}$$

$$\text{for } (u_* k_s/\nu) < 5, \; B_s = 5.5 + \frac{1}{\kappa} \ln \left(\frac{u_* k_s}{\nu} \right) \quad . \tag{35}$$

3.5 Estimation of entrainment rate

The entrainment rate E_s was estimated from the two values of near-bed concentration measured at siphon arrays set at the upstream and downstream locations. As described in the previous section, the entrainment rate matches with near-bed concentration when the flow reaches the equilibrium conditions in time and space; however, spatial equilibrium is almost impossible to achieve in the small-scale flume experiments. Therefore, this study employs the method proposed by Garcia and Parker (1993) to estimate the entrainment rates of basal materials using the following relationship:

$$E_s = \frac{UCH|_{up} - UCH|_{down}}{w_s \Delta x} + \frac{1}{2}\left(c_a|_{up} + c_a|_{down}\right) = c_{ae} \quad , \tag{36}$$

where Δx denotes the distance between locations where two arrays of siphons were set, c_{ae} denotes the near-bed concentration under equilibrium condition. Equation 36 assumes that the decrease in sediment discharge between the upstream and downstream locations indicate the difference between the settling flux and the entrainment rate, and the settling flux can be quantified by products of near-bed concentration and the particle settling velocity.

4 Methodology for data processing

4.1 Data processing of previous studies

The previous research data of entrainment rates of suspension which include both open channel flows and density flows were processed for statistical analysis in this study. The datasets used in this study were obtained from literatures of Kalinske and Pien (1943), Ismail (1952), Brooks (1954), Barton and Lin (1955), Colby and Hembree (1955), Straub, Anderson, and Flammer (1958), Vanoni and Nomicos (1960), Nordin and Dempster (1963), Ashida and Michiue (1964), Coleman (1969), Coleman (1981), Ashida and Okabe (1982), Lyn (1987), Garcia and Parker (1993) and Graf and Cellino (2002) (from Table 2 to Table 3). Most of the data were preliminary processed to indicate the concentrations (and thus entrainment rates) at the reference level $a = 0.05H$ by Garcia and Parker (1991). The near-bed concentration described in Graf and Cellino (2002) was calculated to show the value of volume concentration at the reference level ($a = 0.05H$). The datasets that lack important parameters such as the flow thickness (Jordan, 1965; Sequeiros et al., 2010), dimensionless shear velocity (Montes & Ippen, 1973), the height of the reference level (or the reference level can not be expressed as a fraction of flow thickness) (Cartigny, Eggenhuisen, Hansen, & Postma, 2013; Hubbell & Matejka, 1959; Smith & McLean, 1977; Toffaleti, 1968) were not used in this study. In addition, extremely high concentration that was difficult to judge if it is at near-equilibrium conditions (Einstein, 1955) were excluded in the analysis.

The dataset without temperature data was considered under 20°C, and the kinematic viscosity was in the value of 9.55×10^{-7} m^2/s. The settling velocity of sediment particles in dataset was recalculated using Furguson method (Ferguson & Church, 2004), because the settling velocities calculated using different functions of settling velocity of particles may cause aritificial influence on statistical analysis. In turbidity current dataset, energy slope were calculated from the relationship as $S_e = u_*^2/RCgH$, and here layer-average concentration C was calculated by $C = c_a/2$.

Several data in previous studies were excluded from statistical analysis in this study because of errors in original description. For example, several data in non-uniform experiment show the fraction of the ith grain-size class in the bed $P_i > 1$, which is regarded as a mistake. In some experiments, suspension was observed at the condition $u_* < u_{*ci}$. These dataset was excluded from the whole dataset for multiple regression.

Table 2: The dataset of parameters used to predict entrainment rates of uniform grain-size particles in previous research.

Reference	D_s	R_p	R	S	H	c_{ae}	S_e	R_f	u_*	u_{*ci}	u_{*i}	w_s
Ashida & Michiue (1964)	0.00016	8.14	1.65	0.0040	0.04	0.0040	0.0031	0.31	0.0356	0.0120	0.0335	0.0156
	0.00016	8.14	1.65	0.0023	0.07	0.0038	0.0017	0.31	0.0341	0.0120	0.0319	0.0156
Ashida & Okabe (1982)	0.00017	8.50	1.65	0.0031	0.05	0.0003	0.0013	0.33	0.0246	0.0122	0.0213	0.0172
	0.00017	8.50	1.65	0.0031	0.04	0.0004	0.0012	0.33	0.0224	0.0122	0.0188	0.0172
Barton & Lin (195)	0.00018	10.62	1.65	0.0012	0.15	0.0009	0.0004	0.35	0.0233	0.0120	0.0200	0.0188
	0.00018	10.62	1.65	0.0008	0.22	0.0004	0.0002	0.35	0.0229	0.0120	0.0195	0.0188
	0.00018	10.62	1.65	0.0007	0.42	0.0004	0.0001	0.35	0.0245	0.0120	0.0214	0.0188
	0.00018	10.62	1.65	0.0006	0.31	0.0005	0.0002	0.35	0.0262	0.0120	0.0233	0.0188
	0.00018	10.62	1.65	0.0012	0.18	0.0035	0.0007	0.35	0.0362	0.0120	0.0342	0.0188
	0.00018	10.62	1.65	0.0013	0.21	0.0079	0.0007	0.35	0.0384	0.0120	0.0365	0.0188
	0.00018	10.62	1.65	0.0012	0.24	0.0038	0.0006	0.35	0.0386	0.0120	0.0367	0.0188
	0.00018	10.62	1.65	0.0016	0.21	0.0013	0.0008	0.35	0.0405	0.0120	0.0387	0.0188
	0.00018	10.62	1.65	0.0017	0.19	0.0018	0.0009	0.35	0.0414	0.0120	0.0396	0.0188
	0.00018	10.62	1.65	0.0018	0.20	0.0012	0.0010	0.35	0.0431	0.0120	0.0414	0.0188
	0.00018	10.62	1.65	0.0017	0.23	0.0150	0.0009	0.35	0.0445	0.0120	0.0429	0.0188
	0.00018	10.62	1.65	0.0017	0.23	0.0015	0.0009	0.35	0.0446	0.0120	0.0430	0.0188
	0.00018	10.62	1.65	0.0016	0.17	0.0043	0.0013	0.35	0.0470	0.0120	0.0455	0.0188
	0.00018	10.62	1.65	0.0021	0.16	0.0083	0.0018	0.35	0.0528	0.0120	0.0514	0.0188
Brooks (1954)	0.00015	9.49	1.65	0.0021	0.07	0.0065	0.0015	0.29	0.0326	0.0112	0.0306	0.0141
	0.00009	3.84	1.65	0.0023	0.07	0.0100	0.0016	0.15	0.0334	0.0107	0.0316	0.0059
	0.00009	3.86	1.65	0.0019	0.09	0.0080	0.0012	0.15	0.0313	0.0107	0.0294	0.0059
Coleman (1969)	0.00015	8.84	1.65	0.0016	0.12	0.0028	0.0012	0.29	0.0372	0.0114	0.0354	0.0141
	0.00015	8.84	1.65	0.0031	0.12	0.0057	0.0024	0.29	0.0540	0.0114	0.0528	0.0141
	0.00015	8.84	1.65	0.0052	0.12	0.0210	0.0041	0.29	0.0700	0.0114	0.0691	0.0141
	0.00015	8.84	1.65	0.0009	0.18	0.0009	0.0005	0.29	0.0305	0.0114	0.0283	0.0141
	0.00015	8.84	1.65	0.0012	0.18	0.0041	0.0008	0.29	0.0370	0.0114	0.0352	0.0141
	0.00015	8.84	1.65	0.0018	0.18	0.0094	0.0011	0.29	0.0451	0.0114	0.0436	0.0141
	0.00015	8.84	1.65	0.0007	0.24	0.0008	0.0003	0.29	0.0289	0.0114	0.0266	0.0141

Table 2: Continued 1.

Reference	D_s	R_p	R	S	H	c_{ae}	S_e	R_f	u_*	u_{*ci}	u_{*i}	w_s
Coleman (1969)	0.00015	8.84	1.65	0.0009	0.24	0.0026	0.0004	0.29	0.0318	0.0114	0.0297	0.0141
	0.00021	14.92	1.65	0.0014	0.12	0.0017	0.0009	0.41	0.0330	0.0120	0.0307	0.0236
	0.00021	14.92	1.65	0.0042	0.12	0.0066	0.0032	0.41	0.0648	0.0120	0.0637	0.0236
	0.00021	14.92	1.65	0.0042	0.12	0.0200	0.0032	0.41	0.0618	0.0120	0.0606	0.0236
	0.00021	14.92	1.65	0.0008	0.18	0.0006	0.0004	0.41	0.0280	0.0120	0.0253	0.0236
	0.00021	14.92	1.65	0.0014	0.18	0.0034	0.0010	0.41	0.0424	0.0120	0.0407	0.0236
	0.00021	14.92	1.65	0.0016	0.18	0.0050	0.0009	0.41	0.0400	0.0120	0.0382	0.0236
	0.00021	14.92	1.65	0.0007	0.24	0.0005	0.0003	0.41	0.0286	0.0120	0.0260	0.0236
	0.00021	14.92	1.65	0.0008	0.24	0.0019	0.0005	0.41	0.0338	0.0120	0.0316	0.0236
Coleman (1981)	0.00011	4.72	1.65	0.0020	0.17	0.0189	0.0009	0.20	0.0391	0.0113	0.0374	0.0084
	0.00021	13.36	1.65	0.0020	0.17	0.0096	0.0009	0.41	0.0396	0.0123	0.0376	0.0236
	0.00042	36.82	1.65	0.0022	0.17	0.0020	0.0010	0.68	0.0411	0.0147	0.0384	0.0564
Garcia & Parker (1993)	0.00010	1.23	0.35	0.0800	0.06	0.0010	1.1480	0.06	0.0105	0.0066	0.0082	0.0011
	0.00010	1.23	0.35	0.0800	0.05	0.0019	1.4416	0.06	0.0147	0.0066	0.0131	0.0011
	0.00010	1.23	0.35	0.0800	0.06	0.0010	1.2138	0.06	0.0107	0.0066	0.0084	0.0011
	0.00010	1.23	0.35	0.0800	0.06	0.0041	0.4006	0.06	0.0130	0.0066	0.0112	0.0011
	0.00010	1.23	0.35	0.0800	0.06	0.0026	0.3112	0.06	0.0092	0.0066	0.0064	0.0011
	0.00010	1.23	0.35	0.0800	0.05	0.0027	0.5797	0.06	0.0117	0.0066	0.0097	0.0011
	0.00010	1.23	0.35	0.0800	0.06	0.0021	0.4692	0.06	0.0099	0.0066	0.0074	0.0011
	0.00010	1.23	0.35	0.0800	0.05	0.0023	0.8701	0.06	0.0131	0.0066	0.0113	0.0011
	0.00018	2.98	0.35	0.0800	0.05	0.0030	0.5281	0.13	0.0120	0.0074	0.0095	0.0033
	0.00018	2.98	0.35	0.0800	0.05	0.0013	1.2918	0.13	0.0120	0.0074	0.0095	0.0033
	0.00018	2.98	0.35	0.0800	0.05	0.0018	0.9147	0.13	0.0120	0.0074	0.0095	0.0033
	0.00018	2.98	0.35	0.0800	0.06	0.0019	0.5702	0.13	0.0102	0.0074	0.0070	0.0033
	0.00018	2.98	0.35	0.0800	0.05	0.0021	1.0542	0.13	0.0135	0.0074	0.0113	0.0033
	0.00018	2.98	0.35	0.0800	0.06	0.0018	0.9439	0.13	0.0130	0.0074	0.0107	0.0033
	0.00018	2.98	0.35	0.0800	0.06	0.0043	0.3473	0.13	0.0125	0.0074	0.0101	0.0033
	0.00018	2.98	0.35	0.0800	0.06	0.0018	0.7521	0.13	0.0113	0.0074	0.0086	0.0033

Table 2: Continued 2.

Reference	D_s	R_p	R	S	H	c_{ae}	S_e	R_f	u_*	u_{*ci}	u_{*i}	w_s
Garcia & Parker (1993)	0.00018	2.98	0.35	0.0800	0.06	0.0031	0.3849	0.13	0.0108	0.0074	0.0079	0.0033
	0.00018	2.98	0.35	0.0800	0.06	0.0012	0.7039	0.13	0.0094	0.0074	0.0058	0.0033
Graf & Cellino (2002)	0.00014	6.31	1.65	0.0003	0.12	0.0093	0.0007	0.25	0.0280	0.0117	0.0254	0.0115
	0.00014	6.48	1.65	0.0005	0.12	0.0108	0.0010	0.25	0.0340	0.0116	0.0320	0.0117
	0.00014	6.31	1.65	0.0008	0.12	0.0119	0.0012	0.25	0.0370	0.0117	0.0351	0.0115
	0.00014	6.28	1.65	0.0013	0.12	0.0148	0.0013	0.24	0.0390	0.0117	0.0372	0.0114
	0.00014	6.29	1.65	0.0015	0.12	0.0136	0.0014	0.24	0.0400	0.0117	0.0383	0.0114
	0.00014	6.28	1.65	0.0018	0.12	0.0174	0.0016	0.24	0.0430	0.0117	0.0414	0.0114
	0.00014	6.28	1.65	0.0020	0.12	0.0186	0.0016	0.24	0.0440	0.0117	0.0424	0.0114
	0.00014	6.30	1.65	0.0015	0.12	0.0183	0.0017	0.24	0.0450	0.0117	0.0435	0.0114
	0.00014	6.29	1.65	0.0023	0.12	0.0192	0.0018	0.24	0.0460	0.0117	0.0445	0.0114
	0.00014	6.28	1.65	0.0025	0.12	0.0189	0.0020	0.24	0.0490	0.0117	0.0476	0.0114
	0.00014	6.30	1.65	0.0030	0.12	0.0236	0.0026	0.24	0.0550	0.0117	0.0537	0.0114
	0.00023	14.10	1.65	0.0010	0.12	0.0080	0.0013	0.43	0.0390	0.0127	0.0369	0.0262
	0.00023	13.84	1.65	0.0015	0.12	0.0106	0.0016	0.42	0.0440	0.0128	0.0421	0.0259
	0.00023	14.06	1.65	0.0018	0.12	0.0093	0.0016	0.43	0.0430	0.0127	0.0411	0.0262
	0.00023	14.15	1.65	0.0020	0.12	0.0088	0.0017	0.43	0.0450	0.0127	0.0432	0.0263
	0.00023	13.85	1.65	0.0023	0.12	0.0130	0.0019	0.43	0.0470	0.0128	0.0452	0.0259
	0.00023	13.89	1.65	0.0025	0.12	0.0128	0.0020	0.43	0.0480	0.0128	0.0463	0.0260
Ismail (1952)	0.00010	3.62	1.65	0.0028	0.04	0.0090	0.0019	0.18	0.0280	0.0114	0.0256	0.0071
	0.00010	3.94	1.65	0.0042	0.04	0.0226	0.0033	0.18	0.0334	0.0112	0.0315	0.0071
	0.00010	3.62	1.65	0.0059	0.03	0.0450	0.0046	0.18	0.0390	0.0114	0.0373	0.0071
	0.00010	3.90	1.65	0.0083	0.03	0.0377	0.0064	0.18	0.0447	0.0112	0.0433	0.0071
	0.00010	4.02	1.65	0.0115	0.03	0.0302	0.0103	0.18	0.0592	0.0112	0.0581	0.0071
	0.00010	3.98	1.65	0.0149	0.04	0.0253	0.0114	0.18	0.0639	0.0112	0.0629	0.0071

Table 2: Continued 3.

Reference	D_s	R_p	R	S	H	c_{ae}	S_e	R_f	u_*	u_{*ci}	u_{*i}	w_s
Kalinske & Pien (1943)	0.00018	10.62	1.65	0.0015	0.16	0.0021	0.0011	0.35	0.0416	0.0120	0.0398	0.0188
	0.00018	8.83	1.65	0.0040	0.19	0.0022	0.0015	0.35	0.0520	0.0125	0.0505	0.0188
Lyn (1987)	0.00015	7.45	1.65	0.0024	0.06	0.0047	0.0018	0.29	0.0335	0.0118	0.0313	0.0141
	0.00019	10.78	1.65	0.0025	0.07	0.0046	0.0018	0.37	0.0340	0.0123	0.0317	0.0204
	0.00024	15.41	1.65	0.0030	0.07	0.0039	0.0022	0.46	0.0372	0.0128	0.0349	0.0285
	0.00019	10.75	1.65	0.0030	0.06	0.0040	0.0022	0.37	0.0352	0.0123	0.0330	0.0204
Straub et al. (1958)	0.00016	9.51	1.65	0.0024	0.07	0.0007	0.0012	0.31	0.0302	0.0116	0.0279	0.0156
	0.00016	8.45	1.65	0.0026	0.07	0.0018	0.0014	0.31	0.0312	0.0119	0.0288	0.0156
	0.00016	7.15	1.65	0.0028	0.07	0.0021	0.0015	0.31	0.0323	0.0123	0.0298	0.0156
	0.00016	6.11	1.65	0.0032	0.07	0.0027	0.0016	0.31	0.0332	0.0128	0.0306	0.0156
	0.00016	5.23	1.65	0.0033	0.07	0.0038	0.0017	0.31	0.0342	0.0133	0.0315	0.0156
	0.00016	4.60	1.65	0.0036	0.07	0.0040	0.0019	0.31	0.0352	0.0137	0.0324	0.0156
Vanoni & Nomicos (1960)	0.00011	4.82	1.65	0.0025	0.09	0.0057	0.0005	0.20	0.0205	0.0112	0.0172	0.0084
	0.00011	4.82	1.65	0.0020	0.07	0.0094	0.0011	0.20	0.0289	0.0112	0.0266	0.0084
	0.00011	4.82	1.65	0.0021	0.08	0.0094	0.0013	0.20	0.0316	0.0112	0.0295	0.0084
	0.00016	9.15	1.65	0.0026	0.08	0.0026	0.0014	0.31	0.0330	0.0117	0.0309	0.0156

Table 3: The dataset of parameters used to predict entrainment rates of non-uniform grain-size particles in previous research

Reference	D_i	D_{50}	R_p	R	S	H	c_{ae}	P_i	c_{ae}/P_i	S_e	D_i/D_{50}	R_f	u_*	u_{*ci}	u_{*i}	w_s	σ	λ
Rio Grande River	0.00009	0.00032	3.4	1.65	0.0008	0.78	0.0003	0.03	0.0096	0.0003	0.28	0.152	0.045	0.011	0.044	0.006	0.731	0.847
(Nodin & Dempster, 1963)	0.00009	0.00033	3.0	1.65	0.0008	0.76	0.0002	0.03	0.0067	0.0003	0.27	0.136	0.046	0.011	0.044	0.005	0.731	0.847
	0.00009	0.00030	3.2	1.65	0.0008	0.52	0.0003	0.05	0.0057	0.0004	0.30	0.143	0.043	0.011	0.042	0.005	0.731	0.847
	0.00009	0.00042	3.4	1.65	0.0008	0.72	0.0002	0.02	0.0108	0.0002	0.21	0.152	0.037	0.011	0.035	0.006	0.731	0.847
	0.00009	0.00026	3.4	1.65	0.0008	0.75	0.0001	0.04	0.0035	0.0002	0.35	0.150	0.039	0.011	0.038	0.006	0.731	0.847
	0.00009	0.00026	3.0	1.65	0.0008	0.43	0.0004	0.12	0.0032	0.0002	0.35	0.136	0.031	0.011	0.029	0.005	0.731	0.847
	0.00009	0.00037	3.1	1.65	0.0008	0.44	0.0002	0.05	0.0038	0.0003	0.24	0.138	0.035	0.011	0.033	0.005	0.731	0.847
	0.00009	0.00029	3.1	1.65	0.0008	0.47	0.0003	0.06	0.0044	0.0002	0.31	0.138	0.030	0.011	0.028	0.005	0.731	0.847
	0.00009	0.00031	3.0	1.65	0.0008	0.60	0.0002	0.05	0.0048	0.0002	0.29	0.136	0.036	0.011	0.034	0.005	0.731	0.847
	0.00009	0.00031	3.3	1.65	0.0009	0.41	0.0002	0.05	0.0051	0.0004	0.29	0.146	0.038	0.011	0.036	0.006	0.731	0.847
	0.00009	0.00027	3.9	1.65	0.0009	0.60	0.0003	0.04	0.0079	0.0002	0.33	0.171	0.030	0.011	0.028	0.007	0.731	0.847
	0.00009	0.00031	3.9	1.65	0.0009	0.46	0.0002	0.03	0.0056	0.0003	0.29	0.171	0.036	0.011	0.035	0.007	0.731	0.847
	0.00009	0.00030	3.4	1.65	0.0009	0.59	0.0003	0.04	0.0064	0.0003	0.30	0.150	0.041	0.011	0.039	0.006	0.731	0.847
	0.00018	0.00032	9.7	1.65	0.0008	0.78	0.0003	0.24	0.0014	0.0003	0.56	0.343	0.045	0.012	0.044	0.018	0.731	0.847
	0.00018	0.00033	8.6	1.65	0.0008	0.76	0.0002	0.30	0.0007	0.0003	0.55	0.315	0.046	0.013	0.044	0.017	0.731	0.847
	0.00018	0.00030	9.1	1.65	0.0008	0.52	0.0004	0.27	0.0015	0.0004	0.60	0.327	0.043	0.012	0.041	0.018	0.731	0.847
	0.00018	0.00042	9.7	1.65	0.0008	0.72	0.0002	0.15	0.0013	0.0002	0.43	0.343	0.037	0.012	0.035	0.018	0.731	0.847
	0.00018	0.00026	9.6	1.65	0.0008	0.75	0.0003	0.39	0.0007	0.0002	0.69	0.340	0.039	0.012	0.037	0.018	0.731	0.847
	0.00018	0.00026	8.6	1.65	0.0008	0.43	0.0005	0.33	0.0016	0.0002	0.69	0.315	0.031	0.013	0.028	0.017	0.731	0.847
	0.00018	0.00037	8.7	1.65	0.0008	0.44	0.0003	0.37	0.0008	0.0003	0.49	0.318	0.035	0.013	0.032	0.017	0.731	0.847
	0.00018	0.00029	8.7	1.65	0.0008	0.47	0.0004	0.33	0.0012	0.0002	0.62	0.318	0.030	0.013	0.027	0.017	0.731	0.847
	0.00018	0.00031	8.6	1.65	0.0008	0.60	0.0004	0.30	0.0013	0.0002	0.58	0.315	0.036	0.013	0.033	0.017	0.731	0.847
	0.00018	0.00031	9.3	1.65	0.0009	0.41	0.0003	0.29	0.0012	0.0004	0.58	0.333	0.038	0.012	0.036	0.018	0.731	0.847
	0.00018	0.00027	11.1	1.65	0.0009	0.60	0.0003	0.26	0.0013	0.0002	0.67	0.376	0.030	0.012	0.028	0.020	0.731	0.847
	0.00018	0.00031	11.1	1.65	0.0009	0.46	0.0001	0.31	0.0005	0.0003	0.58	0.376	0.036	0.012	0.034	0.020	0.731	0.847
	0.00018	0.00030	9.6	1.65	0.0009	0.59	0.0004	0.32	0.0012	0.0003	0.60	0.340	0.041	0.012	0.039	0.018	0.731	0.847
	0.00035	0.00032	27.5	1.65	0.0008	0.78	0.0001	0.60	0.0002	0.0003	1.09	0.606	0.045	0.014	0.043	0.046	0.731	0.847
	0.00035	0.00042	27.5	1.65	0.0008	0.72	0.0001	0.42	0.0002	0.0002	0.83	0.606	0.037	0.014	0.034	0.046	0.731	0.847
	0.00035	0.00026	24.3	1.65	0.0008	0.43	0.0001	0.51	0.0002	0.0002	1.35	0.573	0.031	0.014	0.027	0.043	0.731	0.847
	0.00035	0.00029	24.6	1.65	0.0008	0.47	0.0001	0.44	0.0003	0.0002	1.21	0.576	0.030	0.014	0.027	0.043	0.731	0.847
	0.00035	0.00031	24.3	1.65	0.0008	0.60	0.0002	0.45	0.0004	0.0002	1.13	0.573	0.036	0.014	0.033	0.043	0.731	0.847
	0.00035	0.00031	26.4	1.65	0.0009	0.41	0.0001	0.47	0.0003	0.0004	1.13	0.595	0.038	0.014	0.035	0.045	0.731	0.847
	0.00035	0.00027	31.5	1.65	0.0009	0.60	0.0001	0.45	0.0003	0.0002	1.30	0.644	0.030	0.014	0.027	0.048	0.731	0.847

Table 3: Continued 1.

Reference	D_i	D_{50}	R_p	R	S	H	c_{ae}	P_i	c_{ae}/P_i	S_e	D_i/D_{50}	R_f	u_*	u_{*ci}	u_{*i}	w_s	σ	λ
Rio Grande River	0.00035	0.00030	27.1	1.65	0.0009	0.59	0.0001	0.53	0.0002	0.0003	1.17	0.603	0.041	0.014	0.038	0.045	0.731	0.847
(Nodin & Dempster, 1963)	0.00009	0.00017	2.7	1.65	0.0008	0.47	0.0006	0.13	0.0047	0.0003	0.53	0.125	0.036	0.012	0.034	0.005	0.615	0.775
	0.00009	0.00017	2.9	1.65	0.0008	0.31	0.0007	0.16	0.0045	0.0005	0.53	0.130	0.040	0.011	0.038	0.005	0.615	0.775
	0.00009	0.00016	3.3	1.65	0.0010	0.20	0.0006	0.20	0.0031	0.0006	0.56	0.146	0.034	0.011	0.033	0.006	0.615	0.775
	0.00009	0.00021	3.5	1.65	0.0010	0.44	0.0006	0.08	0.0069	0.0003	0.43	0.153	0.036	0.011	0.034	0.006	0.615	0.775
	0.00009	0.00019	3.3	1.65	0.0008	0.35	0.0012	0.13	0.0087	0.0006	0.47	0.148	0.047	0.011	0.046	0.006	0.615	0.775
	0.00009	0.00016	3.2	1.65	0.0008	0.37	0.0020	0.17	0.0117	0.0005	0.56	0.145	0.044	0.011	0.042	0.006	0.615	0.775
	0.00009	0.00015	3.5	1.65	0.0010	0.33	0.0005	0.20	0.0025	0.0004	0.60	0.155	0.036	0.011	0.034	0.006	0.615	0.775
	0.00009	0.00019	3.6	1.65	0.0010	0.28	0.0010	0.09	0.0111	0.0005	0.47	0.159	0.037	0.011	0.035	0.006	0.615	0.775
	0.00009	0.00024	3.5	1.65	0.0009	0.70	0.0051	0.07	0.0693	0.0009	0.38	0.153	0.077	0.011	0.076	0.006	0.615	0.775
	0.00009	0.00025	3.6	1.65	0.0009	0.73	0.0084	0.05	0.1650	0.0009	0.36	0.160	0.078	0.011	0.077	0.006	0.615	0.775
	0.00018	0.00017	7.8	1.65	0.0008	0.47	0.0008	0.51	0.0017	0.0003	1.06	0.292	0.036	0.013	0.034	0.016	0.615	0.775
	0.00018	0.00017	8.1	1.65	0.0008	0.31	0.0010	0.68	0.0014	0.0005	1.06	0.302	0.040	0.013	0.038	0.016	0.615	0.775
	0.00018	0.00016	9.3	1.65	0.0010	0.20	0.0004	0.61	0.0006	0.0006	1.13	0.333	0.034	0.012	0.032	0.018	0.615	0.775
	0.00018	0.00021	9.8	1.65	0.0010	0.44	0.0004	0.57	0.0007	0.0003	0.86	0.346	0.036	0.012	0.034	0.019	0.615	0.775
	0.00018	0.00019	9.5	1.65	0.0008	0.35	0.0016	0.60	0.0026	0.0006	0.95	0.337	0.047	0.012	0.045	0.018	0.615	0.775
	0.00018	0.00016	9.2	1.65	0.0008	0.37	0.0028	0.67	0.0041	0.0005	1.13	0.330	0.044	0.012	0.042	0.018	0.615	0.775
	0.00018	0.00015	10.0	1.65	0.0010	0.33	0.0004	0.61	0.0006	0.0004	1.20	0.349	0.036	0.012	0.034	0.019	0.615	0.775
	0.00018	0.00019	10.2	1.65	0.0010	0.28	0.0021	0.68	0.0031	0.0005	0.95	0.355	0.037	0.012	0.035	0.019	0.615	0.775
	0.00018	0.00024	9.8	1.65	0.0009	0.70	0.0083	0.41	0.0203	0.0009	0.75	0.346	0.077	0.012	0.076	0.019	0.615	0.775
	0.00018	0.00025	10.3	1.65	0.0009	0.73	0.0208	0.41	0.0512	0.0009	0.72	0.358	0.078	0.012	0.077	0.019	0.615	0.775
	0.00035	0.00021	27.8	1.65	0.0010	0.44	0.0001	0.27	0.0003	0.0003	1.67	0.610	0.036	0.014	0.033	0.046	0.615	0.775
	0.00035	0.00024	27.8	1.65	0.0009	0.70	0.0026	0.41	0.0064	0.0009	1.46	0.610	0.077	0.014	0.075	0.046	0.615	0.775
	0.00035	0.00025	29.2	1.65	0.0009	0.73	0.0043	6.20	0.0007	0.0009	1.40	0.623	0.078	0.014	0.077	0.047	0.615	0.775
Niobrara River	0.00009	0.00029	2.2	1.65	0.0017	0.46	0.0002	0.04	0.0051	0.0008	0.31	0.102	0.058	0.012	0.057	0.004	0.686	0.802
(Colby & Hembree, 1955)	0.00009	0.00029	2.2	1.65	0.0017	0.52	0.0004	0.04	0.0111	0.0009	0.31	0.102	0.068	0.012	0.066	0.004	0.686	0.802
	0.00009	0.00029	2.2	1.65	0.0017	0.55	0.0003	0.04	0.0063	0.0008	0.31	0.102	0.065	0.012	0.064	0.004	0.686	0.802
	0.00009	0.00029	2.2	1.65	0.0017	0.67	0.0002	0.04	0.0046	0.0006	0.31	0.102	0.061	0.012	0.060	0.004	0.686	0.802
	0.00009	0.00029	2.2	1.65	0.0017	0.73	0.0002	0.04	0.0044	0.0003	0.31	0.102	0.045	0.012	0.043	0.004	0.686	0.802
	0.00009	0.00031	2.9	1.65	0.0017	0.73	0.0001	0.02	0.0061	0.0003	0.29	0.129	0.048	0.011	0.047	0.005	0.686	0.802
	0.00009	0.00031	2.9	1.65	0.0017	0.76	0.0003	0.02	0.0159	0.0005	0.29	0.129	0.060	0.011	0.058	0.005	0.686	0.802
	0.00009	0.00031	2.9	1.65	0.0017	0.64	0.0004	0.02	0.0221	0.0009	0.29	0.129	0.073	0.011	0.073	0.005	0.686	0.802
	0.00009	0.00031	2.9	1.65	0.0017	0.58	0.0005	0.02	0.0240	0.0007	0.29	0.129	0.065	0.011	0.064	0.005	0.686	0.802

Table 3: Continued 2.

Reference	D_i	D_{50}	R_p	R	S	H	c_{ae}	P_i	c_{ae}/P_i	S_e	D_i/D_{50}	R_f	u_*	u_{*ci}	u_{*i}	w_s	σ	λ
Niobrara River	0.00009	0.00031	2.9	1.65	0.0017	0.52	0.0003	0.02	0.0162	0.0007	0.29	0.129	0.059	0.011	0.058	0.005	0.686	0.802
(Colby & Hembree, 1955)	0.00009	0.00028	3.0	1.65	0.0013	0.64	0.0001	0.01	0.0083	0.0005	0.32	0.137	0.056	0.011	0.055	0.005	0.686	0.802
	0.00009	0.00028	3.0	1.65	0.0013	0.67	0.0000	0.01	0.0039	0.0007	0.32	0.137	0.069	0.011	0.068	0.005	0.686	0.802
	0.00009	0.00028	3.0	1.65	0.0013	0.55	0.0000	0.01	0.0047	0.0008	0.32	0.137	0.068	0.011	0.067	0.005	0.686	0.802
	0.00009	0.00028	3.0	1.65	0.0013	0.61	0.0000	0.01	0.0014	0.0004	0.32	0.137	0.046	0.011	0.045	0.005	0.686	0.802
	0.00018	0.00029	6.2	1.65	0.0017	0.46	0.0005	0.38	0.0014	0.0008	0.62	0.248	0.058	0.014	0.057	0.013	0.686	0.802
	0.00018	0.00029	6.2	1.65	0.0017	0.52	0.0024	0.38	0.0063	0.0009	0.62	0.248	0.068	0.014	0.066	0.013	0.686	0.802
	0.00018	0.00029	6.2	1.65	0.0017	0.55	0.0009	0.38	0.0025	0.0008	0.62	0.248	0.065	0.014	0.063	0.013	0.686	0.802
	0.00018	0.00029	6.2	1.65	0.0017	0.67	0.0004	0.38	0.0011	0.0006	0.62	0.248	0.061	0.014	0.060	0.013	0.686	0.802
	0.00018	0.00029	6.2	1.65	0.0017	0.73	0.0004	0.38	0.0010	0.0003	0.62	0.248	0.045	0.014	0.043	0.013	0.686	0.802
	0.00018	0.00031	8.1	1.65	0.0017	0.73	0.0001	0.32	0.0004	0.0003	0.58	0.301	0.048	0.013	0.046	0.016	0.686	0.802
	0.00018	0.00031	8.1	1.65	0.0017	0.76	0.0006	0.32	0.0020	0.0005	0.58	0.301	0.060	0.013	0.058	0.016	0.686	0.802
	0.00018	0.00031	8.1	1.65	0.0017	0.64	0.0018	0.32	0.0056	0.0009	0.58	0.301	0.073	0.013	0.072	0.016	0.686	0.802
	0.00018	0.00031	8.1	1.65	0.0017	0.58	0.0017	0.32	0.0054	0.0007	0.58	0.301	0.065	0.013	0.064	0.016	0.686	0.802
	0.00018	0.00031	8.1	1.65	0.0017	0.52	0.0005	0.32	0.0016	0.0007	0.58	0.301	0.059	0.013	0.058	0.016	0.686	0.802
	0.00018	0.00028	8.6	1.65	0.0013	0.64	0.0001	0.40	0.0003	0.0005	0.64	0.315	0.056	0.013	0.054	0.017	0.686	0.802
	0.00018	0.00028	8.6	1.65	0.0013	0.67	0.0001	0.40	0.0003	0.0007	0.64	0.315	0.069	0.013	0.068	0.017	0.686	0.802
	0.00018	0.00028	8.6	1.65	0.0013	0.55	0.0003	0.40	0.0008	0.0008	0.64	0.315	0.068	0.013	0.066	0.017	0.686	0.802
	0.00018	0.00028	8.6	1.65	0.0013	0.61	0.0009	0.40	0.0022	0.0004	0.64	0.315	0.046	0.013	0.044	0.017	0.686	0.802
	0.00035	0.00029	17.6	1.65	0.0017	0.46	0.0001	0.34	0.0003	0.0008	1.21	0.485	0.058	0.015	0.056	0.036	0.686	0.802
	0.00035	0.00029	17.6	1.65	0.0017	0.52	0.0005	0.34	0.0015	0.0009	1.21	0.485	0.068	0.015	0.066	0.036	0.686	0.802
	0.00035	0.00029	17.6	1.65	0.0017	0.55	0.0003	0.34	0.0010	0.0008	1.21	0.485	0.065	0.015	0.063	0.036	0.686	0.802
	0.00035	0.00029	17.6	1.65	0.0017	0.67	0.0001	0.34	0.0003	0.0006	1.21	0.485	0.061	0.015	0.059	0.036	0.686	0.802
	0.00035	0.00031	22.9	1.65	0.0017	0.76	0.0009	0.52	0.0017	0.0005	1.13	0.556	0.060	0.014	0.058	0.042	0.686	0.802
	0.00035	0.00031	22.9	1.65	0.0017	0.64	0.0002	0.52	0.0004	0.0009	1.13	0.556	0.073	0.014	0.072	0.042	0.686	0.802
	0.00035	0.00028	24.3	1.65	0.0013	0.67	0.0001	0.51	0.0001	0.0007	1.25	0.573	0.069	0.014	0.068	0.043	0.686	0.802
	0.00035	0.00028	24.3	1.65	0.0013	0.55	0.0001	0.50	0.0002	0.0008	1.25	0.573	0.068	0.014	0.066	0.043	0.686	0.802

As a result, in total 46 datasets from experiments and 70 datasets from field surveys were used for the multiple regression analysis (Table 2 and Table 3). These datasets were then classified into four categories: open channel flows with the uniform sediment, open channel flows with the non-uniform sediment, turbidity currents with the uniform sediment, and turbidity currents with the non-uniform sediment. The previous research of river survey was considered as non-uniform sediment condition, meanwhile the research of laboratory experiment was considered as uniform sediment condition except those explicitly describing that the non-uniform sediment was used in experiments.

4.2 Dimensionless variables analyzed in this study

In this study, the entrainment rate is assumed to be predicted by products of powers of dimensionless variables. Thus, the function to be proposed takes the form:

$$E_s = k\, Q_1^{a1}\, Q_2^{a2}\, Q_3^{a3} \cdots \tag{37}$$

where k is the empirical dimensionless coefficient and Q_j denotes the jth dimensionless variable. The linearized form of these multiple models by taking the logrithm of both sides is subject for multiple linear regression analysis.

Equation 8 and considerations in the section 2.2 imply that five dimensionless variables are candidates of the input variables for the entrainment function:

$$E_s = f\left(\frac{u_{*\mathrm{i}}}{w_\mathrm{s}}, \frac{H}{D_s}, R_\mathrm{p}, R_\mathrm{f}, S_e\right) \quad , \tag{38}$$

where R_p is the particle Reynolds number, and S_e denotes the energy slope defined as $S_e = u_*^2/gH$ in open channel flows. In case of turbidity currents, the value of energy slope reflects the sediment concentration that is subject to estimate in this function, so that the energy slope S_e was excluded from the analysis of the entrainment rates in turbidity currents. The first and second variables $u_{*\mathrm{i}}/w_\mathrm{s}$ and H/D_s are the dimensionless competence shear velocity and dimensionless flow thickness, respectively. R_f is the dimensionless settling velocity of a particle, which is defined as:

$$R_\mathrm{f} = \frac{w_\mathrm{s}}{\sqrt{RgD_s}} \quad , \tag{39}$$

The settling velocity of particle w_{s} was calculated using the following relationship indicated by Ferguson and Church (2004):

$$w_{\mathrm{s}} = \frac{RgD_s^2}{C_1 \nu + (0.75\, C_2 RgD_s^3)^{0.5}} \quad , \tag{40}$$

where C_1 and C_2 take values 18 and 0.4 for smooth spheres, respectively. For typical natural sands they are 18 and 1.0 in sieve diameters, or 20 and 1.1 in nominal diameters, respectively. For very angular sands C_1 and C_2 take values 24 and 1.2, respectively. In this study, the value of $C_1 = 20$ and $C_2 = 1.1$ were chosen.

By the Equation 14, Equation 39, and Equation 40, it is obvious that the dimensionless parameters R_{p} and R_{f} correlate to the same parameters of R, g, D_s and ν. Therefore the dimensionless parameter R_{f} may be substituted by R_{p} because $R_{\mathrm{f}} = f(R_{\mathrm{p}})$.

In the natural rivers or submarine fans, bed materials are rather poorly sorted. Therefore, the entrainment function of uniform sediment needs to be extended to non-uniform case, and the functional relationship takes the form (Garcia & Parker, 1991):

$$E_{s,i} = f\left(\frac{u_{*\mathrm{i}}}{w_{\mathrm{s}i}}, \frac{H}{D_i}, R_{\mathrm{f}}, S_e, \frac{D_i}{D_{50}}, P_i, \lambda\right) \tag{41}$$

where D_i and $w_{\mathrm{s}i}$ are the characteristic geometric diameter and settling velocity of the sediment in the ith grain-size class, respectively. D_{50} denotes the median grain size of sediment mixture, P_i is the volume fraction of the ith grain-size class of sediment in the bed material, and λ is a coefficient ($\lambda = 1 - 0.288\sigma$, suggested by Garcia and Parker (1991)) of which σ is the standard deviation of bed material in ϕ-scale (Figure 2).

4.3 Multiple linear regression and model selection

The multiple linear regression analysis and statistical model selection were utilized to obtain the entrainment function for suspended sediment. The data from open channel flows and density flows were analyzed separately in order to avoid the issue mentioned above. Trends in entrainment rate function were then compared between open channel flows and density flows.

After the entrainment function for the uniform sediment was established, this study explored the correction factor for the entrainment rate of the non-uniform (mixed-grain size) sediment. The following relationship is assumed in the analysis:

$$E_{s,i} = E_{s,uni} f\left(\frac{D_i}{D_{50}}, P_i, \lambda\right) \quad . \tag{42}$$

Since the experimental datasets of mixed-size grains pertaining to density flows were too few to establish the function, the datasets of non-uniform sediment pertaining to two types of flows were combined in the analysis. In this study, the multiple regression was conducted by using the Python libraries statsmodels and sklearn.

After the multiple regression to obtain the exponents of the candidates of the entrainment rate function, the reliability of the models was evaluated by inspecting the significance level of the parameters for each model in statistical hypothesis testing. The remaining reliable models were compared by the method of statistical model selection based on Akaike Information Criterion (AIC) and average value of 10-fold cross-validation (CV). The variance inflation factor (VIF) was employed to quantify the degree of multicollinearity in each model. In this study, VIF larger than 10 is regarded as indicative of a multicollinearity problem, and thus the model was excluded.

The Akaike Information Criterion is an estimator of the relative quality of statistical models for set of data which is based on maximum likelihood estimation. The AIC is defined as follows:

$$\mathrm{AIC} = -2l_{max} + 2\,(k+1) \quad , \tag{43}$$

where l_{max} is the maximum log-likelihood value of each model and k is the number of parameters in the model, $k+1$ is for considering constant coefficient. l_{max} is calculated from the likelihood function which shows how likely a set of particular values of parameters is for a given set of observed data. In a normal distribution with zero mean and independent of the independent variables, the probability density function for the regression residual (ε) and variance of the regression ressidual (σ^2) is difined as:

$$f(\varepsilon \mid \sigma) = \frac{1}{\sqrt{2\pi}\sigma}\, e^{-\frac{\varepsilon^2}{\sigma^2}} \quad . \tag{44}$$

The likelihood funcion of σ for an outcome ε of the regression residual is given by:

$$L(\sigma \mid \varepsilon) = f(\varepsilon \mid \sigma) \quad . \tag{45}$$

Then, the log-likelihood function of σ for a set of outcomes $(\varepsilon_1, \varepsilon_2, \cdots, \varepsilon_n)$ can be rewritten as:

$$l(\sigma \mid \varepsilon_1, \varepsilon_2, \cdots, \varepsilon_n) = \ln L = \sum_{i=1}^{n} \ln f(\varepsilon_i \mid \sigma) = -\frac{n(1 + \ln(2\pi\sigma^2))}{2} \quad , \tag{46}$$

where n denotes the size of dataset, ε_i denotes the individual regression residuals.

The maximum log-likelihood function for the model is given by:

$$l_{max} \approx -\frac{n(1 + \ln(2\pi\sigma_i^2))}{2} = -\frac{n \ln \sigma_i^2}{2} - \frac{n(1 + \ln 2\pi)}{2} \quad , \tag{47}$$

where σ_i^2 denotes resultant estimated value of σ^2. Since the population mean of ε is zero, the central limit theorem shows an unbiased estimator of σ_i^2 as:

$$\sigma_i^2 = \sum_{i=1}^{n} \frac{\varepsilon_i^2}{n-k} \quad . \tag{48}$$

The Bayesian Information Criterion (BIC) was also calculated in this study. The BIC is defined as:

$$\mathrm{BIC} = -2l_{max} + (k+1)\ \ln n \quad . \tag{49}$$

Since BIC has a consistency property, it tends to suggest the correct model when the unknown true model is included in the candidate models. BIC introduce a penalty term of the sample size as well as the number of parameters while AIC does not. In this study, however, the first priority is to realize the greater generalization performance in predicting entrainment rate of suspension, and the correct form of the function is not necessarily expected. Therefore AIC is used for the model selection at the first priority, and the BIC is used as a reference of robustness on selection.

On the other hand, cross-validation assess the model by the degree how much the statistical model can be generalized to an independent data set. At first, it divided the dataset into two part: one used to train a model and the other used to validate the model. To reduce variability, multiple rounds of cross-validation are performed using different partitions, so that each dataset will be under validated, at last the validation results are averaged over the rounds to infer an estimation of the predictive performance of the model. In this case, the K-fold cross-validation method was used, and K is set to 10. The average value of mean square error between model and test data was calculated in one round, for 10-fold cross-validation in this study, CV value is the average value of the total ten rounds. Since cross-validation is a non-parametric method and does not assume any particular probability distribution for the regression residuals. CV is robust against violations of the assumption of normality of residuals.

By the definition of the value of AIC, BIC and CV, the smallest value represents best fitness and prediction in model selecting. If these criteria were interference with another which is difficult to choose the preferred model, the AIC and CV are primary criterion for model selection in this study.

5 Experimental results

A steady quasi-equilibrium condition of density flows for each experimental run was attained with the constant thickness of the erodible bed and migrating small scale bedforms. A quasi-equilibrium condition was confirmed by the observation, and then measurements were conducted. In several experiments of this study, only one set of siphon was able to install in the flume. In such cases, the equilibrium state of flow conditions was judged carefully with longer duration of experimental flows.

5.1 Description for representative experiments

Here several results of representative experiments are introduced.

In the Run 10 using the uniform sediment of plastic particles **P** with density of 1.45 g/cm^3, the mean value of the grain-size distribution in the mixing tank was 2.67 ϕ. The value of D_5, D_{50} and D_{95} were 1.91 ϕ, 2.50 ϕ, 3.39 ϕ, respectively. The volume concentration of particles in the mixing tanks was 1.0% before the initiation of each experiment. The flume was set in one straight slope at 10%, without any sediment on bed. Two arrays of siphons were set at the distance 2.5 m and 3.5 m respectively from inlet, the upstream one was set 5 mm above bed, the downstream was fitted close to bed. ADVP was set at the distance 2.9 m from inlet, and 45 mm above bed. Since the flow start to be stable, the ADVP was lifted 5 mm up per minute since 2 min. 31 sec. in the experiment to adjust the bed sediment thickness. Temperature of water was 15.8°C in the flume.

The flow thickness of this experiment was 20 cm by observation from the video record. Layer-average flow velocity and boundary shear velocity was 0.19 m/s and 0.0106 m/s, respectively. The concentration of sediment at $0.05H$ was 0.25% at upstream siphon and 0.12% at downstream siphon (Figure 8). The settling velocity of the particle was calculated under Furguson method, which is 0.0047 m/s. R_p and R_f which are the dimensionless parameters of particle diameters were resulted in 4.06 and 0.172, respectively.

In the Run 16 using the non-uniform sediment, plastic particles **P** with density of 1.45 g/cm^3 and natural sand **S** with density of 2.65 g/cm^3 were used. The distribution of the grain-size was shown in Figure 4. The mean value of the grain-size of mixed particles is 2.64 ϕ under analyzed in the density of 1.45 g/cm^3. The value of D_5, D_{50}, D_{95} is 0.80 ϕ, 2.65 ϕ, 3.95 ϕ, respectively. The measured volume concentration of particles in mixing

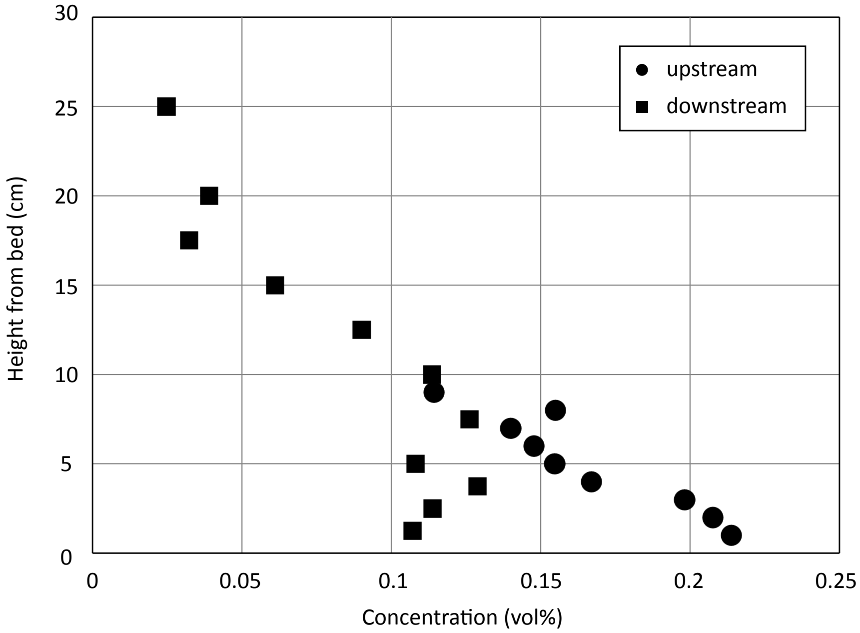

Fig. 8: The vertical distribution profile of concentrantion of suspended particles (upstream and downstream) in Run 10 by using uniform grain-size sediment.

tank was 2% with a proportion of **S**:**P** = 1:2 before experiment start. The flume was set in one straight slope at 12%, with preparatory 22 mm thickness of sediment on bed. One set of siphon was set at the distance 2.35 m from inlet, and 15 mm above bed. ADVP was set at the distance 2.75 m from inlet, 85 mm above bed before experiment start and remain at the place during the experiment. Temperature of water was 12.8°C in the flume.

The flow thickness of this experiment was 11 cm by checking the video record. Layer-average flow velocity and boundary shear velocity was 0.11 m/s and 0.0098 m/s, respectively. The volume concentration of sediment at $0.05H$ was 0.26%, 0.27% and 0.04% in 2–3 ϕ, 3–4 ϕ and 4–5 ϕ of grain-size class range, respectively (concentrations of grain-size class were shown in Figure 10, total concentration was shown in Figure 9). The settling velocity of the particle was calculated under Furguson method, which is 0.0049 m/s, 0.0014 m/s, 0.0003 m/s, respectively. R_p and R_f which are the dimensionless parameters of particle diameters were resulted in 4.06 and 0.18, 1.44 and 0.07, 0.51 and 0.02 in that grain-size class range, respectively. After experiment, the sediment on bed was covered by plastic particles, the sand was barely existed on the surface of bed material. Sample result of proportion in 2–3 ϕ, 3–4 ϕ and 4–5 ϕ of grain-size class range on the bed material surface was

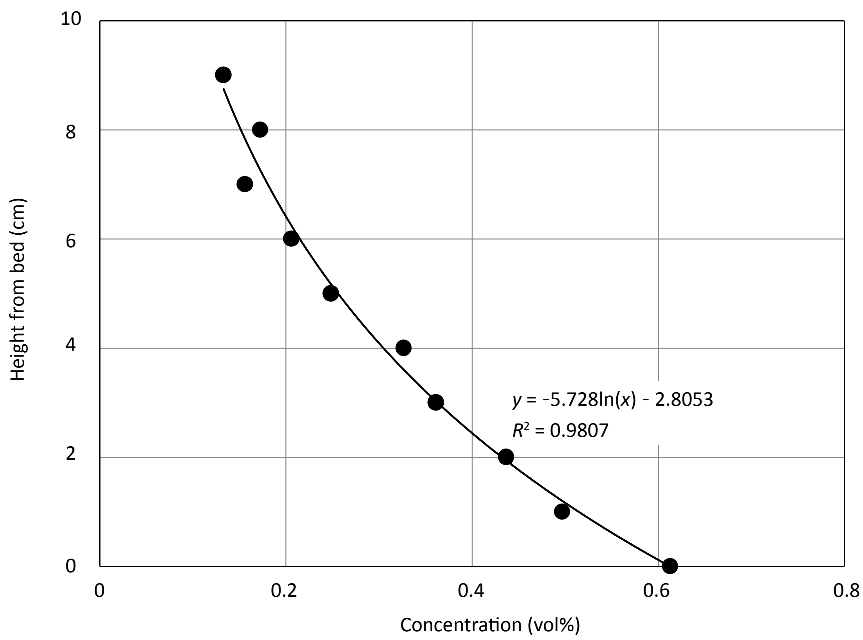

Fig. 9: The vertical distribution profile of concentrantion of suspended particles (total concentration of all grain-size class) in Run 16 by using non-uniform grain-size sediment.

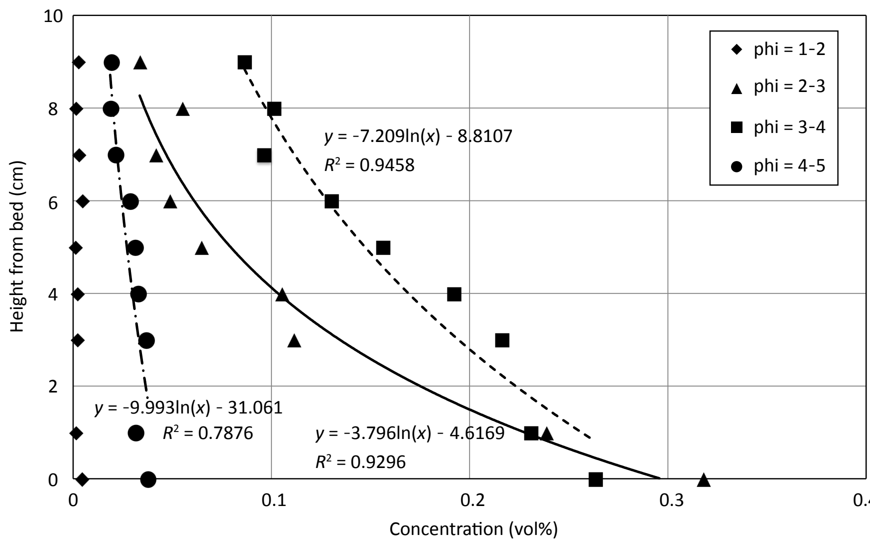

Fig. 10: The vertical distribution profile of concentrantion of suspended particles (concentration in individual grain-size class) in Run 16 by using non-uniform grain-size sediment.

Table 4: The calculated result of parameters in experiments using uniform grains.

Run	D_s	R_p	R	S	H	c_{ae}	S_e	R_f	u_*	u_{*ci}	u_{*i}	w_s
5	0.00014	3.11	0.45	0.10	0.35	0.0090	0.029	0.136	0.0142	0.0071	0.007	0.0034
6	0.00014	2.68	0.45	0.10	0.13	0.0008	0.350	0.120	0.0092	0.0073	0.008	0.0029
7	0.00012	2.09	0.45	0.10	0.13	0.0005	0.553	0.095	0.0090	0.0073	0.007	0.0022
8	0.00014	2.7	0.45	0.10	0.18	0.0015	0.178	0.120	0.0104	0.0073	0.008	0.0030
9	0.00012	2.1	0.45	0.10	0.18	0.0011	0.250	0.096	0.0102	0.0073	0.007	0.0022
10	0.00017	4.06	0.45	0.10	0.20	0.0025	0.103	0.172	0.0106	0.0075	0.008	0.0047
11	0.00016	3.6	0.45	0.10	0.20	0.0011	0.217	0.155	0.0105	0.0074	0.007	0.0040

51%, 42%, 6%, respectively. Standard deviation of particles grain-size σ was 0.54, which derived the value of parameter λ in 0.84.

5.2 Layer averaged values of experimental flows and shear velocity

The layer averaged velocity U ranges from 0.11 to 0.28 m/s, which was capable to entrain and transport sediment along the flume. The layer averaged concentration C ranges from 0.03% to 1.2%, even though the volume concentration in mixing tank was extremely larger than this in flume. The flow thickness H ranges from 0.11 to 0.35 m in steady conditions (see in Table 1).

The boundary shear velocity were calculated from ADVP data, and the computed results of u_* were shown in Table 4 and Table 5. As a whole, u_* ranged from 0.009 m/s to 0.03 m/s, and values of u_{*i} ranged from 0.005 m/s to 0.03 m/s. In cases of experiments using the uniform sediment, u_* ranged from 0.009 to 0.014 m/s (Table 4). In the cases of the experiments using the non-uniform sediment, u_* ranged from 0.01 to 0.03 m/s (Table 5).

5.3 Near-bed sediment concentration and grain-size distributions of bed materials

The near-bed concentration of sediment was calculated from the vertical concentration distribution of particles, and the grain-size distribution of bed materials was also analyzed. The near-bed concentration (at 0.05H) ranged 0.05%–0.90% and 0.02%–1.36% in cases of experiments using the uniform and the non-uniform sediments respectively. In the cases of the non-uniform sediment, proportion of each grain-size class on the bed ranged from 3% to 71%, and the standard deviation of their grain-size were in a range of 0.4–1.2.

Table 5: The calculated result of parameters in experiments using non-uniform grains.

Run	D_i	D_{50}	R_p	R	S	H	c_{ae}	P_i	c_{ae}/P_i	S_e	D_i/D_{50}	R_f	u_*	u_{*ci}	u_{*i}	w_s	σ	λ
1	0.000180	0.000152	4.97	0.45	0.05	0.22	0.0136	0.519	0.0263	0.0117	1.18	0.207	0.0124	0.0074	0.0099	0.0058	0.924	0.734
	0.000090	0.000152	1.76	0.45	0.05	0.22	0.0108	0.348	0.0310	0.0117	0.59	0.083	0.0124	0.0066	0.0104	0.0017	0.924	0.734
	0.000044	0.000152	0.62	0.45	0.05	0.22	0.0024	0.076	0.0317	0.0117	0.29	0.030	0.0124	0.0056	0.0110	0.0004	0.924	0.734
2	0.000180	0.000173	3.70	0.45	0.05	0.20	0.0084	0.644	0.0130	0.0214	1.04	0.162	0.0112	0.0080	0.0078	0.0046	0.800	0.770
	0.000090	0.000173	1.31	0.45	0.05	0.20	0.0049	0.300	0.0162	0.0214	0.52	0.063	0.0112	0.0070	0.0087	0.0013	0.800	0.770
3	0.000180	0.000198	5.04	0.45	0.10	0.25	0.0060	0.648	0.0092	0.0291	0.91	0.210	0.0136	0.0074	0.0114	0.0059	0.590	0.830
	0.000090	0.000198	1.78	0.45	0.10	0.25	0.0046	0.246	0.0185	0.0291	0.46	0.085	0.0136	0.0066	0.0119	0.0017	0.590	0.830
	0.000044	0.000198	0.63	0.45	0.10	0.25	0.0010	0.030	0.0333	0.0291	0.22	0.030	0.0136	0.0056	0.0124	0.0004	0.590	0.830
4	0.000180	0.000301	5.10	0.45	0.10	0.25	0.0010	0.213	0.0045	0.7955	0.60	0.212	0.0294	0.0074	0.0285	0.0060	1.212	0.651
	0.000090	0.000301	1.80	0.45	0.10	0.25	0.0010	0.338	0.0030	0.7955	0.30	0.085	0.0294	0.0066	0.0287	0.0017	1.212	0.651
12	0.000180	0.000176	4.23	0.45	0.10	0.14	0.0051	0.714	0.0072	0.1706	1.02	0.181	0.0193	0.0077	0.0177	0.0051	0.537	0.845
	0.000090	0.000176	1.50	0.45	0.10	0.14	0.0017	0.228	0.0075	0.1706	0.51	0.072	0.0193	0.0068	0.0180	0.0014	0.537	0.845
	0.000044	0.000176	0.53	0.45	0.10	0.14	0.0002	0.027	0.0083	0.1706	0.25	0.026	0.0193	0.0057	0.0184	0.0004	0.537	0.845
13	0.000180	0.000137	4.23	0.45	0.10	0.14	0.0013	0.500	0.0026	0.3840	1.32	0.181	0.0193	0.0077	0.0177	0.0051	0.495	0.857
	0.000090	0.000137	1.50	0.45	0.10	0.14	0.0016	0.436	0.0037	0.3840	0.66	0.072	0.0193	0.0068	0.0180	0.0014	0.495	0.857
	0.000044	0.000137	0.53	0.45	0.10	0.14	0.0002	0.055	0.0042	0.3840	0.32	0.026	0.0193	0.0057	0.0184	0.0004	0.495	0.857
14	0.000180	0.000152	4.90	0.45	0.10	0.18	0.0036	0.648	0.0056	0.0488	1.18	0.205	0.0108	0.0075	0.0078	0.0058	0.471	0.864
	0.000090	0.000152	1.73	0.45	0.10	0.18	0.0024	0.348	0.0070	0.0488	0.59	0.082	0.0108	0.0067	0.0085	0.0016	0.471	0.864
15	0.000180	0.000140	4.90	0.45	0.10	0.18	0.0017	0.538	0.0032	0.0945	1.29	0.205	0.0108	0.0075	0.0078	0.0058	0.446	0.872
	0.000090	0.000140	1.73	0.45	0.10	0.18	0.0014	0.457	0.0031	0.0945	0.64	0.082	0.0108	0.0067	0.0085	0.0016	0.446	0.872
16	0.000180	0.000137	4.06	0.45	0.12	0.11	0.0026	0.508	0.0050	0.0693	1.31	0.175	0.0098	0.0078	0.0059	0.0049	0.539	0.845
	0.000090	0.000137	1.44	0.45	0.12	0.11	0.0027	0.421	0.0065	0.0693	0.66	0.069	0.0098	0.0069	0.0070	0.0014	0.539	0.845
	0.000044	0.000137	0.51	0.45	0.12	0.11	0.0004	0.060	0.0071	0.0693	0.32	0.025	0.0098	0.0058	0.0079	0.0003	0.539	0.845
17	0.000180	0.000373	3.71	0.45	0.12	0.15	0.0022	0.290	0.0075	0.0912	0.48	0.163	0.0096	0.0080	0.0054	0.0046	0.785	0.774
	0.000090	0.000373	1.31	0.45	0.12	0.15	0.0010	0.102	0.0096	0.0912	0.24	0.064	0.0096	0.0070	0.0065	0.0013	0.785	0.774

5.4 Result of other dimensionless parameter

For the purpose of the statistical analysis, all the measured values were converted to the dimensionless parameters. All dimensionless parameters obtained in this study were shown in Table 4 and Table 5.

In the uniform grains experiment, R_{f} and R_{p} which related to grain-size were constant around 0.1–0.2 and 2–4 respectively. The bed slpoe S was always set up at 10%, whereas S_e which related to flow thickness and concentration was in a range from 0.03 to 0.55 (Table 4).

In the cases of the experiments using the non-uniform sediment, R_{f} and R_{p} related to not only grain-size class but also the density difference between plastic particle and siliciclastic sand. As a result, R_{f} and R_{p} ranged 0.03–0.21 and 0.5–5.1, respectively (Table 5).

The bed slope S in the experiments using the non-uniform sediment ranged from 5% to 10%, while the energy slope varied from 0.01–0.8.

6 Results of multiple regression analysis

6.1 Open channel flows with the uniform sediment

Total 79 data of open channel flows with uniform grains were analyzed. The relationship between the observed entrainment rate c_{ae} and each parameters was shown in Figure 11. The observed concentration of suspended particles at $0.05H$ of the flow has not over the range of 10^{-4}–10^{-1}. The parameters of dimensionless competence shear velocity $u_{*\mathrm{i}}/w_{\mathrm{s}}$ is in the range from 1–10, the other parameters S_e, R_{f}, R_p, and H/D_s are in the range of 10^{-4}–10^{-2}, 10^{-1}–1, 1–10^2, and 10^2–10^4, respectively. It is obvious that the dimensionless parameter $u_{*\mathrm{i}}/w_{\mathrm{s}}$ reveal a primary correlation to entrainment rate, whereas the other parameters may only have secondary correlation to entrainment rate.

As described in methodology, the models which use two parameters to describe the same characteristics were excluded. Four parameters combinations were analyzed under mutiple regression. The details of each model were shown in Table 6.

In Table 6, the AIC and CV of each model were shown at first. The coefficient of individual parameters and their p-values were shown at right part. The p-value for t-test statistic of parameters represents the probability to observe an equal or more extreme two-tailed t-value than actually observed one presuming the null hypothesis. The number 0.05 of a significance level was used in this analysis to reject a true null hypothesis in statistical test.

As a result, the model No.1, 2, 8, 10, 11, 12, 14, 17, 21, 22, 25, 26, 28, 30, 31 were excluded at the significant level of 0.05. Considering the parameter of $u_{*\mathrm{i}}/w_{\mathrm{s}}$ reveal a primary correlation to entrainment, models No.3, 4, 5, 6, and 7 are candidates of the best model. Between these models, the value of AIC is in the range of 47.8–49.3, and in each model the value of CV is 0.14. The VIF of these models were shown in Table 7.

As a result, the value of AIC indicates Model No.3 is the best model, with the value of VIF of individual parameters smaller than 10. In describing dimensional parameters with approximation $R_{\mathrm{f}} \sim w_{\mathrm{s}}^1$, the relationship of Model No.3 is given by:

$$\text{Model No.3}: \; E_s \propto \left(\frac{H}{D_s}\right)^{-0.4} R_{\mathrm{f}}^{2.0} \left(\frac{u_{*\mathrm{i}}}{w_{\mathrm{s}}}\right)^{2.75} \approx u_{*\mathrm{i}}^{2.75} w_{\mathrm{s}}^{-0.75} H^{-0.4} \quad . \tag{50}$$

Thus, this model gives a result on dimensional parameter of $u_{*\mathrm{i}}$ about 2.75. The function of entrainment rate prediction was suggested as :

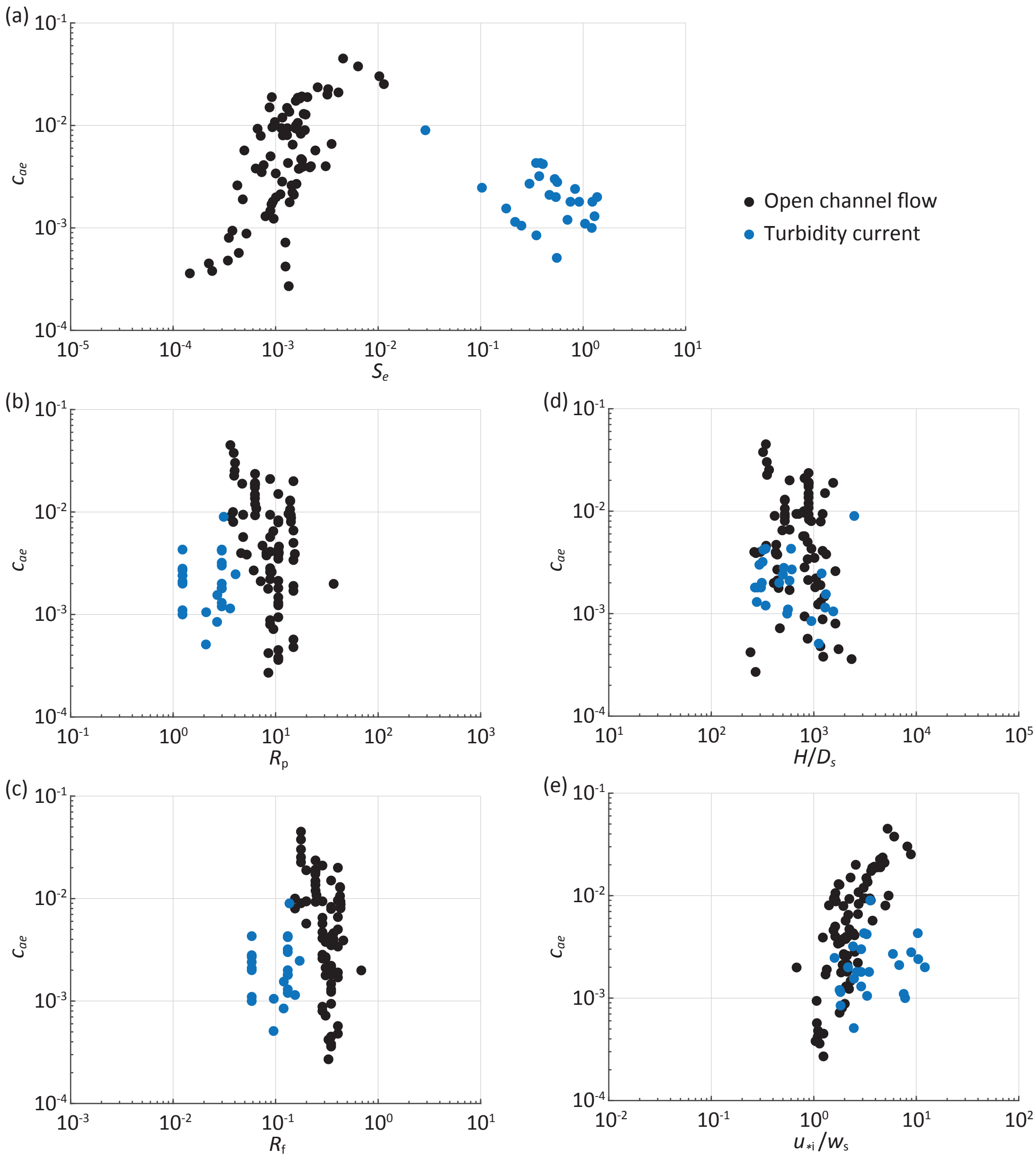

Fig. 11: The relationship between each parameters and the measured value of near-bed concentration in open channel flow with uniform sediment. Figure 11(a)(b)(c)(d)(e) represent the correlation between near-bed concentration and the energy slope S_e, particle Reynolds number R_p, dimensionless flow thickness H/D_s, the dimensionless grain-size R_f, dimensionless competence shear velocity u_{*i}/w_s, respectively.

Table 6: The result of multiple regression analysis and information criteria analysis of open channel flow with uniform grain-size particles

Model				constant			R_p			H/D_s			S_e			R_f			u_i/w_s		
No.	Combination of parameters	AIC	CV	coef	p	std. err.	coef	p	std. err.	coef	p	std. err.	coef	p	std. err.	coef	p	std. err.	coef	p	std. err.
1	$\log H/D_s$, $\log S_e$, $\log R_f$, $\log u_i/w_s$	44.91	0.14	0.37	6.70×10^{-1}	0.86				**−7.73**	**2.50×10^{-2}**	**3.38**	**−7.28**	**3.30×10^{-2}**	**3.35**	**14.18**	**1.40×10^{-2}**	**5.66**	**15.61**	**1.00×10^{-2}**	**5.92**
2	$\log R_p$, $\log H/D_s$, $\log S_e$, $\log R_f$, $\log u_i/w_s$	46.9	0.14	0.3	8.30×10^{-1}	1.42	0.04	9.50×10^{-1}	0.68	**−7.7**	**2.90×10^{-2}**	**3.45**	**−7.24**	**3.80×10^{-2}**	**3.43**	**14.06**	**2.40×10^{-2}**	**6.09**	**15.54**	**1.30×10^{-2}**	**6.08**
3	$\log H/D_s$, $\log R_f$, $\log u_i/w_s$	47.8	0.14	**−1.16**	**2.40×10^{-2}**	**0.5**				**−0.4**	**1.60×10^{-2}**	**0.16**				**1.93**	**2.60×10^{-4}**	**0.5**	**2.75**	**3.00×10^{-14}**	**0.29**
4	$\log S_e$, $\log R_f$, $\log u_i/w_s$	48.32	0.14	**−1.29**	**7.90×10^{-3}**	**0.47**							**0.38**	**2.10×10^{-2}**	**0.16**	**1.29**	**2.70×10^{-2}**	**0.57**	**2.07**	**3.20×10^{-6}**	**0.41**
5	$\log R_p$, $\log S_e$, $\log u_i/w_s$	48.49	0.14	**−2.27**	**1.30×10^{-3}**	**0.68**	**0.67**	**3.00×10^{-2}**	**0.3**				**0.46**	**2.60×10^{-3}**	**0.15**				**1.84**	**4.20×10^{-7}**	**0.33**
6	$\log R_p$, $\log H/D_s$, $\log u_i/w_s$	49.22	0.14	**−2.83**	**1.70×10^{-6}**	**0.55**	**1.08**	**5.40×10^{-4}**	**0.3**	**−0.5**	**3.80×10^{-3}**	**0.17**							**2.57**	**7.90×10^{-15}**	**0.27**
7	$\log H/D_s$, $\log S_e$, $\log u_i/w_s$	49.34	0.14	**−1.43**	**4.60×10^{-3}**	**0.49**				**0.69**	**4.80×10^{-2}**	**0.34**	**1.08**	**5.80×10^{-4}**	**0.3**				**0.78**	**2.20×10^{-2}**	**0.34**
8	$\log R_p$, $\log H/D_s$, $\log R_f$, $\log u_i/w_s$	49.57	0.14	−1.62	1.50×10^{-1}	1.12	0.31	6.50×10^{-1}	0.68	**−0.43**	**1.60×10^{-2}**	**0.17**				1.45	2.20×10^{-1}	1.16	**2.74**	**6.50×10^{-14}**	**0.3**
9	$\log H/D_s$, $\log S_e$, $\log R_f$	49.99	0.14	**−1.5**	**4.00×10^{-3}**	**0.51**				**1.14**	**7.20×10^{-6}**	**0.24**	**1.54**	**8.50×10^{-14}**	**0.17**	**−0.7**	**3.20×10^{-2}**	**0.32**			
10	$\log R_p$, $\log S_e$, $\log R_f$, $\log u_i/w_s$	50.11	0.14	−1.74	1.20×10^{-1}	1.12	0.3	6.60×10^{-1}	0.68				**0.41**	**2.10×10^{-2}**	**0.17**	0.78	5.50×10^{-1}	1.29	**2.01**	**1.80×10^{-5}**	**0.44**
11	$\log R_p$, $\log H/D_s$, $\log S_e$, $\log u_i/w_s$	50.47	0.14	**−2.18**	**2.60×10^{-2}**	**0.96**	0.59	3.70×10^{-1}	0.65	0.1	8.90×10^{-1}	0.74	0.55	4.10×10^{-1}	0.66				1.7	1.20×10^{-1}	1.07
12	$\log R_p$, $\log H/D_s$, $\log S_e$	51.14	0.14	−0.86	8.40×10^{-2}	0.49	−0.4	6.00×10^{-2}	0.21	**1.21**	**1.50×10^{-6}**	**0.23**	**1.57**	**2.00×10^{-14}**	**0.17**						
13	$\log S_e$, $\log u_i/w_s$	51.48	0.14	**−1.19**	**1.60×10^{-2}**	**0.48**							**0.55**	**3.40×10^{-4}**	**0.15**				**1.29**	**1.90×10^{-7}**	**0.23**
14	$\log R_p$, $\log H/D_s$, $\log S_e$, $\log R_f$	51.67	0.14	−2.05	7.20×10^{-2}	1.12	0.38	5.80×10^{-1}	0.69	**1.1**	**3.80×10^{-5}**	**0.25**	**1.53**	**1.80×10^{-13}**	**0.17**	−1.27	2.40×10^{-1}	1.08			
15	$\log R_f$, $\log u_i/w_s$	51.99	0.14	**−2.32**	**5.00×10^{-19}**	**0.2**										**1.92**	**4.40×10^{-4}**	**0.52**	**2.75**	**9.40×10^{-14}**	**0.3**
16	$\log H/D_s$, $\log S_e$	52.9	0.13	**−1.11**	**2.50×10^{-2}**	**0.48**				**1.29**	**3.90×10^{-7}**	**0.23**	**1.69**	**4.10×10^{-17}**	**0.16**						
17	$\log R_p$, $\log R_f$, $\log u_i/w_s$	53.8	0.14	−1.84	1.10×10^{-1}	1.15	−0.28	6.70×10^{-1}	0.66							**2.34**	**4.40×10^{-2}**	**1.14**	**2.77**	**1.30×10^{-13}**	**0.31**
18	$\log R_p$, $\log u_i/w_s$	56.11	0.15	**−4.08**	**2.50×10^{-17}**	**0.37**	**0.92**	**3.70×10^{-3}**	**0.31**										**2.47**	**1.80×10^{-13}**	**0.28**
19	$\log H/D_s$, $\log u_i/w_s$	59.91	0.15	**−1.86**	**5.00×10^{-4}**	**0.51**				**−0.39**	**2.90×10^{-2}**	**0.18**							**1.83**	**1.20×10^{-15}**	**0.18**
20	$\log u_i/w_s$	62.92	0.15	**−2.99**	**7.70×10^{-52}**	**0.08**													**1.84**	**2.50×10^{-15}**	**0.19**
21	$\log R_p$, $\log S_e$, $\log R_f$	67.9	0.17	−2.28	7.30×10^{-2}	1.25	1.33	7.20×10^{-2}	0.73				**1**	**1.20×10^{-10}**	**0.13**	**−3.08**	**7.00×10^{-3}**	**1.11**			
22	$\log S_e$, $\log R_f$	69.34	0.16	−0.16	7.40×10^{-1}	0.48							**0.95**	**4.50×10^{-10}**	**0.13**	**−1.15**	**1.50×10^{-3}**	**0.35**			
23	$\log R_p$, $\log S_e$	73.61	0.17	**1.04**	**8.50×10^{-3}**	**0.38**	**−0.59**	**1.50×10^{-2}**	**0.24**				**0.97**	**9.30×10^{-10}**	**0.14**						
24	$\log S_e$	77.84	0.17	**0.86**	**3.10×10^{-2}**	**0.39**							**1.1**	**3.90×10^{-12}**	**0.13**						
25	$\log H/D_s$, $\log R_f$	107.02	0.27	**−2.18**	**3.40×10^{-3}**	**0.72**				−0.41	9.00×10^{-2}	0.24				**−1.96**	**1.30×10^{-5}**	**0.42**			
26	$\log R_p$, $\log H/D_s$, $\log R_f$	107.95	0.27	**−3.61**	**2.60×10^{-2}**	**1.59**	0.99	3.20×10^{-1}	0.98	−0.5	5.40×10^{-2}	0.25				**−3.42**	**2.60×10^{-2}**	**1.51**			
27	$\log R_f$	108.02	0.27	**−3.35**	**4.00×10^{-24}**	**0.23**										**−1.98**	**1.40×10^{-5}**	**0.43**			
28	$\log R_p$, $\log R_f$	109.9	0.27	**−3.9**	**1.80×10^{-2}**	**1.62**	0.32	7.40×10^{-1}	0.94							−2.45	9.60×10^{-2}	1.45			
29	$\log R_p$	110.8	0.27	**−1.21**	**2.00×10^{-5}**	**0.27**	**−1.19**	**5.60×10^{-5}**	**0.28**												
30	$\log R_p$, $\log H/D_s$	111.18	0.28	−0.37	6.10×10^{-1}	0.72	**−1.15**	**1.10×10^{-4}**	**0.28**	−0.31	2.10×10^{-1}	0.25									
31	$\log H/D_s$	124.85	0.33	−1.07	1.70×10^{-1}	0.77				−0.44	1.00×10^{-1}	0.27									

Table 7: The value of variance inflation factor (VIF) of candidates models in open channel flow.

Model No.	VIF				
	$\log u_{*i}/w_s$	$\log R_f$	$\log R_p$	$\log S_e$	$\log H/D_s$
3	3.094	3.094			1.001
4	6.045	3.951		2.192	
5	3.923		2.640	1.849	
6	2.485		2.526		1.031
7	3.958			7.480	4.362

$$E_{s,open} = 10^{-1.16} \left(\frac{u_{*\mathrm{i}}}{w_{\mathrm{s}}} \right)^{2.75} R_{\mathrm{f}}^{1.93} \left(\frac{H}{D_s} \right)^{-0.40} \quad . \tag{51}$$

6.2 Result of turbidity currents with uniform grains

Total 25 data of turbidity currents with uniform grains was analyzed. The relationship between the observed entrainment rate c_{ae} and each parameters was shown in Figure 11. The observed concentration of suspended particles at $0.05H$ of the flow has not over the range of 10^{-3}–10^{-2}. The parameters of dimensionless competence shear velocity $u_{*\mathrm{i}}/w_{\mathrm{s}}$ is in the range from 1–10, the other parameters S_e, R_{f}, R_p, and H/D_S are in the range of 10^{-2}–1, 10^{-2}–1, 1–10, and 10^2–10^4, respectively. As described above, considering the energy slope S_e was excluded in the analysis of turbidity currents.

Comparison between data sets pertaining to open channel flows and turbidity currents are shown in Figure 11. The datasets of open channel flow represents a obvious trend of the correlation between parameter $u_{*\mathrm{i}}/w_{\mathrm{s}}$, energy slope S_e to the equilibrium near-bed concentration c_{ae}. Because the parameters $u_{*\mathrm{i}}/w_{\mathrm{s}}$ and c_a in datasets of the experiments of turbidity currents show very small ranges (from 1 to 10 and from 10^{-3} to 10^{-2} respectively, it was difficult to observe clear trends in relations of these parameters with entrainment rates. However, it is obvious that the distributions of those parameters in the parametric space are different from those of open channel flow data.

At the equilibrium condition, energy slope S_e is supposed equal to slope. However, the value of S_e is extremely deviate from value of S (see dataset of Garcia and Parker (1993) in Table 2, and dataset of this study in Table 4, 5).

As a result, the model No.3, 4, 5, 6, 7, 8, 9, 10, 11, 12, 13, 14, 15 were excluded at

Table 8: The result of multiple regression analysis and information criteria analysis of turbidity currents with uniform grain-size particles

Model				constant			R_p			H/D_s			S_e			R_f			u_{*i}/w_s		
No.	Combination of parameters	AIC	CV	coef	p	std. err.	coef	p	std. err.	coef	p	std. err.	coef	p	std. err.	coef	p	std. err.	coef	p	std. err.
1	$\log R_p$, $\log u_{*i}/w_s$	−4.78	0.06	**−4.46**	$\mathbf{2.40\times10^{-10}}$	**0.41**	**2.31**	$\mathbf{4.60\times10^{-4}}$	**0.56**										**1.67**	$\mathbf{2.80\times10^{-4}}$	**0.39**
2	$\log R_f$, $\log u_{*i}/w_s$	−4.57	0.06	**−1.14**	$\mathbf{1.40\times10^{-2}}$	**0.43**										**2.52**	$\mathbf{5.10\times10^{-4}}$	**0.62**	**1.67**	$\mathbf{3.00\times10^{-4}}$	**0.39**
3	$\log R_p$, $\log R_f$, $\log u_{*i}/w_s$	−3.47	0.11	−28.32	3.70×10^{-1}	31.06	18.84	3.90×10^{-1}	21.53							−18.19	4.50×10^{-1}	23.67	**1.59**	$\mathbf{7.00\times10^{-4}}$	**0.4**
4	$\log R_p$, $\log H/D_s$,] $\log u_{*i}/w_s$	−3.22	0.07	**−4.8**	$\mathbf{7.70\times10^{-7}}$	**0.69**	**2.4**	$\mathbf{5.50\times10^{-4}}$	**0.59**	0.1	5.50×10^{-1}	0.16							**1.73**	$\mathbf{3.50\times10^{-4}}$	**0.41**
5	$\log H/D_s$, $\log R_f$, $\log u_{*i}/w_s$	−3.03	0.07	**−1.35**	$\mathbf{2.30\times10^{-2}}$	**0.55**				0.1	5.40×10^{-1}	0.16				**2.63**	$\mathbf{6.00\times10^{-4}}$	**0.65**	**1.74**	$\mathbf{3.80\times10^{-4}}$	**0.41**
6	$\log R_p$, $\log H/D_s$, $\log R_f$, $\log u_{*i}/w_s$	−1.75	0.25	−25.88	4.30×10^{-1}	32.06	17.04	4.50×10^{-1}	22.26	0.08	6.40×10^{-1}	0.17				−16.12	5.20×10^{-1}	24.5	**1.65**	$\mathbf{9.80\times10^{-4}}$	**0.43**
7	$\log u_{*i}/w_s$	7.45	0.09	**−2.83**	$\mathbf{5.80\times10^{-17}}$	**0.13**													0.22	3.00×10^{-1}	0.2
8	$\log H/D_s$	8.46	0.12	**−2.47**	$\mathbf{2.00\times10^{-4}}$	**0.56**				−0.09	6.70×10^{-1}	0.2									
9	$\log R_p$, $\log R_f$	8.53	0.25	−56.12	1.70×10^{-1}	39.11	37.18	1.90×10^{-1}	27.18							−40.56	1.90×10^{-1}	29.72			
10	$\log R_p$	8.56	0.1	**−2.74**	$\mathbf{1.90\times10^{-17}}$	**0.12**	0.09	7.70×10^{-1}	0.3												
11	$\log R_f$	8.57	0.1	**−2.61**	$\mathbf{6.80\times10^{-8}}$	**0.34**										0.09	7.80×10^{-1}	0.33			
12	$\log H/D_s$, $\log u_{*i}/w_s$	9.32	0.12	**−2.64**	$\mathbf{1.70\times10^{-4}}$	**0.58**				−0.07	7.40×10^{-1}	0.2							0.21	3.20×10^{-1}	0.21
13	$\log R_p$, $\log H/D_s$, $\log R_f$	10.15	0.46	−58.09	1.60×10^{-1}	39.89	38.77	1.80×10^{-1}	27.75	−0.11	5.80×10^{-1}	0.2				−42.3	1.80×10^{-1}	30.35			
14	$\log R_p$, $\log H/D_s$	10.36	0.13	**−2.5**	$\mathbf{2.90\times10^{-4}}$	**0.58**	0.09	7.80×10^{-1}	0.31	−0.09	6.80×10^{-1}	0.21									
15	$\log H/D_s$, $\log R_f$	10.37	0.13	**−2.38**	$\mathbf{1.50\times10^{-3}}$	**0.66**				−0.09	6.80×10^{-1}	0.21				0.09	7.90×10^{-1}	0.34			

Table 9: The value of variance inflation factor (VIF) of candidates models in turbidity current.

Model No.	VIF		
	$\log u_{*i}/w_s$	$\log R_f$	$\log R_p$
1	6.089		6.089
2	6.158	6.158	

the significant level of 0.05. Whereas only the model No.1 and 2 were candidates as the best model. The value of CV in both two models are 0.06, and the value of AIC in the two models are −4.78, −4.57, respectively. The VIF of two models were shown in Table 9. Both model uses the two dimensionless variales, and takes the form:

$$\text{Model No.1}: \; E_s = 10^{-4.46} R_{\mathrm{p}}^{2.31} \left(\frac{u_{*\mathrm{i}}}{w_{\mathrm{s}}} \right)^{1.67} \quad , \tag{52}$$

$$\text{Model No.2}: \; E_s = 10^{-1.14} R_{\mathrm{f}}^{2.52} \left(\frac{u_{*\mathrm{i}}}{w_{\mathrm{s}}} \right)^{1.67} \quad . \tag{53}$$

In the two models, both the value of VIF approximate to 6 that is below the criterion of the multicollinearity.

The model selection method based on AIC suggest the model 1 as the best model. However, considering the dataset of turbidity current was using the light particles with very small grain-size range, the model 2 which uses parameter R_{f} may show a better prediction for larger grain-size case. In both models, it was indicated that the exponent of $u_{*\mathrm{i}}/w_{\mathrm{s}}$ was 1.67 in both model, which is obviously smaller than that in open channel flow type.

6.3 Result of non-uniform sediment

Total 118 data of non-uniform grains was analyzed into 7 models. The relationship between the observed entrainment rate c_{ae} and each parameters was shown in Figure 12. The observed concentration of suspended particles at $0.05H$ of the flow are in the range of 10^{-5}–10^{-1}. The parameters of proportion of ith size grains at bed P_i are in the range from 10^{-2}–10, the dimensionless relative grain-size D_i/D_{50} are in the range from 10^{-1}–1, the coefficient of grain-size deviation λ are around a value of 0.8. It is obvious that the dimensionless parameter P_i reveal a primary correlation to entrainment rate.

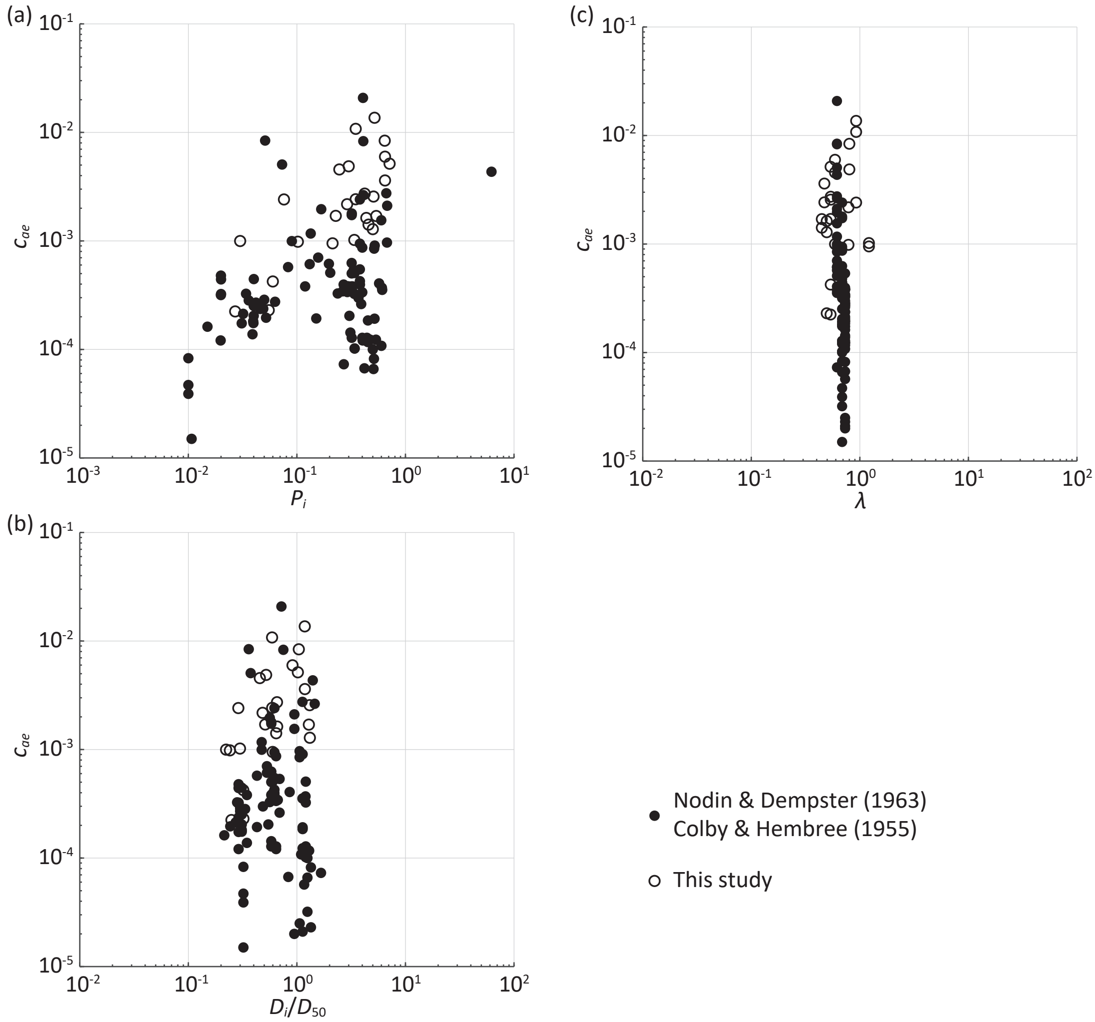

Fig. 12: The relationship between each parameters and the measured value of near-bed concentration with non-uniform sediment. Figure 12(a)(b)(c) represent the correlation between near-bed concentration and dimensionless relative grain-size D_i/D_{50}, the proportion of ith size grains at bed P_i, the coefficient of grain-size deviation λ, respectively.

As described above, the statistical analysis of non-uniform sediment was conducted based on the combined datasets pertaning to both types of flows, because number of datasets pertaining to turbidity currents are too small to analyze independenty. The details of each model was shown in Table 10.

Based on the entrainment rate function for uniform grains, the combination of the three parameters P_i, D_i/D_{50} and λ produced 7 models. The values of AIC of model No.1, 2, 3, and 4 show narrow range, and these model were all containing the parameter P_i, which shows significance of P_i for estimating the entrainment rate of individual grain-size classes. The model No.4 used only P_i, and No.6, 7 used individual parameter of D_i/D_{50}, λ, respectively. The value of CV suggests that model No.4 using one parameter of P_i with a exponent of 1.24 is best model for predicting, whereas the AIC of other models suggest different estimation.

The result suggested that new empirical function for non-uniform grains follow the relationship as:

$$\text{Model No.4}: \; E_{s,i} = E_{s,uni} P_i^{1.24} \quad , \tag{54}$$

for considering P_i is the primary parameter above all which also has the smallest CV. On the other hand, the relationship can also be suggested as:

$$\text{Model No.1}: \; E_{s,i} = E_{s,uni} P_i^{1.36} \left(\frac{D_i}{D_{50}} \right)^{-0.95} \lambda^{2.50} \quad , \tag{55}$$

for considering the model has smallest AIC.

The result revealed that proportion of each grain-size class on the bed P_i is the primary and only dominant parameter between entrainment rate function from uniform grains applied to non-uniform grains. Under the thought that flow condition gives no influence of bed material proportion, the exponent, standard error and 95% confidence interval of P_i are 1.24, 0.06, [1.12, 1.36], respectively with two types of flow combined condition.

The value of P_i will be always ≤ 1, so the individual value of entrainment rate of each grain-size will not exceed the value of uniform grain-size. If the P_i value is very close to 1, which means the grains-size distribution narrow down to a uniform case, then the value of entrainment rate of non-uniform grain-size particles approach with the uniform grain-size case.

Table 10: The result of multiple regression analysis and information criteria analysis of non-uniform grain-size particles

Model						P_i			D_i/D_{50}			λ		
No.	R^2	AIC	BIC	I_{max}	CV	coef	std.err.	p	coef	std.err.	p	coef	std.err.	p
1	0.808	203.2	211.5	-98.6	0.412	**1.36**	**0.18**	**0.00**	**-0.95**	**0.42**	**0.03**	**2.50**	**0.89**	**0.01**
2	0.799	206.4	211.9	-101.2	0.408	**1.01**	**0.09**	**0.00**				**2.81**	**0.89**	**0.00**
3	0.795	209.1	214.6	-102.6	0.395	**1.62**	**0.16**	**0.00**	**-1.13**	**0.43**	**0.01**			
4	0.782	214.0	216.8	-106.0	0.393	**1.24**	**0.06**	**0.00**						
5	0.711	249.6	255.1	-122.8	0.569				**1.81**	**0.26**	**0.00**	**6.04**	**0.92**	**0.00**
6	0.604	284.5	287.3	-141.3	0.552				**2.97**	**0.22**	**0.00**			
7	0.591	288.4	291.2	-143.2	0.714							**10.41**	**0.80**	**0.00**

Table 11: Comparision between proposed function and previous functions with uniform grain-size particles in open channel flows.

	k	n	AIC	J_{log}
$E_{s,open}$	3	79	47.80	8.97
E_s (Garcia and Parker, 1991)	2	79	92.13	13.41
E_s (Dorrell et al., 2018)	3	79	98.26	13.95
E_s (van Rijn, 1984)	3	79	112.81	16.77

Table 12: Comparision between proposed function and previous functions with uniform grain-size particles in turbidity currents.

	k	n	AIC	J_{log}
$E_{s,turbi}$	2	25	-4.57	1.76
E_s (Garcia and Parker, 1993)	2	25	61.86	12.58
E_s (Dorrell et al., 2018)	3	25	63.38	11.80
E_s (van Rijn, 1984)	3	25	53.75	8.03

6.4 Comparison of new function with previous study

The empirical functions of entrainment rate proposed in previous study were analyzed with this new function. The statistical criterion value between observation and prediction was calculated, by sum of squared residuals (the value between empirical function of E_s and observed equilibrium near-bed concentration c_{ae} in logrithmic form J_{log}) and AIC.

With regard to the open channel flow condition with uniform grains, the fuction proposed in this study shows the best performance comparing to previous studies. Although prediction of three pre-existing function shows relatively good fittness with the observation, predictions by Dorrell et al. (2018) and van Rijn (1984) represent a overestimating trend (Figure 13). The statistical criterion value of AIC and J_{log} in each estimation was under inspected (Table 11). The value of AIC in the new function (Equation 51), Garcia function (Equation 20), Dorrell function (Equation 19) and van Rijn function (Equation 15) are 47.80, 92.13, 98.26, and 112.81, respectively. The J_{log} value of the four functions are 8.97, 13.41, 13.95, and 16.77, respectively.

With regard to the turbidity current condition with uniform grains, the newly proposed function here also shows the best performance comparing to previous three functions, whereas all predictions including this study show larger deviation from observed values (Figure 14). The statistical criterion value of AIC and J_{log} in each estimation was under

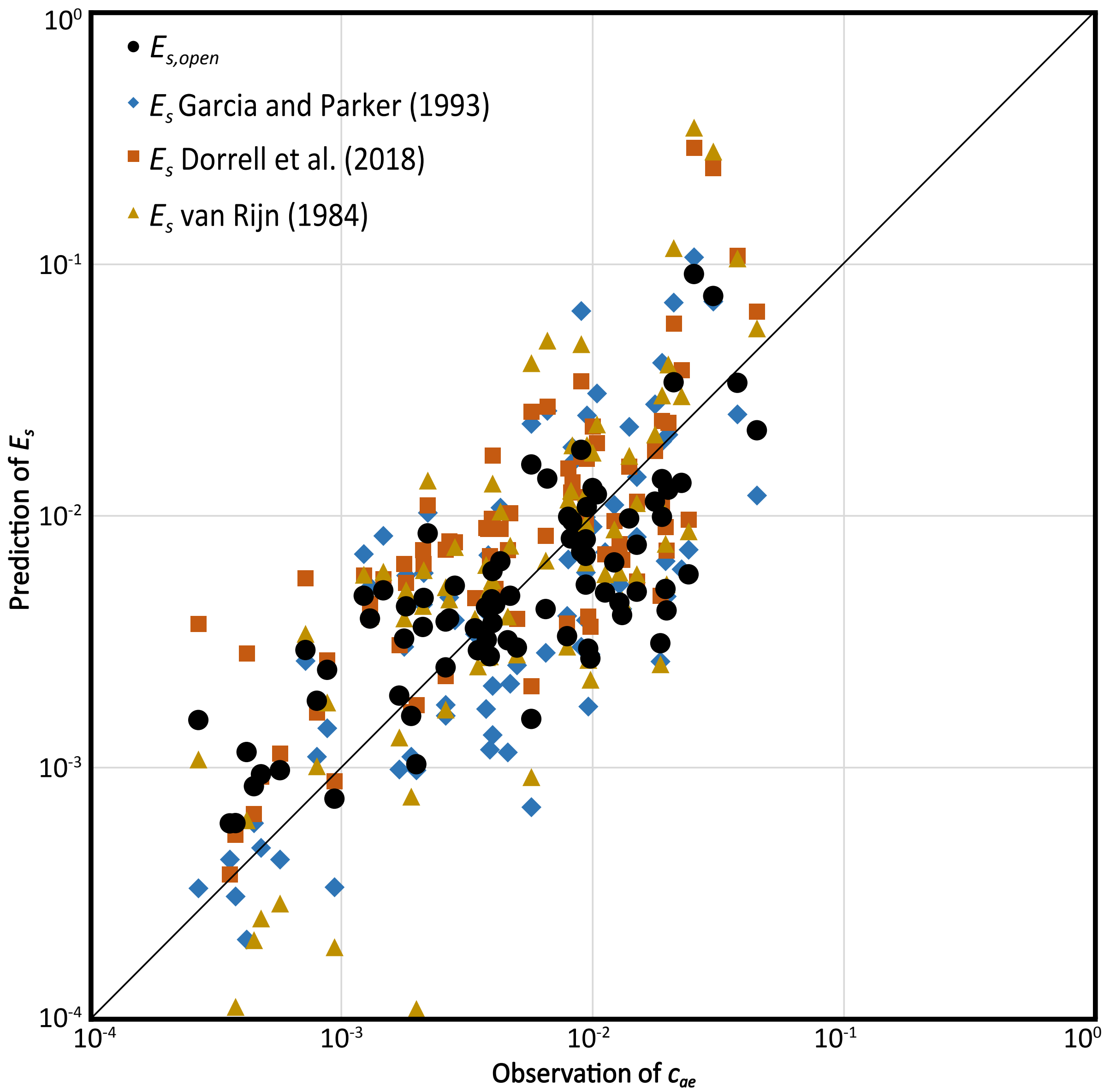

Fig. 13: Comparision between proposed function and previous functions with uniform grain-size particles in open channel flows.

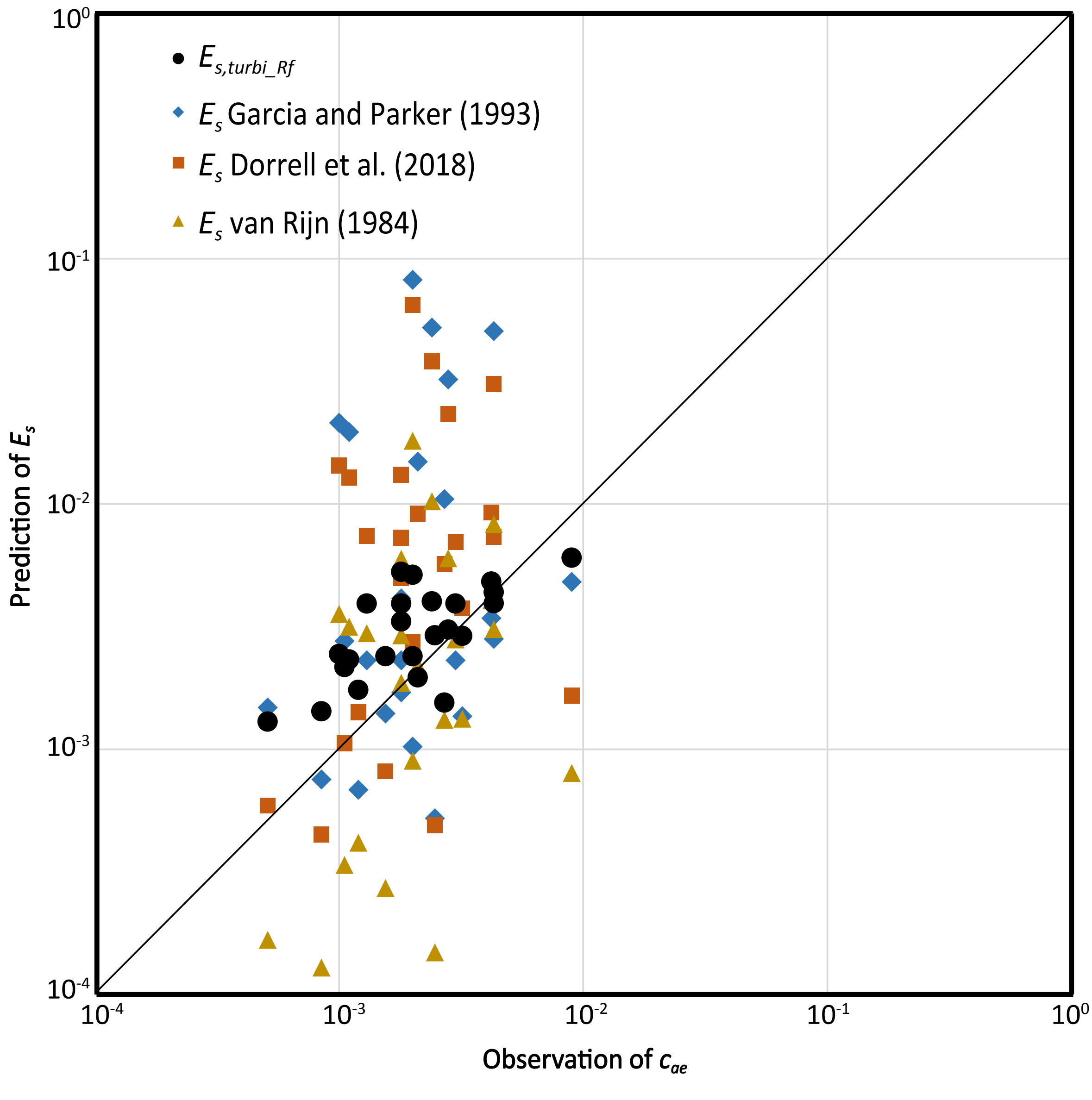

Fig. 14: Comparision between proposed function and previous functions with uniform grain-size particles in turbidity currents.

Table 13: Comparision between proposed function and previous functions with non-uniform grain-size particles.

	k	n	AIC	J_{log}
E_{si}	2	118	214.0	44.2
E_{si} (Elhakeem and Sattar, 2015)	5	118	356.4	128.7
E_{si} (Dorrell et al., 2018)	3	118	311.1	91.5
E_{si} (Wright and Parker, 2004)	4	118	286.2	71.8

inspected (Table 12). The value of AIC in the new function (Equation 53), Garcia function (Equation 20), Dorrell function (Equation 19) and van Rijn function (Equation 15) are −4.57, 61.86, 63.38, and 53.75, respectively. The J_{log} value of the four functions are 1.76, 12.58, 11.80, and 8.03, respectively. The questions in this fitness is discussed In Section 7.

In the non-uniform grain-size case, the new function (Equation 55) obtained from dataset that combined two types of flow was compared with the pre-existing empirical functions from Elhakeem (Equation 26), Dorrell (Equation 19) and Wright (Equation 24).

From comparison result of all functions, the new empirical function suggested a better estimation of entrainment rate judging from the values of information criterion (Table 13). The prediction value of this function with non-uniform grains agreed the observation value better than previous research both in open channel flows and turbidity currents (Figure 15).

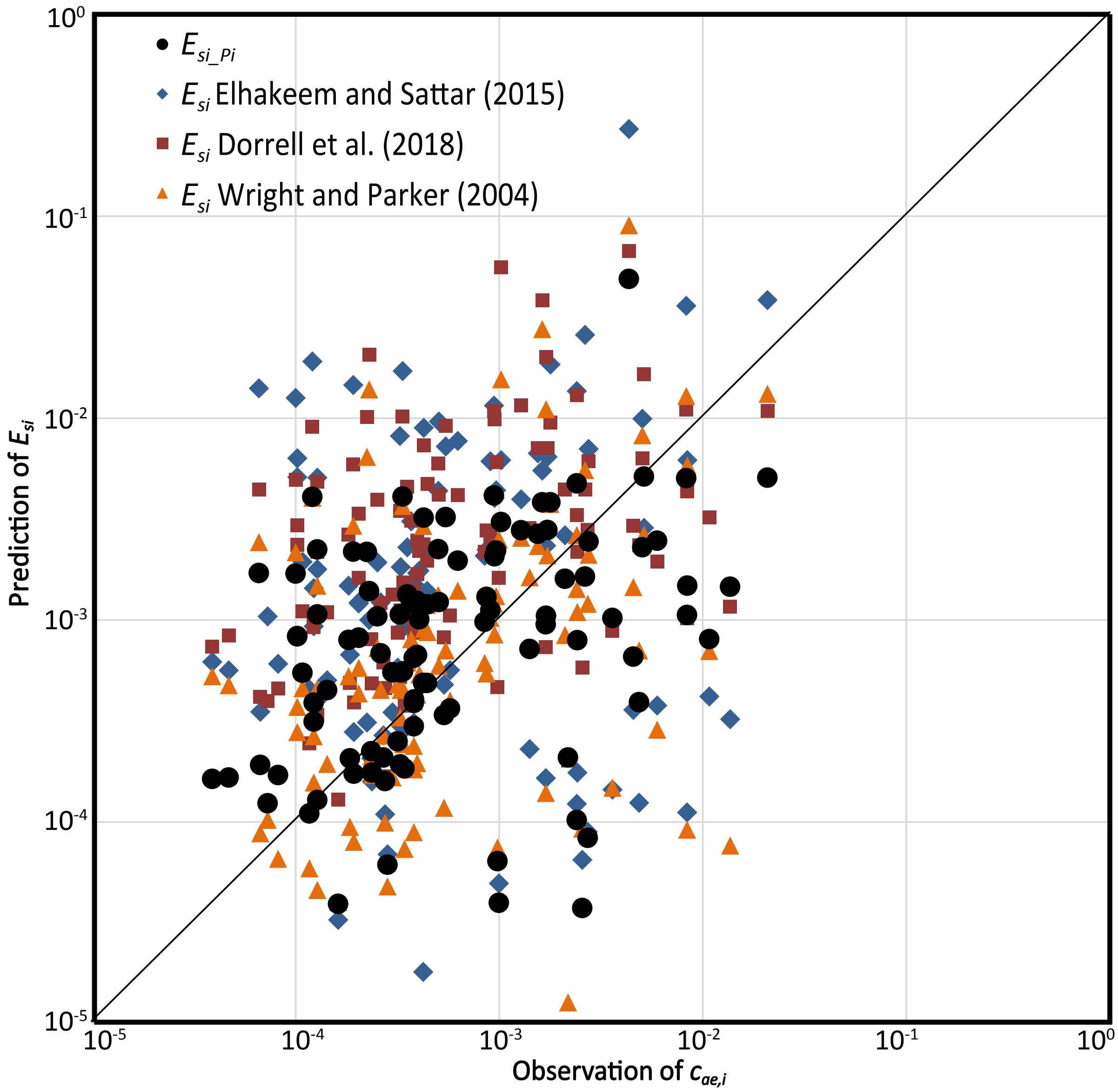

Fig. 15: Comparision between proposed function and previous functions with non-uniform grain-size particles.

7 Discussion

7.1 Comparison of the entrainment function for open-channel flows with previous studies

Comparing to previous studies, this research is characterized by the automated selection of the combinations of model input variables by using the information criteria. It was indicated that the new function of entrainment rate in open channel flows show the better fitness between the observed value of near-bed concentration and the predicted entrainment rates than previous studies (Figure 13). In this study, the residuals from the prediction are evenly distributed above and below in any value range (Figure 13). In contrast, the function of Dorrell et al. (2018) have an overestimation in all range of c_{ae}. The functions of Garcia and Parker (1991, 1993) and van Rijn (1984) are less biased, but they show larger variance than the function proposed in this study. The AIC also represents that the new funcion of $E_{s,open}$ has the better generalized performance. In summary, the new function can be expected to provide more precise predictions of entrainment rates for unknown data above all the other existing functions.

It is also noteworthy that the approach of this study can be easily improved when additional data set becomes available. Since the selection of significant model variables are not arbitrarily chosen in this study. In the previous research, the selection of variables were depended on insights of researchers with trials and errors that requires larger efforts to researchers. In contrast, automated approach of this study is promising to be more efficient for future expansion to unknown variables and data sets.

7.2 Physical significance of input variables chosen in the new functions

The new function proposed in this study was established by purely empirical approach, but dimensionless variables chosen by the model selection provides several insights to consider governing factors of the sediment entrainment process. First, the primary variable for predicting entrainment rate was the dimensionless competence shear velocity $u_{*\mathrm{i}}/w_{\mathrm{s}}$. This variable was adopted in all of the empirical functions of previous research, but its exponent was highly variable. The exponent of $u_{*\mathrm{i}}$ ranges from 3 to 10 fixed in existing functions (Akiyama & Fukushima, 1985; Parker et al., 1987; Garcia & Parker, 1991; Izumi et al., 2003). The force balance theory predicted that the value 3 is appropriate for estimating capacity of suspension (Celik & Rodi, 1991; Garcia, 2008; Dorrell et al., 2018), but it was not proved that this value is effective also for the entrainment rate at the specific reference level in the flow. The result of this study proposed that the exponent of $u_{*\mathrm{i}}$ is roughly 2.8, which is close to this physical prediction. Thus, the result of this study provides a supportive evidence to the force-balance theory. Also, this physical plausibility may give possibility of validity of the function even when it is applied to the condition that is out of the range of observational data.

Also, the exponents of $u_{*\mathrm{i}}$ in the new functions of open channel flow and turbidity current were largely different. Although the cause of difference in entrainment rates is unknown, this result may be attributed to difference in the vertical profile of flow velocity between different flow types. The result of this study casts a question about the applicability of the function established from the open channel data to the turbidity currents.

Secondly, it was revealed that the entrainment models using H/D_s or S_e tend to be selected by the information criteria, that is, the flow height H is also an influential variable on sediment entrainment rate. In some previous research, the flow thickness was excluded from the input variables of the function (Akiyama & Fukushima, 1985; Parker et al., 1987; Garcia & Parker, 1991), or fixed at -1 (Dorrell et al., 2018). Again, this highlights the difference between open channel and density flows. In turbidity current where water entrainment at the surface between the flow and ambient water occurs, it is hard to decide the clear boundary between them. If based on the logrithmic relationship between $u_{*\mathrm{i}}$ and U, the H should be valued by the distance from bed to the horizon of the velocity maximum.

Thirdly, the variable R_f tends to be judged better than R_p in the model selection. Particle Reynolds number R_p is not appropriate for considering the parametric space wider than the datasets, because the value of R_p grows extremely large value as grain diameter increases. In contrast, the variable R_f has advantage in extending the entrainment rate function in all grain-size without overestimate. The particle Reynolds number was widely used in many fields, but it will generate contradiction in predicting the sediment entrainment. On the other hand, R_f makes a more smooth fitness of entrainment rate, especially in the gravel regime of grains (Figure 16 and Figure 17) .

In previous studies, it was suggested that E_s positively correlates with R_p (Garcia & Parker, 1991; Wright & Parker, 2004a), which generated a paradox that the larger grains are entrained at higher rate. The new function E_s that is correlated to R_f solve this problem

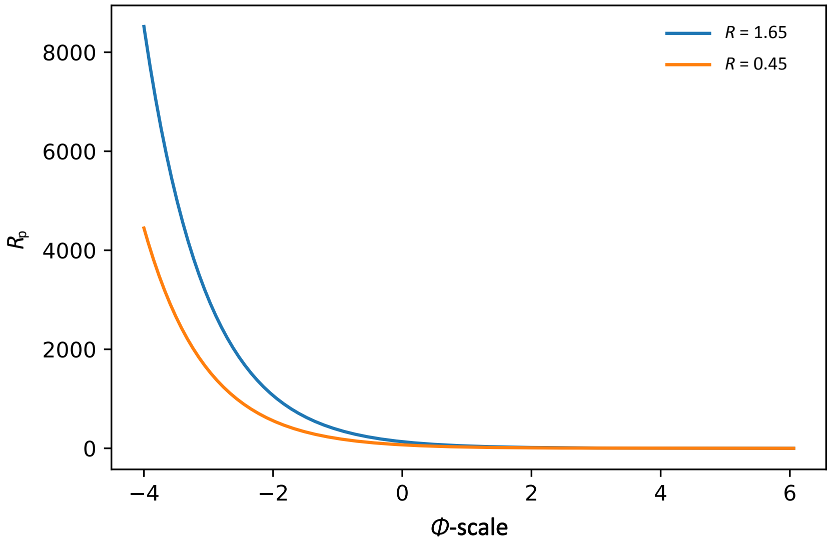

Fig. 16: The difference between R_p and R_f with the dimensionless density at 1.65 and 0.45 under 20°C.

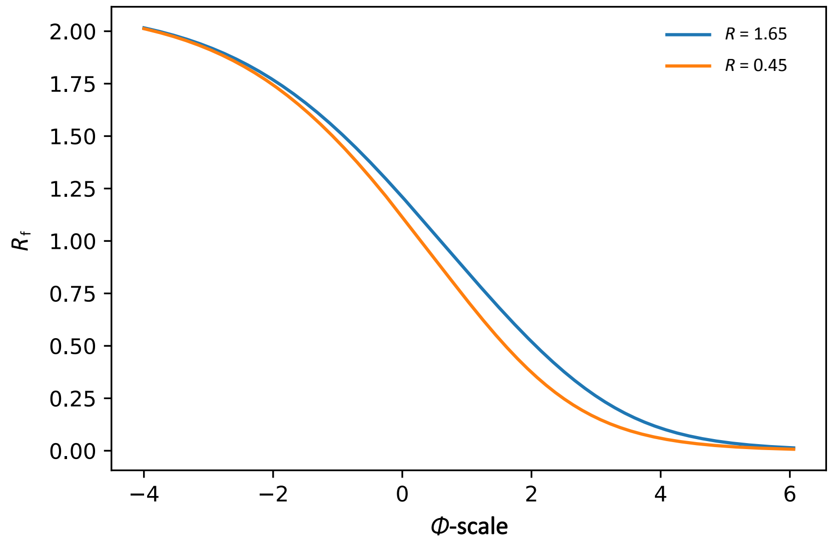

Fig. 17: The difference between R_p and R_f with the dimensionless density at 1.65 and 0.45 under 20°C.

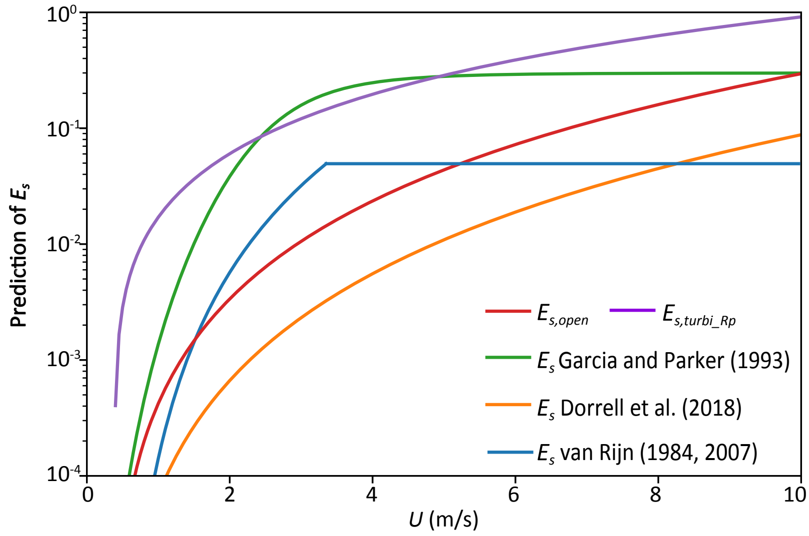

Fig. 18: The empirical functions of uniform grain-size particles under the conditions of D = 0.2 mm, H = 5 m, at 20°C. The prediction of entrainment rate in turbidity current condition used Equation 52.

because R_{f} becomes nealy constant as grain size becomes larger. Also, this is not supportive to the thought that grain-size has no influence on entrainment rates of suspension (Eggenhuisen et al., 2017).

7.3 Application of the new function to natural flows

When the empirical functions are applied to conditions in wider range in velocity, most of previous functions predict extremely large entrainment rates (Figure 18, Figure 19). Compared with the pre-existing functions, however, the new function of $E_{s,open}$ shows a reasonable values smaller than the function proposed by Garcia and Parker (1991), whereas it shows a parallel curve to the function proposed by Dorrell et al. (2018). The function of van Rijn (2007) showed a similarity to the prediction of Garcia and Parker (1991) with a smaller value. As a summary, the entrainment rate will take a maximum value of 0.3 and 0.05 even the flow velocity less than 4 m/s, based on the empirical function of Garcia and Parker (1993); van Rijn (2007), respectively. On the other hand, new function from this study and the prediction of Dorrell et al. (2018) shows a smooth curve along flow velocity.

On the other hand, the dataset of turbidity current was in a very small range of flow

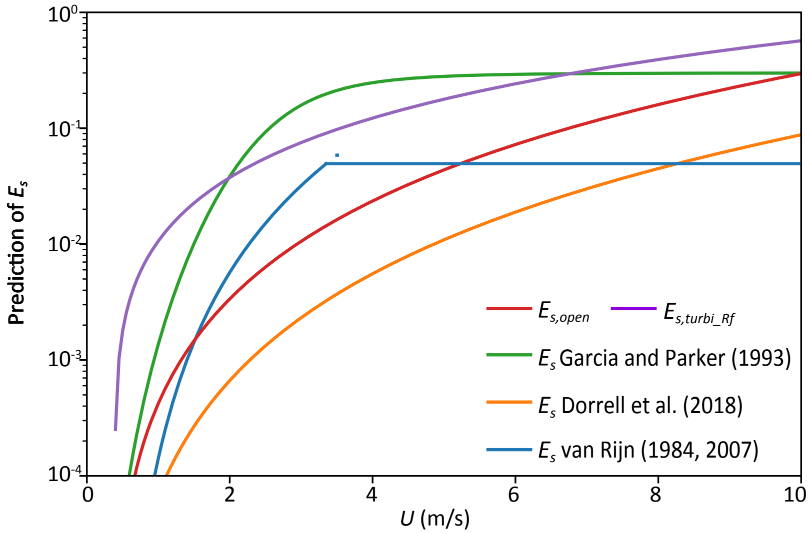

Fig. 19: The empirical functions of uniform grain-size particles under the conditions of D = 0.2 mm, H = 5 m, at 20°C. The prediction of entrainment rate in turbidity current condition used Equation 53.

velocity (< 30 cm/s), and the entrainment rate of particles was obviously larger than the predictions from previous research in this regime. The entrainment rate function shows a smaller value of which using R_{f} than using R_p.

The relationship between predicted entrainment rate and grain-size of uniform particles was shown in Figure 20 and Figure 21. It is obvious that the new function has similar value and trend with the empirical function proposed by Dorrell et al. (2018) in open channel flow type.

Under a certain condition (U = 1 m/s, H = 0.5 m, at 20°C), the function of van Rijn (2007) suggested that only the particles smaller than 1.7 ϕ can be entrained, and the flow concentration maitains 0.002 even particle grain-size close to silt size. The empirical prediction of Garcia and Parker (1993) suggested the minimum value of entrainment rate at 0.001 by the grain-size around roughly 1.2 ϕ. However, no matter the particles grain-size bigger or smaller than 1.2 ϕ, the value of entrainment rate will increase, even the particles grain-size close to gravel size.

On the other hand, the prediction of entrainment rate in turbidity current from Equation 52 used R_p shows a value more than 1 in the grain-size range from -0.5 to -1.8 ϕ, which

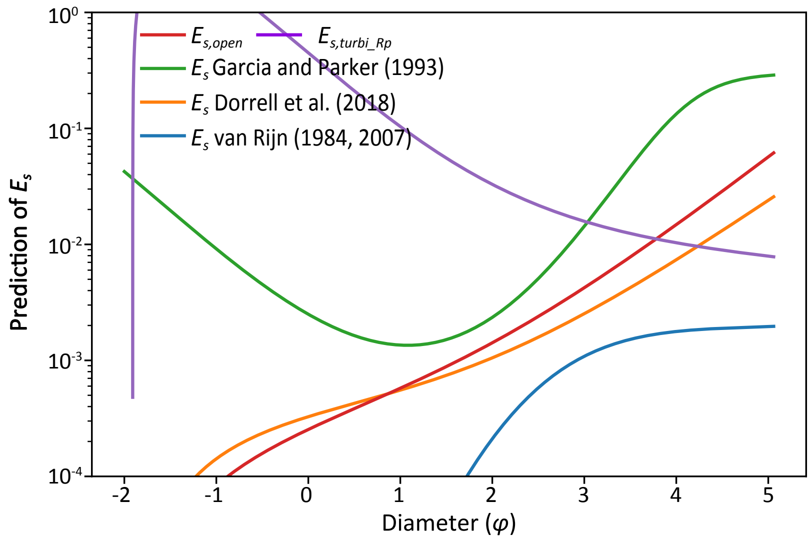

Fig. 20: The empirical functions of uniform grain-size particles in a grain-size range under the conditions of U = 1 m/s, H = 0.5 m, at 20°C. The prediction of entrainment rate in turbidity current condition used Equation 52.

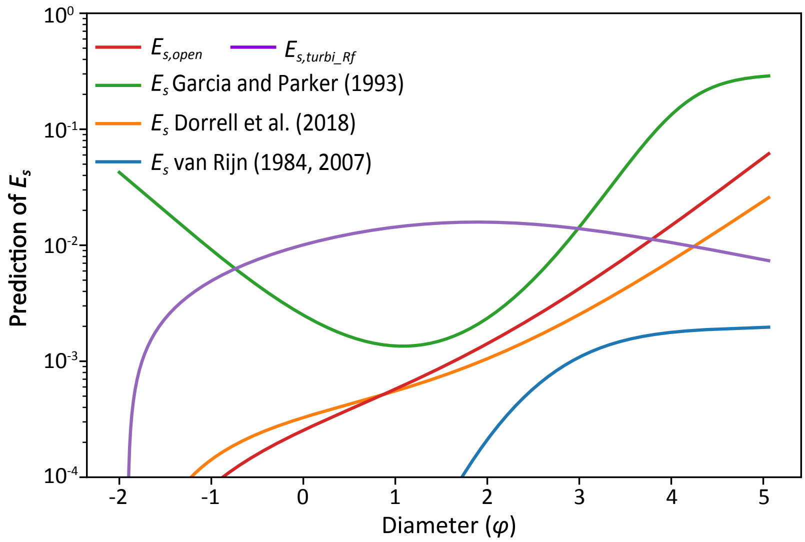

Fig. 21: The empirical functions of uniform grain-size particles in a grain-size range under the conditions of U = 1 m/s, H = 0.5 m, at 20°C. The prediction of entrainment rate in turbidity current condition used Equation 53.

is totally impossible. The Equation 53 used R_f shows a reasonable prediction for particles bigger than 0 ϕ. The predicted flow concentration has a maximum value around 0.02 for grain-size in 0–4 ϕ range, which is also rational.

Applicability of the new function in wider range of grain-size distribution may make it possible to develop the morpohdynamic models of sediment sorting for considering transition from gravel-bed to sand bed rivers. This phenomenon was interpreted to relate to onset of deposition of suspended load, but the modeling was difficult because the previous function cannot be applied to the mixture of sand and gravels. Also, the new function provides physically plausible estimates for very high-velocity flows without any artificial thresholds, suggesting that it is appropriate to apply destructive flows such as tsunamis or megafloods.

7.4 Future task

The problem in the entrainment function proposed here is the narrow range of the observed parameters u_{*i}/w_s, which is not enough to apply for suspended loads in a large-scale flow such as tsunamis or turbidity currents. Especially in turbidity currents cases, it is difficult to perform experiments with very large or small entrainment rates of particles due to limitation of experiment facilities. Therefore, the entrainment rates in turbidity currents cases have a very small range (from 10^{-3}–10^{-2} in measurement), and the relationship between entrainment rates and u_{*i}/w_s was ambiguous. Thus, the extrapolation of the empirical function is currently inevitable for such purposes. To this end, it is necessary to conduct in-situ measurements of turbidity currents or tsunamis with highly accurate facilities for sediment concentration.

8 Summary

Multiple regression analysis with model selection using the information criteria and cross-validation were used to establish new entrainment functions for predicting entrainment rate of suspended load. The new functions show the better fit to the observation than previous studies, as well as the variables completely employed in the function provides several insights for understandings of entrainment processes. The result shows that the dimensionless competence shear velocity $u_{*\mathrm{i}}$ and the dimensionless settling velocity R_f as well as the dimensionless flow height H/D_s have the dominant influence on the entrainment. The empirical exponent of the shear velocity confirmed the theoretical assumptions of the force-balance model of suspended load.

In addition, result of this study suggests that the function cannot directly expand from open channel flows to turbidity currents. Statistical analysis indicated difference in trends of entrainment between two types of flows. The new function resolved the questions in previous research, and gives a statistical answer which is still reasonable and consistent between different types of flows and grains.

Acknowledgments

I would like to express my sincere gratitude to my advisor, Prof. Hajime Naruse of the Kyoto University, Department of Earth and Planetary Sciences, for his continuous support and encouragement of my Ph.D study. His guidance has been an indispensable force in enlightening and motivating me during my time of research and writing of this thesis. His advice on both my research and my career has been invaluable.

My gratitude must also go to Prof. Takao Ubukata, who provided me with insightful comments and constructive criticisms on the statistical analysis of my data throughout my Ph.D studies. The tough questions always incented me to widen my knowledge and perspective.

I deeply appreciate the work of Koji Ohata and Kei Wakamori, who provided me with valuable suggestions on the composition and visual representation of my thesis. I would like to thank Dr. Kazuki Kikuchi and Zhirong Cai for aiding me during experiments and supporting me during my thesis writing.

My acknowledgement also goes to my labmates for the stimulating discussions during seminars and for their help along the way of my Ph.D studies.

The reference in this paper was under APA style.

References

Akiyama, J., & Fukushima, Y. (1985). Entrainment of noncohesive bed sediment into suspension. In *Third international symposium on river sedimentation* (pp. 804–813).

Ashida, K., & Michiue, M. (1964). Laboratory study of suspended load discharge in alluvial channels. In *Disaster prevention research institute annuals, (10).*

Ashida, K., & Okabe, T. (1982). On the calculation method of the concentration of suspended sediment under non-equilibrium condition. In *Proceedings of the japanese conference on hydraulics* (Vol. 26, pp. 153–158).

Bagnold, R. A. (1966). *An approach to the sediment transport problem from general physics*. US government printing office.

Barton, J., & Lin, P. (1955). A study of the sediment transport in alluvial streams. *Civil Engineering Department Report*.

Brooks, N. H. (1954). *Laboratory studies of the mechanics of streams flowing over a movable bed of fine sand* (Unpublished doctoral dissertation). California Institute of Technology.

Cantero, M. I., Cantelli, A., Pirmez, C., Balachandar, S., Mohrig, D., Hickson, T. A., Yeh, T., Naruse, H., & Parker, G. (2012). Emplacement of massive turbidites linked to extinction of turbulence in turbidity currents. *Nature Geoscience*, *5*(1), 42–45.

Cartigny, M. J., Eggenhuisen, J. T., Hansen, E. W., & Postma, G. (2013). Concentration-dependent flow stratification in experimental high-density turbidity currents and their relevance to turbidite facies models. *Journal of Sedimentary Research*, *83*(12), 1047–1065.

Celik, I., & Rodi, W. (1991). Suspended sediment-transport capacity for open channel flow. *Journal of Hydraulic Engineering*, *117*(2), 191–204.

Colby, B. R., & Hembree, C. H. (1955). *Computations of total sediment discharge, Niobrara River near Cody, Nebraska*. US Government Printing Office.

Coleman, N. L. (1969). A new examination of sediment suspension in open channels-journ. *Rech. Hyd.(AIRH)-VoL*, *7*.

Coleman, N. L. (1981). Velocity profiles with suspended sediment. *Journal of Hydraulic Research*, *19*(3), 211–229.

Dorrell, R., Amy, L., Peakall, J., & McCaffrey, W. (2018). Particle size distribution controls the threshold between net sediment erosion and deposition in suspended load dominated flows. *Geophysical Research Letters*, *45*(3), 1443–1452.

Eggenhuisen, J. T., Cartigny, M. J., & de Leeuw, J. (2017). Physical theory for near-bed turbulent particle suspension capacity. *Earth surface dynamics.*, *5*(2), 269–281.

Einstein, H. A. (1955). Effect of heavy sediment concentration near the bed on velocity and sediment distribution. *MRD Series*(8).

Elhakeem, M., & Sattar, A. M. (2015). An entrainment model for non-uniform sediment. *Earth Surface Processes and Landforms*, *40*(9), 1216–1226.

Engelund, F., & Fredsøe, J. (1976). A sediment transport model for straight alluvial channels. *Hydrology Research*, *7*(5), 293–306.
Ferguson, R., & Church, M. (2004). A simple universal equation for grain settling velocity. *Journal of sedimentary Research*, *74*(6), 933–937.
Garcia, M. H. (2008). Sediment transport and morphodynamics. In *Sedimentation engineering: Processes, measurements, modeling, and practice* (pp. 21–163).
Garcia, M. H., & Parker, G. (1991). Entrainment of bed sediment into suspension. *Journal of Hydraulic Engineering*, *117*(4), 414–435.
Garcia, M. H., & Parker, G. (1993). Experiments on the entrainment of sediment into suspension by a dense bottom current. *Journal of Geophysical Research: Oceans*, *98*(C3), 4793–4807.
Gibbs, R. J. (1974). A settling tube system for sand-size analysis. *Journal of Sedimentary Research*, *44*(2), 583–588.
Graf, W., & Cellino, M. (2002). Suspension flows in open channels; experimental study. *Journal of hydraulic research*, *40*(4), 435–447.
Hubbell, D. W., & Matejka, D. Q. (1959). *Investigations of sediment transportation, Middle Loup River at Dunning, Nebraska: With application of data from turbulence flume*. Geological Survey (U.S.).
Ismail, H. M. (1952). Turbulent transfer mechanism of suspended sediment in closed channels. *Trans. ASCE*, *117*, 1–26.
Izumi, N., Tanaka, H., Tsuboi, K., & Date, M. (2003). Inceptive topography of fluvial-dominated river mouth terraces: Experiments. In *Doboku gakkai ronbunshu* (Vol. 2003, pp. 109–120). Japan Society of Civil Engineers.
Jordan, P. R. (1965). *Fluvial sediment of the mississippi river at st. louis, missouri*. US Government Printing Office Washington, DC.
Kalinske, A. A., & Pien, C. (1943). Experiments on eddy-diffusion and suspended-material transportation in open channels. *Eos, Transactions American Geophysical Union*, *24*(2), 530–536.
Kostic, S., & Parker, G. (2006). The response of turbidity currents to a canyon–fan transition: internal hydraulic jumps and depositional signatures. *Journal of Hydraulic Research*, *44*(5), 631–653.
Lauer, J. W., & Parker, G. (2008). Modeling framework for sediment deposition, storage, and evacuation in the floodplain of a meandering river: Theory. *Water Resources Research*, *44*(4), W04425.
Lawler, J., Parker, J., Anderson, L., & Fitzsimmons, W. (1977). Nanosecond time-resolved spectroscopy of the n= 2 levels in a high-pressure he discharge. *Physical Review Letters*, *39*(9), 543.
Lyn, D. A. (1987). *Turbulence and turbulent transport in sediment-laden open-channel flows* (Unpublished doctoral dissertation). California Institute of Technology.
Ma, H., Nittrouer, J., Naito, K., Fu, X., Zhang, Y., Moodie, A., Wang, Y., Wu, B., & Parker, G. (2017). The exceptional sediment load of fine-grained dispersal systems: Example of the yellow river, china. *Science advances*, *3*(5), e1603114.
Middleton, G. (1993). Sediment deposition from turbidity currents. *Annual review of earth and planetary sciences*, *21*(1), 89–114.

Montes, J. S., & Ippen, A. T. (1973). *Interaction of two-dimensional turbulent flow with suspended particles*. Ralph M. Parsons Laboratory for Water Resources and Hydrodynamics.

Naruse, H. (2005). Usage and advantages of an application program Stube for settling tube grain-size analysis. *Journal of the Sedimentological Society of Japan*, *62*(62), 55–61.

Nordin, C. F., & Dempster, G. R. (1963). *Vertical distribution of velocity and suspended sediment, middle rio grande, new mexico*. US Government Printing Office.

Parker, G., Fukushima, Y., & Pantin, H. M. (1986). Self-accelerating turbidity currents. *Journal of Fluid Mechanics*, *171*, 145–181.

Parker, G., Garcia, M., Fukushima, Y., & Yu, W. (1987). Experiments on turbidity currents over an erodible bed. *Journal of Hydraulic Research*, *25*(1), 123–147.

Rouse, H. (1937). Modern conceptions of the mechanics or fluid turbulence. *Transactions of the American Society of Civil Engineers*, *102*(1), 463–505.

Sarre, R. (1987). Aeolian sand transport. *Progress in Physical Geography*, *11*(2), 157–182.

Sequeiros, O. E., Spinewine, B., Beaubouef, R. T., Sun, T., García, M. H., & Parker, G. (2010). Characteristics of velocity and excess density profiles of saline underflows and turbidity currents flowing over a mobile bed. *Journal of Hydraulic Engineering*, *136*(7), 412–433.

Smith, J. D., & McLean, S. (1977). Spatially averaged flow over a wavy surface. *Journal of Geophysical research*, *82*(12), 1735–1746. doi: 10.1029/JC082i012p01735

Soulsby, R. (1997). *Dynamics of marine sands: a manual for practical applications*. Thomas Telford.

Straub, L. G., Anderson, A., & Flammer, G. (1958). *Experiments on the influence of temperature on the sediment load* (No. 10). US Army Engineer Division, Missouri River.

Syvitski, J. P., Vorosmarty, C. J., Kettner, A. J., & Green, P. (2005). Impact of humans on the flux of terrestrial sediment to the global coastal ocean. *Science*, *308*(5720), 376–380.

Toffaleti, F. (1968). *A procedure for computation of the total river sand discharge and detailed distribution, bed to surface.* Corps pf Engineers, U.S.Army.

van Rijn, L. C. (1984). Sediment transport, part II: suspended load transport. *Journal of hydraulic engineering*, *110*(11), 1613–1641.

van Rijn, L. C. (2007). Unified view of sediment transport by currents and waves. II: Suspended transport. *Journal of Hydraulic Engineering*, *133*(6), 668–689.

Vanoni, V. A., & Nomicos, G. N. (1960). Resistance properties of sediment-laden streams. *Transactions of the American Society of Civil Engineers*, *125*(1), 1140–1167.

Wright, S., & Parker, G. (2004a). Density stratification effects in sand-bed rivers. *Journal of Hydraulic Engineering*, *130*(8), 783–795.

Wright, S., & Parker, G. (2004b). Flow resistance and suspended load in sand-bed rivers: simplified stratification model. *Journal of Hydraulic Engineering*, *130*(8), 796–805.

Appendix

Experimental data sets

Two kinds of tables were shown in this appendix.

In individual experiment, the first type of table shows the mass information of samples from mixing-tank and each layer of siphon. M_c, M_s, and M_d denote the mass of container, suspension with container, dried sediment with container, respectively. c (wt%) and c (vol%) indicate the total wight concentration and total volumetric concentration.

The second type of table shows the volumetric concentration c (vol%) at different elevation z of flow in each grain-size range. As an explanation, the concentration value of a given grain-size describes the interval before its grain-size. For example, in Appendix Table 2 the value of volumetric concentration under 3 ϕ at z = 0 is 0.86, which means the volumetric concentration between 2.8 ϕ–3 ϕ at z = 0 is 0.86%.

Table 1: Data of mass information and calculated value of total concentration in Run 1.

	Tank	Vertical Elevation z (cm)						
	Sample	0	2	4	6	11	16	21
M_c (g)	137.0	6.60	6.60	6.60	6.60	6.60	6.60	6.60
M_s (g)	334.3	143.8	144.5	136.0	135.9	139.7	138.7	153.0
M_d (g)	149.17	12.80	10.72	10.01	9.60	9.26	8.00	7.68
c (wt%)	6.168	4.519	2.988	2.635	2.320	1.998	1.060	0.738
c (vol%)	4.337	3.161	2.080	1.832	1.612	1.387	0.733	0.510

Table 2: Data of volumetric concentration at each elevation in different grain-size range in Run 1.

z (cm)	Grain size (Φ -scale)																								
	0	0.2	0.4	0.6	0.8	1	1.2	1.4	1.6	1.8	2	2.2	2.4	2.6	2.8	3	3.2	3.4	3.6	3.8	4	4.2	4.4	4.6	4.8	5
0	0.03	0.00	0.00	0.00	0.03	0.00	0.02	0.00	0.02	0.00	0.02	0.02	0.03	0.19	0.64	0.86	0.49	0.30	0.16	0.11	0.10	0.08	0.06	0.05	0.03	0.03
2	0.00	0.00	0.00	0.00	0.02	0.00	0.00	0.00	0.02	0.00	0.00	0.02	0.02	0.11	0.37	0.57	0.39	0.15	0.15	0.09	0.07	0.07	0.02	0.04	0.04	0.02
4	0.00	0.02	0.00	0.00	0.00	0.00	0.00	0.02	0.00	0.00	0.00	0.03	0.00	0.06	0.26	0.48	0.36	0.18	0.20	0.06	0.08	0.03	0.00	0.09	0.08	0.00
6	0.00	0.00	0.00	0.00	0.02	0.00	0.00	0.02	0.00	0.00	0.00	0.00	0.00	0.07	0.16	0.36	0.41	0.20	0.11	0.07	0.07	0.05	0.03	0.05	0.03	0.03
11	0.00	0.00	0.00	0.00	0.00	0.00	0.00	0.00	0.00	0.00	0.00	0.02	0.00	0.05	0.17	0.28	0.33	0.19	0.09	0.09	0.06	0.05	0.03	0.05	0.02	0.03
16	0.00	0.02	0.00	0.00	0.00	0.00	0.00	0.00	0.00	0.00	0.01	0.00	0.00	0.02	0.03	0.15	0.14	0.11	0.08	0.06	0.04	0.03	0.03	0.02	0.02	0.01
21	0.01	0.00	0.00	0.00	0.00	0.00	0.00	0.01	0.00	0.00	0.00	0.00	0.01	0.00	0.02	0.06	0.11	0.08	0.07	0.04	0.04	0.02	0.02	0.01	0.01	0.01

Table 3: Data of mass information and calculated value of total concentration in Run 2.

	Tank	Vertical Elevation z (cm)											
	Sample	0	1.25	2.5	3.75	5	7.5	10	12.5	15	17.5	20	25
M_c (g)	119.50	118.57	116.07	117.04	118.08	120.43	119.32	117.79	47.75	47.38	47.77	47.34	63.91
M_s (g)	380.14	364.44	332.64	378.35	337.42	414.15	422.02	307.68	158.53	154.99	147.91	145.44	188.60
M_d (g)	134.34	124.85	120.04	121.58	121.53	124.57	122.54	120.26	48.75	47.64	48.00	47.46	64.01
c (wt%)	5.694	2.554	1.833	1.737	1.573	1.410	1.064	1.301	0.903	0.242	0.230	0.122	0.080
c (vol%)	3.997	1.776	1.271	1.205	1.090	0.976	0.736	0.901	0.624	0.167	0.159	0.084	0.055

Table 4: Data of volumetric concentration at each elevation in different grain-size range in Run 2.

z (cm)	Grain size (Φ -scale)																									
	0	0.2	0.4	0.6	0.8	1	1.2	1.4	1.6	1.8	2	2.2	2.4	2.6	2.8	3	3.2	3.4	3.6	3.8	4	4.2	4.4	4.6	4.8	5
0	0.00	0.00	0.00	0.00	0.00	0.00	0.00	0.00	0.00	0.00	0.02	0.04	0.09	0.33	0.34	0.30	0.19	0.12	0.09	0.06	0.04	0.02	0.01	0.00	0.02	0.00
1.25	0.00	0.00	0.00	0.00	0.01	0.00	0.00	0.00	0.00	0.01	0.00	0.02	0.05	0.12	0.31	0.26	0.18	0.11	0.07	0.06	0.04	0.02	0.01	0.00	0.02	0.00
2.5	0.00	0.00	0.00	0.00	0.00	0.00	0.00	0.00	0.00	0.00	0.00	0.00	0.02	0.09	0.31	0.28	0.17	0.12	0.09	0.06	0.03	0.02	0.01	0.00	0.00	0.02
3.75	0.00	0.00	0.00	0.00	0.00	0.00	0.00	0.00	0.00	0.00	0.00	0.01	0.02	0.08	0.30	0.24	0.14	0.11	0.08	0.05	0.03	0.02	0.01	0.00	0.00	0.01
5	0.00	0.00	0.00	0.06	0.00	0.00	0.00	0.00	0.00	0.00	0.00	0.01	0.01	0.05	0.22	0.19	0.12	0.09	0.08	0.06	0.03	0.01	0.01	0.00	0.00	0.05
7.5	0.00	0.00	0.00	0.00	0.00	0.00	0.00	0.00	0.00	0.00	0.00	0.00	0.01	0.07	0.17	0.14	0.10	0.10	0.05	0.04	0.02	0.01	0.01	0.00	0.00	0.00
10	0.00	0.00	0.00	0.00	0.00	0.00	0.00	0.00	0.00	0.00	0.00	0.01	0.02	0.08	0.20	0.15	0.13	0.10	0.07	0.06	0.04	0.02	0.01	0.01	0.00	0.00
12.5	0.00	0.00	0.00	0.00	0.00	0.00	0.00	0.00	0.00	0.00	0.00	0.00	0.00	0.01	0.14	0.14	0.11	0.08	0.06	0.04	0.03	0.01	0.01	0.00	0.00	0.00
15	0.00	0.00	0.00	0.00	0.00	0.00	0.00	0.00	0.00	0.00	0.00	0.00	0.00	0.00	0.00	0.00	0.01	0.04	0.02	0.02	0.01	0.01	0.00	0.00	0.00	0.04
17.5	0.00	0.00	0.00	0.00	0.00	0.00	0.00	0.00	0.00	0.00	0.00	0.00	0.00	0.00	0.00	0.00	0.02	0.03	0.04	0.03	0.01	0.01	0.00	0.01	0.01	0.00
20	0.01	0.00	0.00	0.00	0.00	0.00	0.00	0.00	0.00	0.00	0.00	0.01	0.00	0.01	0.00	0.03	0.01	0.00	0.00	0.00	0.00	0.00	0.00	0.00	0.00	0.00
25																										

Table 5: Data of mass information and calculated value of total concentration in Run 3.

	Tank	Vertical Elevation z (cm)										
	Sample	0	1.25	2.5	3.75	5	7.5	10	12.5	15	17.5	20	25
M_c (g)	154.98	154.23	152.65	152.23	153.41	153.18	154.35	153.05	153.19	153.96	155.86	153.12	153.98
M_s (g)	457.50	352.50	377.00	332.50	369.00	335.50	360.20	404.00	406.00	374.50	424.00	398.00	445.00
M_d (g)	168.89	161.55	156.26	154.76	156.24	155.46	157.04	156.01	156.04	156.54	156.69	153.91	154.76
c (wt%)	4.596	3.696	1.610	1.406	1.312	1.250	1.307	1.179	1.126	1.172	0.308	0.323	0.268
c (vol%)	3.216	2.578	1.116	0.974	0.909	0.865	0.905	0.816	0.779	0.811	0.213	0.223	0.185

Table 6: Data of volumetric concentration at each elevation in different grain-size range in Run 3.

z (cm)	Grain size (Φ -scale)																							
	0.2	0.4	0.6	0.8	1	1.2	1.4	1.6	1.8	2	2.2	2.4	2.6	2.8	3	3.2	3.4	3.6	3.8	4	4.2	4.4	4.6	4.8	5
0	0.00	0.00	0.00	0.01	0.00	0.02	0.00	0.00	0.04	0.13	0.16	0.45	0.48	0.33	0.27	0.23	0.17	0.11	0.07	0.05	0.03	0.02	0.02	0.00	0.01
1.25	0.00	0.00	0.00	0.00	0.00	0.00	0.00	0.00	0.00	0.00	0.01	0.07	0.13	0.21	0.18	0.12	0.12	0.10	0.07	0.04	0.03	0.02	0.00	0.00	0.00
2.5	0.00	0.00	0.00	0.00	0.00	0.00	0.00	0.01	0.00	0.01	0.02	0.05	0.10	0.20	0.16	0.13	0.10	0.07	0.05	0.03	0.02	0.01	0.01	0.01	0.01
3.75	0.00	0.00	0.00	0.00	0.00	0.00	0.01	0.00	0.01	0.00	0.00	0.00	0.11	0.20	0.15	0.13	0.09	0.05	0.04	0.03	0.02	0.01	0.00	0.07	0.01
5	0.00	0.00	0.00	0.00	0.00	0.00	0.00	0.00	0.01	0.00	0.00	0.02	0.08	0.16	0.19	0.13	0.09	0.06	0.05	0.04	0.02	0.01	0.01	0.00	0.00
7.5	0.00	0.00	0.00	0.00	0.00	0.00	0.00	0.01	0.00	0.00	0.03	0.04	0.10	0.18	0.14	0.12	0.10	0.06	0.04	0.03	0.02	0.01	0.01	0.00	0.00
10	0.00	0.00	0.00	0.00	0.00	0.00	0.00	0.01	0.01	0.02	0.02	0.04	0.09	0.16	0.10	0.11	0.08	0.05	0.04	0.03	0.02	0.01	0.01	0.01	0.00
12.5	0.00	0.00	0.00	0.00	0.00	0.00	0.00	0.00	0.02	0.01	0.03	0.04	0.09	0.16	0.13	0.10	0.07	0.05	0.03	0.02	0.02	0.01	0.00	0.00	0.00
15	0.00	0.00	0.00	0.00	0.00	0.00	0.00	0.00	0.01	0.01	0.01	0.02	0.07	0.13	0.14	0.11	0.09	0.07	0.05	0.03	0.02	0.01	0.02	0.00	0.00
17.5	0.00	0.00	0.00	0.00	0.00	0.00	0.00	0.00	0.00	0.00	0.00	0.00	0.01	0.03	0.05	0.05	0.03	0.02	0.01	0.01	0.01	0.00	0.00	0.00	0.00
20	0.00	0.00	0.01	0.00	0.00	0.00	0.00	0.00	0.00	0.00	0.00	0.00	0.02	0.04	0.05	0.03	0.02	0.02	0.01	0.01	0.01	0.00	0.00	0.00	0.00
25																									

Table 7: Data of mass information and calculated value of total concentration in Run 4.

	Tank	Vertical Elevation z (cm)										
	Sample	0	1.25	2.5	3.75	5	7.5	10	12.5	15	17.5	20	25
M_c (g)	152.808	155.617	158.486	155.768		155.544	154.128	153.004	157.857	152.428	157.515	152.984	
M_s (g)	405.530	386.806	374.328	352.565		372.934	380.415	401.719	387.024	376.828	360.894	363.238	
M_d (g)	176.436	156.918	159.654	156.562		156.120	154.699	153.565	158.378	152.940	158.001	153.298	
c (wt%)	9.349	0.563	0.541	0.403		0.265	0.252	0.226	0.227	0.228	0.239	0.149	
c (vol%)	6.641	0.389	0.374	0.279		0.183	0.174	0.156	0.157	0.157	0.165	0.103	

Table 8: Data of volumetric concentration at each elevation in different grain-size range in Run 4.

z (cm)	Grain size (Φ -scale)																				
	-0.5	-0.25	0	0.25	0.5	0.75	1	1.25	1.5	1.75	2	2.25	2.5	2.75	3	3.25	3.5	3.75	4	4.25	4.5
0	0.004	0.000	0.000	0.001	0.005	0.010	0.020	0.035	0.015	0.014	0.011	0.014	0.014	0.012	0.022	0.024	0.027	0.034	0.014	0.011	0.011
1.25	0.007	0.000	0.000	0.000	0.004	0.013	0.023	0.020	0.017	0.015	0.014	0.012	0.012	0.018	0.022	0.027	0.025	0.023	0.018	0.013	0.006
2.5	0.008	0.000	0.000	0.000	0.001	0.005	0.009	0.010	0.010	0.011	0.007	0.014	0.015	0.013	0.023	0.027	0.028	0.024	0.015	0.008	0.010
3.75																					
5	0.021	0.000	0.000	0.000	0.000	0.000	0.000	0.000	0.000	0.000	0.000	0.000	0.000	0.000	0.000	0.043	0.068	0.017	0.030	0.013	0.013
7.5	0.012	0.000	0.000	0.000	0.000	0.000	0.003	0.000	0.002	0.002	0.003	0.000	0.000	0.000	0.016	0.073	0.041	0.022	0.019	0.006	0.000
10	0.000	0.000	0.000	0.000	0.000	0.000	0.000	0.000	0.000	0.000	0.000	0.003	0.009	0.005	0.014	0.023	0.035	0.029	0.022	0.011	0.005
12.5	0.000	0.000	0.001	0.000	0.000	0.000	0.002	0.001	0.000	0.003	0.000	0.004	0.006	0.006	0.011	0.039	0.034	0.026	0.017	0.009	0.009
15	0.000	0.001	0.003	0.004	0.003	0.001	0.000	0.000	0.001	0.000	0.000	0.003	0.005	0.009	0.009	0.036	0.034	0.028	0.020	0.010	0.011
17.5	0.000	0.001	0.004	0.000	0.008	0.006	0.005	0.004	0.002	0.003	0.003	0.008	0.008	0.007	0.004	0.022	0.022	0.020	0.008	0.008	0.000
20	0.000	0.002	0.003	0.005	0.004	0.000	0.000	0.000	0.000	0.001	0.000	0.000	0.001	0.005	0.000	0.019	0.029	0.019	0.012	0.014	0.010
25																					

Table 9: Data of mass information and calculated value of total concentration in Run 5.

	Tank	Vertical Elevation z (cm)											
	Sample	0	1.25	2.5	3.75	5	7.5	10	12.5	15	17.5	20	25
M_c (g)	154.827	154.036	158.478	155.759	153.881	155.539	154.120	153.001	153.002	153.748	155.714	154.286	154.607
M_s (g)	399.533	394.604	348.848	400.844	361.877	419.661	406.581	383.363	379.516	411.885	370.217	408.122	411.396
M_d (g)	160.813	157.090	160.229	157.252	155.158	156.495	155.152	153.493	153.606	154.769	156.346	155.045	155.602
c (wt%)	2.446	1.269	0.920	0.609	0.614	0.362	0.409	0.214	0.267	0.396	0.295	0.299	0.387
c (vol%)	1.700	0.879	0.636	0.421	0.424	0.250	0.282	0.147	0.184	0.273	0.203	0.206	0.268

Table 10: Data of volumetric concentration at each elevation in different grain-size range in Run 5.

z (cm)	Grain size (*Φ* -scale)																				
	1	1.2	1.4	1.6	1.8	2	2.2	2.4	2.6	2.8	3	3.2	3.4	3.6	3.8	4	4.2	4.4	4.6	4.8	5
0	0.000	0.000	0.000	0.002	0.002	0.000	0.007	0.096	0.316	0.165	0.112	0.086	0.041	0.026	0.017	0.010	0.000	0.000	0.000	0.000	0.000
1.25	0.000	0.000	0.000	0.000	0.000	0.000	0.000	0.062	0.217	0.122	0.092	0.062	0.036	0.019	0.012	0.012	0.000	0.000	0.000	0.000	0.000
2.5	0.000	0.000	0.000	0.000	0.000	0.004	0.000	0.010	0.144	0.107	0.063	0.039	0.027	0.012	0.012	0.006	0.000	0.000	0.000	0.000	0.000
3.75	0.003	0.001	0.000	0.001	0.000	0.000	0.001	0.021	0.135	0.109	0.060	0.041	0.022	0.014	0.008	0.007	0.000	0.000	0.000	0.000	0.000
5	0.000	0.000	0.000	0.000	0.000	0.000	0.000	0.000	0.041	0.090	0.046	0.028	0.020	0.011	0.012	0.002	0.000	0.000	0.000	0.000	0.000
7.5	0.001	0.000	0.000	0.001	0.001	0.000	0.001	0.008	0.067	0.076	0.055	0.033	0.021	0.011	0.009	0.001	0.000	0.000	0.000	0.000	0.000
10	0.000	0.001	0.000	0.001	0.000	0.003	0.000	0.003	0.013	0.047	0.037	0.021	0.012	0.007	0.004	0.003	0.000	0.000	0.000	0.000	0.000
12.5	0.000	0.000	0.000	0.000	0.000	0.000	0.000	0.000	0.000	0.064	0.053	0.030	0.015	0.009	0.006	0.006	0.000	0.000	0.000	0.000	0.000
15	0.000	0.002	0.000	0.001	0.000	0.000	0.000	0.004	0.042	0.094	0.046	0.041	0.022	0.012	0.009	0.004	0.000	0.000	0.000	0.000	0.000
17.5	0.011	0.000	0.001	0.000	0.000	0.001	0.000	0.004	0.020	0.070	0.045	0.016	0.011	0.009	0.007	0.009	0.000	0.000	0.000	0.000	0.000
20	0.000	0.001	0.000	0.000	0.003	0.000	0.001	0.004	0.000	0.082	0.043	0.037	0.012	0.013	0.010	0.009	0.000	0.000	0.000	0.000	0.000
25	0.000	0.000	0.000	0.000	0.000	0.000	0.000	0.004	0.069	0.075	0.048	0.035	0.020	0.009	0.008	0.000	0.000	0.000	0.000	0.000	0.000

Table 11: Data of mass information and calculated value of total concentration in Run 6.

	Tank	Vertical Elevation z (cm)									
	Sample	0	1	2	3	4	5	6	7	8	9
M_c (g)	152.370	153.470	152.270	151.470	153.270	152.470	153.470	152.370	152.470	153.270	155.270
M_s (g)	441.270	381.770	377.770	385.270	380.270	397.270	384.270	388.270	382.770	384.770	397.270
M_d (g)	153.783	153.738	152.505	151.788	153.572	152.709	153.643	152.551	152.688	153.406	155.398
c (wt%)	0.489	0.117	0.104	0.136	0.133	0.098	0.075	0.077	0.095	0.059	0.053
c (vol%)	0.338	0.081	0.072	0.094	0.092	0.067	0.052	0.053	0.065	0.041	0.036

Table 12: Data of volumetric concentration at each elevation in different grain-size range in Run 6.

z (cm)	Grain size (Φ -scale)																
	1	1.25	1.5	1.75	2	2.25	2.5	2.75	3	3.25	3.5	3.75	4	4.25	4.5	4.75	5
0	0.000	0.001	0.000	0.000	0.001	0.001	0.003	0.012	0.021	0.014	0.008	0.007	0.004	0.003	0.002	0.002	0.001
1	0.000	0.000	0.000	0.000	0.000	0.000	0.002	0.007	0.016	0.015	0.011	0.006	0.005	0.004	0.002	0.002	0.001
2	0.000	0.001	0.000	0.000	0.001	0.002	0.002	0.015	0.021	0.015	0.013	0.007	0.004	0.005	0.001	0.002	0.000
3	0.000	0.000	0.000	0.000	0.000	0.002	0.003	0.017	0.024	0.013	0.012	0.007	0.004	0.003	0.003	0.002	0.002
4	0.000	0.000	0.000	0.000	0.000	0.000	0.003	0.006	0.021	0.009	0.011	0.006	0.004	0.004	0.002	0.001	0.001
5	0.001	0.000	0.000	0.000	0.002	0.000	0.002	0.004	0.011	0.013	0.006	0.006	0.004	0.003	0.002	0.001	0.002
6	0.000	0.000	0.000	0.000	0.000	0.000	0.001	0.004	0.010	0.012	0.007	0.006	0.004	0.003	0.002	0.001	0.001
7	0.000	0.000	0.000	0.000	0.000	0.002	0.002	0.009	0.010	0.015	0.009	0.006	0.004	0.004	0.002	0.002	0.001
8	0.000	0.000	0.000	0.000	0.000	0.001	0.002	0.005	0.010	0.007	0.005	0.003	0.002	0.001	0.001	0.001	0.001
9	0.000	0.000	0.000	0.000	0.000	0.001	0.002	0.004	0.009	0.007	0.004	0.003	0.002	0.002	0.002	0.001	0.001

Table 13: Data of mass information and calculated value of total concentration in Run 7.

	Tank	Vertical Elevation z (cm)											
	Sample	0	1.25	2.5	3.75	5	7.5	10	12.5	15	17.5	20	25
M_c (g)	152.370	155.170	158.070	155.370		155.070	153.770	152.570	157.270	151.870	156.970	153.670	154.070
M_s (g)	441.270	377.270	374.770	374.770		380.770	394.270	416.770	403.770	397.770	393.770	380.770	394.770
M_d (g)	153.783	155.335	158.220	155.517		155.200	153.898	152.722	157.434	152.063	157.135	153.807	154.221
c (wt%)	0.489	0.074	0.069	0.067		0.058	0.053	0.058	0.067	0.078	0.070	0.060	0.063
c (vol%)	0.338	0.051	0.048	0.046		0.040	0.037	0.040	0.046	0.054	0.048	0.042	0.043

Table 14: Data of volumetric concentration at each elevation in different grain-size range in Run 7.

z (cm)	Grain size (Φ -scale)																
	1	1.25	1.5	1.75	2	2.25	2.5	2.75	3	3.25	3.5	3.75	4	4.25	4.5	4.75	5
0																	
1.25	0.000	0.000	0.000	0.000	0.000	0.000	0.002	0.003	0.010	0.010	0.007	0.005	0.004	0.003	0.002	0.002	0.002
2.5	0.000	0.000	0.000	0.000	0.000	0.000	0.001	0.002	0.007	0.008	0.009	0.005	0.004	0.003	0.002	0.001	0.003
3.75																	
5	0.000	0.001	0.000	0.000	0.000	0.000	0.003	0.003	0.005	0.007	0.006	0.005	0.003	0.003	0.002	0.001	0.003
7.5	0.000	0.000	0.000	0.000	0.000	0.000	0.001	0.002	0.005	0.008	0.006	0.005	0.003	0.003	0.002	0.001	0.001
10	0.000	0.000	0.000	0.000	0.000	0.000	0.000	0.002	0.007	0.007	0.005	0.005	0.003	0.003	0.001	0.004	0.003
12.5	0.000	0.000	0.000	0.000	0.000	0.000	0.000	0.003	0.004	0.006	0.009	0.007	0.004	0.004	0.003	0.003	0.004
15	0.000	0.000	0.000	0.000	0.000	0.000	0.000	0.003	0.001	0.008	0.010	0.008	0.007	0.006	0.004	0.004	0.003
17.5	0.000	0.000	0.000	0.006	0.000	0.000	0.000	0.004	0.002	0.004	0.004	0.008	0.004	0.006	0.004	0.002	0.006
20	0.000	0.000	0.000	0.000	0.000	0.000	0.000	0.006	0.000	0.003	0.006	0.003	0.011	0.003	0.006	0.006	0.000
25	0.000	0.000	0.000	0.000	0.002	0.004	0.002	0.004	0.006	0.000	0.002	0.004	0.000	0.000	0.004	0.002	0.002

Table 15: Data of mass information and calculated value of total concentration in Run 8.

	Tank	Vertical Elevation z (cm)									
	Sample	0	1	2	3	4	5	6	7	8	9
M_c (g)	154.417	136.575	151.588	155.239	152.579	151.622	153.363	153.283	152.753	153.037	157.724
M_s (g)	432.813	428.224	430.247	430.870	463.197	428.369	419.352	442.753	430.300	429.939	409.965
M_d (g)	157.594	137.202	152.116	155.781	153.126	152.041	153.705	153.591	153.105	153.418	158.036
c (wt%)	1.141	0.215	0.189	0.197	0.176	0.151	0.129	0.106	0.127	0.138	0.124
c (vol%)	0.790	0.148	0.131	0.136	0.122	0.104	0.089	0.073	0.088	0.095	0.085

Table 16: Data of volumetric concentration at each elevation in different grain-size range in Run 8.

z (cm)	Grain size (Φ -scale)															
	1	1.25	1.5	1.75	2	2.25	2.5	2.75	3	3.25	3.5	3.75	4	4.25	4.5	4.75	5
0	0.000	0.001	0.000	0.000	0.001	0.002	0.006	0.023	0.038	0.026	0.015	0.012	0.007	0.005	0.003	0.004	0.002
1	0.000	0.000	0.000	0.000	0.000	0.000	0.003	0.013	0.029	0.027	0.020	0.012	0.010	0.008	0.004	0.004	0.002
2	0.000	0.001	0.000	0.000	0.001	0.003	0.003	0.022	0.030	0.021	0.018	0.010	0.006	0.007	0.001	0.003	0.000
3	0.000	0.000	0.000	0.000	0.000	0.002	0.004	0.022	0.032	0.017	0.015	0.009	0.005	0.004	0.004	0.003	0.003
4	0.000	0.000	0.000	0.000	0.000	0.000	0.004	0.009	0.033	0.014	0.017	0.009	0.007	0.007	0.003	0.001	0.001
5	0.001	0.000	0.000	0.000	0.003	0.000	0.003	0.006	0.019	0.022	0.010	0.010	0.007	0.005	0.003	0.002	0.003
6	0.000	0.000	0.000	0.000	0.000	0.000	0.002	0.005	0.013	0.017	0.010	0.008	0.006	0.004	0.003	0.002	0.002
7	0.000	0.000	0.000	0.000	0.000	0.003	0.002	0.012	0.013	0.020	0.012	0.008	0.005	0.005	0.003	0.002	0.001
8	0.000	0.000	0.001	0.000	0.001	0.002	0.006	0.011	0.023	0.017	0.012	0.007	0.004	0.002	0.002	0.002	0.002
9	0.000	0.000	0.000	0.000	0.000	0.003	0.004	0.010	0.021	0.016	0.010	0.006	0.005	0.004	0.004	0.002	0.002

Table 17: Data of mass information and calculated value of total concentration in Run 9.

	Tank	Vertical Elevation z (cm)											
	Sample	0	1.25	2.5	3.75	5	7.5	10	12.5	15	17.5	20	25
M_c (g)	154.417	155.275	158.120	155.417	153.272	155.200	153.778	152.666	157.484	152.063	152.575	153.452	154.221
M_s (g)	432.813	434.730	454.026	442.473	442.054	447.586	448.092	441.313	435.428	446.984	435.639	421.535	451.898
M_d (g)	157.594	155.687	158.480	155.786	153.557	155.472	154.134	152.890	157.683	152.251	152.650	153.488	154.270
c (wt%)	1.141	0.147	0.122	0.129	0.099	0.093	0.121	0.078	0.072	0.064	0.026	0.013	0.016
c (vol%)	0.790	0.102	0.084	0.089	0.068	0.064	0.083	0.054	0.049	0.044	0.018	0.009	0.011

Table 18: Data of volumetric concentration at each elevation in different grain-size range in Run 9.

z (cm)	Grain size (Φ -scale)																
	1	1.25	1.5	1.75	2	2.25	2.5	2.75	3	3.25	3.5	3.75	4	4.25	4.5	4.75	5
0																	
1.25	0.000	0.000	0.000	0.000	0.000	0.000	0.003	0.005	0.017	0.018	0.013	0.008	0.006	0.005	0.003	0.004	0.003
2.5	0.000	0.000	0.000	0.000	0.000	0.000	0.002	0.004	0.013	0.016	0.017	0.009	0.008	0.006	0.004	0.003	0.006
3.75	0.000	0.000	0.000	0.000	0.000	0.000	0.002	0.003	0.010	0.017	0.010	0.010	0.005	0.004	0.003	0.004	0.001
5	0.000	0.002	0.000	0.000	0.000	0.000	0.004	0.004	0.008	0.012	0.010	0.008	0.004	0.005	0.003	0.002	0.004
7.5	0.000	0.000	0.000	0.000	0.000	0.000	0.003	0.005	0.011	0.017	0.014	0.010	0.007	0.007	0.004	0.003	0.003
10	0.000	0.000	0.000	0.000	0.000	0.000	0.000	0.002	0.010	0.009	0.007	0.007	0.004	0.004	0.001	0.005	0.004
12.5	0.000	0.000	0.000	0.000	0.000	0.000	0.000	0.003	0.004	0.007	0.010	0.008	0.005	0.004	0.003	0.003	0.004
15	0.000	0.000	0.000	0.000	0.000	0.000	0.000	0.003	0.001	0.006	0.008	0.006	0.005	0.004	0.004	0.004	0.003
17.5	0.000	0.000	0.000	0.002	0.000	0.000	0.000	0.002	0.001	0.002	0.002	0.003	0.002	0.002	0.002	0.001	0.002
20	0.000	0.000	0.000	0.000	0.000	0.000	0.000	0.001	0.000	0.001	0.001	0.001	0.002	0.001	0.001	0.001	0.000
25	0.000	0.000	0.000	0.000	0.001	0.001	0.001	0.001	0.002	0.000	0.001	0.001	0.000	0.000	0.001	0.001	0.001

Table 19: Data of mass information and calculated value of total concentration in Run 10.

	Tank	Vertical Elevation z (cm)									
	Sample	0	1	2	3	4	5	6	7	8	9
M_c (g)	152.408	136.579	151.602	155.252	152.592	151.635	153.375	153.298	152.764	153.047	157.736
M_s (g)	410.876	400.364	416.660	413.005	400.965	412.553	413.586	388.742	396.917	430.090	434.192
M_d (g)	156.229	137.724	152.423	156.027	153.305	152.266	153.958	153.802	153.259	153.669	158.194
c (wt%)	1.478	0.434	0.310	0.301	0.287	0.242	0.224	0.214	0.203	0.225	0.166
c (vol%)	1.024	0.300	0.214	0.208	0.198	0.167	0.155	0.148	0.140	0.155	0.114

Table 20: Data of volumetric concentration at each elevation in different grain-size range in Run 10.

z (cm)	Grain size (Φ -scale)																
	1	1.25	1.5	1.75	2	2.25	2.5	2.75	3	3.25	3.5	3.75	4	4.25	4.5	4.75	5
0	0.000	0.000	0.000	0.000	0.004	0.016	0.054	0.095	0.051	0.040	0.019	0.012	0.003	0.003	0.001	0.000	0.000
1	0.000	0.000	0.000	0.000	0.000	0.008	0.026	0.064	0.058	0.027	0.017	0.008	0.005	0.001	0.000	0.000	0.000
2	0.000	0.000	0.000	0.000	0.000	0.010	0.030	0.065	0.052	0.027	0.014	0.005	0.002	0.002	0.000	0.000	0.000
3	0.000	0.000	0.000	0.000	0.002	0.006	0.024	0.070	0.048	0.025	0.013	0.005	0.002	0.001	0.000	0.000	0.000
4	0.000	0.000	0.000	0.000	0.000	0.009	0.021	0.063	0.040	0.023	0.010	0.001	0.000	0.000	0.000	0.000	0.000
5	0.000	0.000	0.000	0.000	0.000	0.008	0.020	0.046	0.042	0.017	0.010	0.002	0.001	0.000	0.000	0.010	0.000
6	0.000	0.000	0.000	0.000	0.000	0.004	0.020	0.042	0.043	0.020	0.009	0.005	0.003	0.000	0.000	0.000	0.000
7	0.000	0.000	0.000	0.000	0.000	0.002	0.013	0.046	0.033	0.022	0.010	0.006	0.002	0.001	0.004	0.001	0.000
8	0.000	0.000	0.000	0.000	0.000	0.008	0.021	0.046	0.037	0.022	0.011	0.006	0.001	0.002	0.000	0.000	0.001
9	0.000	0.000	0.000	0.000	0.000	0.005	0.015	0.036	0.029	0.015	0.008	0.003	0.002	0.000	0.000	0.001	0.000

Table 21: Data of mass information and calculated value of total concentration in Run 11.

	Tank	Vertical Elevation z (cm)											
	Sample	0	1.25	2.5	3.75	5	7.5	10	12.5	15	17.5	20	25
M_c (g)	152.408	155.221	158.078	155.360	153.277	155.138	153.728	152.602	157.442	152.030	152.582	153.452	154.212
M_s (g)	410.876	434.102	399.606	416.789	438.787	435.338	454.639	461.244	440.633	438.599	410.658	434.887	453.176
M_d (g)	156.229	155.966	158.453	155.791	153.810	155.577	154.278	153.110	157.812	152.284	152.703	153.611	154.319
c (wt%)	1.478	0.267	0.155	0.165	0.187	0.157	0.183	0.165	0.131	0.089	0.047	0.056	0.036
c (vol%)	1.024	0.184	0.107	0.114	0.129	0.108	0.126	0.114	0.090	0.061	0.032	0.039	0.025

Table 22: Data of volumetric concentration at each elevation in different grain-size range in Run 11.

z (cm)	Grain size (Φ -scale)																
	1	1.25	1.5	1.75	2	2.25	2.5	2.75	3	3.25	3.5	3.75	4	4.25	4.5	4.75	5
0	0.001	0.000	0.000	0.000	0.003	0.002	0.011	0.063	0.049	0.029	0.012	0.008	0.004	0.003	0.000	0.000	0.000
1.25	0.000	0.000	0.000	0.000	0.000	0.000	0.009	0.026	0.037	0.017	0.010	0.004	0.002	0.001	0.000	0.000	0.000
2.5	0.000	0.000	0.000	0.000	0.000	0.002	0.005	0.019	0.045	0.015	0.015	0.007	0.003	0.002	0.000	0.000	0.000
3.75	0.000	0.000	0.000	0.000	0.000	0.000	0.007	0.031	0.041	0.022	0.014	0.008	0.003	0.001	0.000	0.001	0.000
5	0.000	0.000	0.000	0.000	0.000	0.000	0.003	0.020	0.040	0.023	0.012	0.004	0.002	0.001	0.001	0.000	0.000
7.5																	
10	0.000	0.000	0.000	0.000	0.000	0.000	0.006	0.012	0.042	0.018	0.013	0.006	0.006	0.002	0.003	0.004	0.003
12.5	0.000	0.000	0.000	0.000	0.000	0.000	0.006	0.010	0.024	0.022	0.015	0.007	0.005	0.001	0.000	0.000	0.000
15	0.000	0.000	0.000	0.000	0.000	0.003	0.002	0.003	0.007	0.017	0.012	0.007	0.003	0.003	0.001	0.001	0.000
17.5	0.000	0.000	0.000	0.000	0.000	0.004	0.006	0.004	0.002	0.008	0.006	0.002	0.000	0.002	0.000	0.000	0.000
20	0.000	0.000	0.000	0.000	0.000	0.004	0.001	0.004	0.003	0.008	0.004	0.004	0.003	0.003	0.001	0.003	0.003
25	0.000	0.000	0.000	0.000	0.000	0.003	0.004	0.001	0.003	0.003	0.003	0.001	0.001	0.001	0.001	0.001	0.000

Table 23: Data of mass information and calculated value of total concentration in Run 12.

	Tank	Vertical Elevation z (cm)									
	Sample	0	1	2	3	4	5	6	7	8	9
M_c (g)	164.278	136.573	151.597	155.245	152.588	151.634	153.372	153.290	152.760	153.042	157.734
M_s (g)	639.760	429.830	452.696	495.353	453.574	457.779	467.224	461.221	464.893	487.424	475.546
M_d (g)	183.788	139.893	154.005	157.393	153.941	152.576	154.228	153.886	153.075	153.288	157.905
c (wt%)	4.103	1.132	0.800	0.632	0.450	0.308	0.273	0.194	0.101	0.074	0.054
c (vol%)	2.866	0.784	0.553	0.436	0.310	0.212	0.188	0.134	0.070	0.051	0.037

Table 24: Data of volumetric concentration at each elevation in different grain-size range in Run 12.

z (cm)	Grain size (Φ -scale)																
	1	1.25	1.5	1.75	2	2.25	2.5	2.75	3	3.25	3.5	3.75	4	4.25	4.5	4.75	5
0	0.000	0.000	0.002	0.002	0.020	0.112	0.182	0.146	0.120	0.088	0.051	0.027	0.013	0.008	0.005	0.005	0.004
1	0.000	0.001	0.000	0.000	0.006	0.088	0.135	0.093	0.083	0.061	0.037	0.020	0.012	0.006	0.005	0.004	0.003
2	0.000	0.002	0.000	0.000	0.005	0.025	0.111	0.085	0.071	0.055	0.034	0.020	0.010	0.006	0.006	0.003	0.003
3	0.002	0.000	0.000	0.002	0.000	0.009	0.060	0.083	0.051	0.040	0.027	0.015	0.008	0.005	0.005	0.004	0.003
4	0.001	0.000	0.000	0.001	0.000	0.004	0.023	0.063	0.043	0.031	0.020	0.011	0.006	0.002	0.004	0.004	0.002
5	0.000	0.000	0.001	0.000	0.002	0.000	0.008	0.043	0.043	0.035	0.021	0.013	0.008	0.006	0.004	0.004	0.003
6	0.001	0.001	0.001	0.000	0.000	0.000	0.005	0.020	0.041	0.022	0.017	0.009	0.007	0.004	0.004	0.004	0.002
7	0.000	0.003	0.000	0.001	0.000	0.002	0.000	0.007	0.016	0.014	0.011	0.007	0.003	0.002	0.003	0.004	0.002
8	0.000	0.000	0.000	0.000	0.000	0.000	0.002	0.006	0.012	0.009	0.007	0.004	0.003	0.003	0.001	0.001	0.003
9	0.001	0.000	0.002	0.001	0.000	0.001	0.000	0.003	0.007	0.009	0.005	0.005	0.002	0.001	0.002	0.001	0.002

Table 25: Data of mass information and calculated value of total concentration in Run 13.

	Tank	Vertical Elevation z (cm)											
	Sample	0	1.25	2.5	3.75	5	7.5	10	12.5	15	17.5	20	25
M_c (g)	164.278	155.211	158.072	155.359	153.272	155.139	153.730	152.603	157.439	152.030	157.098	153.890	154.22
M_s (g)	639.760	443.333	479.922	464.591	504.568	471.365	458.912	488.688	522.057	482.237	445.445	461.079	446.32
M_d (g)	183.788	156.462	159.225	156.268	154.114	155.715	154.072	152.875	157.569	152.090	157.123	153.914	154.23
c (wt%)	4.103	0.434	0.358	0.294	0.240	0.182	0.112	0.081	0.036	0.018	0.009	0.008	0.006
c (vol%)	2.866	0.300	0.247	0.203	0.165	0.126	0.077	0.056	0.025	0.013	0.006	0.005	0.004

Table 26: Data of volumetric concentration at each elevation in different grain-size range in Run 13.

z (cm)	Grain size (Φ -scale)																
	1	1.25	1.5	1.75	2	2.25	2.5	2.75	3	3.25	3.5	3.75	4	4.25	4.5	4.75	5
0	0.000	0.001	0.000	0.001	0.001	0.000	0.013	0.077	0.062	0.053	0.040	0.025	0.014	0.009	0.007		
1.25	0.002	0.000	0.002	0.000	0.001	0.001	0.007	0.052	0.050	0.048	0.036	0.023	0.013	0.009	0.008		
2.5	0.000	0.000	0.001	0.001	0.000	0.001	0.006	0.031	0.044	0.042	0.031	0.021	0.012	0.009	0.006		
3.75	0.000	0.001	0.000	0.000	0.000	0.002	0.003	0.020	0.038	0.035	0.025	0.018	0.011	0.007	0.006		
5	0.001	0.001	0.000	0.000	0.000	0.002	0.002	0.009	0.029	0.025	0.022	0.014	0.009	0.007	0.005		
7.5	0.000	0.000	0.000	0.001	0.000	0.001	0.000	0.003	0.011	0.018	0.014	0.011	0.008	0.007	0.004		
10	0.000	0.000	0.000	0.000	0.000	0.001	0.001	0.001	0.003	0.012	0.013	0.008	0.006	0.004	0.003	0.003	0.003
12.5	0.001	0.000	0.000	0.001	0.000	0.001	0.001	0.001	0.002	0.005	0.004	0.004	0.002	0.002	0.002	0.002	0.002
15	0.000	0.000	0.001	0.000	0.000	0.000	0.001	0.001	0.001	0.001	0.002	0.003	0.001	0.001	0.000	0.001	0.003
17.5																	
20																	
25																	

Table 27: Data of mass information and calculated value of total concentration in Run 14.

	Tank	Vertical Elevation z (cm)									
	Sample	0	1	2	3	4	5	6	7	8	9
M_c (g)	164.449	155.470	153.518	152.768	154.046	153.624	155.275	153.899	152.174	153.632	153.454
M_s (g)	605.477	426.572	445.008	443.893	451.353	420.109	413.840	488.071	491.486	419.239	427.317
M_d (g)	181.805	158.766	155.861	154.745	155.478	154.708	155.954	154.680	152.810	153.987	153.752
c (wt%)	3.935	1.216	0.804	0.679	0.482	0.407	0.263	0.234	0.187	0.134	0.109
c (vol%)	2.748	0.842	0.556	0.469	0.333	0.281	0.181	0.161	0.129	0.092	0.075

Table 28: Data of volumetric concentration at each elevation in different grain-size range in Run 14.

z (cm)	Grain size (Φ -scale)																	
	0	0.25	0.5	0.75	1	1.25	1.5	1.75	2	2.25	2.5	2.75	3	3.25	3.5	3.75	4	4.25
0	0.000	0.003	0.000	0.000	0.000	0.000	0.000	0.000	0.000	0.009	0.100	0.243	0.179	0.122	0.085	0.049	0.030	0.021
1	0.000	0.000	0.000	0.000	0.000	0.000	0.000	0.000	0.000	0.003	0.022	0.145	0.133	0.095	0.065	0.043	0.030	0.019
2	0.000	0.000	0.000	0.000	0.000	0.000	0.000	0.000	0.000	0.000	0.014	0.155	0.097	0.081	0.063	0.032	0.018	0.009
3	0.000	0.000	0.000	0.000	0.000	0.000	0.000	0.000	0.000	0.000	0.007	0.077	0.079	0.065	0.047	0.029	0.017	0.010
4	0.000	0.000	0.000	0.000	0.000	0.000	0.000	0.000	0.000	0.002	0.005	0.058	0.066	0.055	0.041	0.025	0.017	0.011
5	0.000	0.000	0.000	0.000	0.000	0.000	0.000	0.000	0.000	0.000	0.004	0.017	0.058	0.035	0.025	0.018	0.013	0.010
6	0.000	0.000	0.000	0.000	0.001	0.000	0.000	0.000	0.000	0.000	0.003	0.024	0.045	0.030	0.023	0.017	0.011	0.009
7	0.000	0.000	0.000	0.000	0.000	0.000	0.000	0.000	0.000	0.000	0.003	0.020	0.034	0.026	0.017	0.012	0.009	0.008
8	0.000	0.000	0.000	0.000	0.000	0.000	0.000	0.000	0.000	0.000	0.002	0.007	0.025	0.021	0.013	0.009	0.009	0.006
9	0.000	0.000	0.000	0.000	0.000	0.000	0.000	0.000	0.000	0.000	0.002	0.006	0.015	0.017	0.013	0.009	0.007	0.006

Table 29: Data of mass information and calculated value of total concentration in Run 15.

	Tank	Vertical Elevation z (cm)											
	Sample	0	1.25	2.5	3.75	5	7.5	10	12.5	15	17.5	20	25
M_c (g)	164.449	154.355	158.213	152.764	157.224	153.803	152.595	120.213	157.630	155.359	151.874	152.807	119.277
M_s (g)	605.477	498.326	447.185	474.422	496.937	444.329	435.700	403.218	524.688	448.771	433.958	461.192	413.853
M_d (g)	181.805	156.962	159.536	153.950	158.272	154.479	153.206	120.647	158.049	155.578	152.016	152.902	119.33
c (wt%)	3.935	0.758	0.458	0.369	0.308	0.233	0.216	0.153	0.114	0.075	0.050	0.031	0.018
c (vol%)	2.748	0.524	0.316	0.255	0.213	0.161	0.149	0.106	0.079	0.051	0.035	0.021	0.012

Table 30: Data of volumetric concentration at each elevation in different grain-size range in Run 15.

z (cm)	Grain size (Φ -scale)																	
	0	0.25	0.5	0.75	1	1.25	1.5	1.75	2	2.25	2.5	2.75	3	3.25	3.5	3.75	4	4.25
0																		
1.25	0.000	0.000	0.000	0.000	0.000	0.001	0.000	0.000	0.000	0.002	0.021	0.081	0.063	0.061	0.043	0.026	0.012	0.007
2.5	0.000	0.000	0.000	0.000	0.000	0.000	0.000	0.000	0.000	0.000	0.007	0.051	0.062	0.051	0.038	0.023	0.014	0.008
3.75	0.000	0.000	0.000	0.000	0.000	0.000	0.000	0.000	0.000	0.000	0.004	0.045	0.055	0.040	0.033	0.019	0.011	0.005
5	0.000	0.000	0.002	0.000	0.000	0.000	0.000	0.000	0.000	0.000	0.000	0.031	0.048	0.028	0.022	0.014	0.009	0.008
7.5	0.000	0.000	0.000	0.000	0.000	0.000	0.000	0.000	0.000	0.000	0.002	0.016	0.049	0.028	0.024	0.014	0.010	0.006
10	0.000	0.000	0.000	0.000	0.000	0.002	0.001	0.000	0.000	0.002	0.001	0.005	0.029	0.022	0.016	0.012	0.009	0.008
12.5	0.000	0.000	0.000	0.000	0.000	0.000	0.000	0.000	0.000	0.000	0.000	0.003	0.021	0.018	0.014	0.010	0.007	0.006
15																		
17.5																		
20																		
25																		

Table 31: Data of mass information and calculated value of total concentration in Run 16.

	Tank	Vertical Elevation z (cm)									
	Sample	0	1	2	3	4	5	6	7	8	9
M_c (g)	162.784	152.582	154.410	155.485	152.667	151.628	152.413	118.222	117.506	118.898	117.694
M_s (g)	541.267	429.409	431.572	488.709	444.036	451.443	432.065	380.949	394.126	375.197	372.910
M_d (g)	173.669	155.036	156.403	157.592	154.191	153.046	153.420	119.007	118.132	119.539	118.186
c (wt%)	2.876	0.886	0.719	0.632	0.523	0.473	0.360	0.299	0.226	0.250	0.193
c (vol%)	2.001	0.613	0.497	0.437	0.361	0.327	0.249	0.206	0.156	0.173	0.133

Table 32: Data of volumetric concentration at each elevation in different grain-size range in Run 16.

z (cm)	Grain size (Φ -scale)																				
	0	0.25	0.5	0.75	1	1.25	1.5	1.75	2	2.25	2.5	2.75	3	3.25	3.5	3.75	4	4.25	4.5	4.75	5
0	0.000	0.000	0.000	0.000	0.002	0.000	0.000	0.000	0.004	0.006	0.038	0.142	0.132	0.109	0.081	0.048	0.025	0.017	0.010	0.008	0.002
1	0.000	0.000	0.000	0.000	0.001	0.000	0.001	0.000	0.000	0.001	0.027	0.117	0.093	0.090	0.068	0.043	0.029	0.016	0.001	0.014	0.000
2																					
3	0.000	0.000	0.000	0.000	0.001	0.002	0.000	0.000	0.000	0.002	0.006	0.034	0.069	0.077	0.064	0.047	0.028	0.015	0.010	0.006	0.005
4	0.000	0.000	0.000	0.000	0.001	0.000	0.001	0.000	0.001	0.001	0.007	0.032	0.065	0.069	0.060	0.039	0.023	0.016	0.007	0.006	0.003
5	0.000	0.000	0.000	0.000	0.000	0.000	0.001	0.000	0.000	0.002	0.001	0.016	0.045	0.054	0.047	0.032	0.023	0.014	0.006	0.006	0.004
6	0.000	0.000	0.001	0.000	0.000	0.000	0.002	0.000	0.002	0.000	0.002	0.010	0.036	0.044	0.040	0.026	0.020	0.013	0.008	0.004	0.003
7	0.000	0.000	0.000	0.000	0.000	0.001	0.000	0.001	0.001	0.001	0.001	0.009	0.030	0.032	0.028	0.023	0.013	0.009	0.005	0.004	0.004
8	0.000	0.000	0.001	0.000	0.000	0.000	0.000	0.000	0.001	0.000	0.002	0.008	0.045	0.041	0.026	0.020	0.014	0.008	0.004	0.003	0.003
9	0.000	0.000	0.000	0.000	0.001	0.001	0.000	0.001	0.000	0.001	0.001	0.005	0.026	0.032	0.026	0.019	0.008	0.010	0.007	0.002	0.000

Table 33: Data of mass information and calculated value of total concentration in Run 17.

	Tank	Vertical Elevation z (cm)									
	Sample	0	1	2	3	4	5	6	7	8	9
M_c (g)	164.420	155.458	153.501	152.746	154.024	153.595	155.250	153.879	152.150	153.603	153.429
M_s (g)	703.739	522.114	520.158	504.260	514.917	478.874	486.382	495.262	513.037	494.955	485.898
M_d (g)	232.698	161.434	158.732	157.393	158.587	157.383	158.658	157.189	155.452	156.437	155.977
c (wt%)	12.660	1.630	1.427	1.322	1.264	1.165	1.029	0.970	0.915	0.830	0.766
c (vol%)	5.186	0.761	0.681	0.644	0.604	0.567	0.514	0.471	0.433	0.406	0.379

Table 34: Data of volumetric concentration at each elevation in different grain-size range in Run 17.

z (cm)	Grain size (Φ -scale)																			
	0	0.25	0.5	0.75	1	1.25	1.5	1.75	2	2.25	2.5	2.75	3	3.25	3.5	3.75	4	4.25	4.5	4.75	5
0	0.000	0.000	0.003	0.025	0.055	0.095	0.114	0.099	0.057	0.075	0.050	0.052	0.044	0.034	0.023	0.012	0.008	0.005	0.000	0.005	0.004
1	0.000	0.000	0.004	0.016	0.043	0.071	0.103	0.086	0.050	0.059	0.051	0.051	0.043	0.038	0.026	0.014	0.010	0.006	0.006	0.002	0.002
2	0.000	0.000	0.003	0.019	0.042	0.068	0.082	0.072	0.046	0.061	0.054	0.055	0.040	0.037	0.023	0.016	0.011	0.009	0.001	0.002	0.005
3	0.000	0.000	0.004	0.019	0.042	0.067	0.085	0.073	0.042	0.051	0.042	0.047	0.039	0.032	0.020	0.011	0.010	0.008	0.006	0.004	0.004
4	0.000	0.001	0.002	0.016	0.035	0.058	0.073	0.066	0.041	0.050	0.038	0.042	0.041	0.032	0.024	0.017	0.010	0.006	0.008	0.004	0.003
5	0.000	0.000	0.001	0.011	0.028	0.047	0.058	0.065	0.031	0.050	0.044	0.042	0.035	0.033	0.025	0.016	0.010	0.009	0.003	0.004	0.004
6	0.000	0.000	0.002	0.012	0.028	0.048	0.059	0.058	0.040	0.054	0.047	0.030	0.030	0.023	0.015	0.010	0.006	0.004	0.001	0.004	0.001
7	0.000	0.000	0.001	0.013	0.028	0.047	0.060	0.065	0.032	0.031	0.035	0.043	0.018	0.015	0.021	0.007	0.007	0.003	0.004	0.002	0.004
8	0.000	0.000	0.002	0.009	0.024	0.040	0.051	0.049	0.031	0.044	0.023	0.041	0.026	0.020	0.018	0.010	0.003	0.004	0.002	0.003	0.003
9	0.000	0.000	0.001	0.008	0.022	0.036	0.045	0.046	0.029	0.039	0.030	0.034	0.029	0.019	0.014	0.006	0.006	0.005	0.005	0.003	0.003

Notation

a	reference level for near-bed
A, B	constant parameters in sediment entrainment relations
B_s	roughness function
c	local sediment concentration
c_a	sediment concentration at the near-bed
c_{ae}	sediment concentration at the near-bed under equilibrium condition
c_u	Kramer coefficient of uniformity
C	layer-averaged concentration
C_i	layer-averaged sediment concentration in ith size range
C_1, C_2	constant parameters in sediment settling velocity relations
D	sediment diameter
D_*	dimensionless diameter of sediment
D_i	characteristic geometric diameter of i-th size range
D_s	geometric diameter of representative sediment grains
D_5	sediment diameter such that 5% of the bed material is finer
D_{50}	median diameter of sediment
D_{95}	sediment diameter such that 95% of the bed material is finer
E	sediment entrainment rate
E_s	dimensionless entrainment rate
$E_{s,i}$	dimensionless entrainment rate in ith size range
$E_{s,open}$	dimensionless entrainment rate in open-channel flow
$E_{s,turbi}$	dimensionless entrainment rate in turbidity current
$E_{s,uni}$	dimensionless entrainment rate in uniform flow
g	gravity acceleraton
G_s	specific gravity of the sediment
H	flow thickness
$\mathrm{J}_{\log}$	sum of squared residuals from least squares method
k	number of parameters in the model of AIC
k_s	roughness height
l_{max}	maximum log-likelihood value
m	exponent describing hiding effect

M_c	mass of container
M_d	mass of dried sediment and container
M_s	mass of suspension and container
n	size of dataset used in information criteria
P_i	volume fraction of bed materia in ith size range
r_0	ratio of near-bottom concentration to the layer-averaged sediment concentration
R	submerged specific density of sediment
R_f	dimensionless settling velocity
R_p	particle Reynolds number
S	bed slope
S_e	energy slope
U	layer averaged velocity
u, v	horizontal velocities
u_*	shear velocity
$u_{*\mathrm{i}}$	competence shear velocity
$u_{*\mathrm{ci}}$	critical shear velocity for incipient motion
u_z	local flow velcoity
w	vertical component of flow velocity
w_s	settling velocity of sediments
$w_{\mathrm{s}i}$	settling velocity of sediments of ith size range
x, y	horizontal coordinates
z	vertical coordinate
Z	Rouse number
β	empirical coefficient in sediment diffusion relations
Δx	distance between locations where two arrays of siphons
Δ	bed-form height
ε	regression residual
ϵ	eddy viscocity of the fluid
$\epsilon_{xs}, \epsilon_{ys}, \epsilon_{zs}$	diffusion coefficients along the x, y, and z axes
κ	von Karman constant
λ	coefficient of grain-size deviation
ν	kinematic viscosity of water
ρ_f	density of fluid
ρ_s	density of sediment

σ standard deviation on phi-scale of bed material

τ_c critical Shields stress of the sediment

τ_{*g} Shields stress of D_{50}

τ_{*cg} critical Shields stress of D_{50}